ANALYSIS OF VIBRIO PARAHAEMOLYTICUS VIRULENCE SYSTEMS

APPROVED BY SUPERVISORY COMMITTEE

Kim Orth, Ph. D.

Vanessa Sperandio, Ph. D.

Beatriz Fontoura, Ph. D.

Kevin Gardner Ph. D.

ACKNOWLEDGEMENT

I would like to acknowledge many people that have helped make this work possible. First, I would like to give special thanks to my mentor Kim Orth for her guidance and support over the last 5 years. Her mentorship and commitment to designing logical, well-controlled experiments really helped me grow as a scientist. Kim is also very enthusiastic and passionate about her work, which is a quality that I will strive to emulate in my future career.

I would also like to thank the members of my thesis committee, Dr. Vanessa Sperandio, Dr. Beatriz Fontoura, and Dr. Kevin Gardner, for their advice and helpful ideas towards my project. Additionally, I greatly appreciate Dr. Alto and his lab members for many beneficial discussions during shared lab meetings and for sharing lab equipment and reagents. While working on this project, I also enjoyed a very rewarding collaboration with Dr. Lisa Kinch, whose bioinformatics expertise was instrumental in characterizing VPA1380.

Everyone in the Orth lab has been extremely friendly and collaborative. I would like to thank all the members of the Orth lab for sharing their knowledge and expertise with me over the last 5 years. I am grateful to Dr. Dor Salomon for his “menDorship” and guidance. Additionally, I greatly appreciate Alex Klimko, Dr. Marcela Santos, and Dr. Jessie Fernandez for their contributions to this project. Also, my graduate school experience would not have been the same without my bench-mate and best friend, Hyeilin Ham. I would like to thank Hyeilin for her amazing level of kindness, for her support in lab, and for all the fun times outside of lab.

Finally, I would like to thank my family for their love and support. Throughout graduate school they continually provided encouragement during the moments of stress and

cheered me on during the moments of success. My eagerness to strive for a higher education stems from wanting to mimic their own qualities of working hard and over-achieving. Thank you Mom, Dad, Steve, Kristi, Bella, and Jude! This work is dedicated to you.

ANALYSIS OF VIBRIO PARAHAEMOLYTICUS VIRULENCE SYSTEMS

by

THOMAS JAMES CALDER

DISSERTATION / THESIS

Presented to the Faculty of the Graduate School of Biomedical Sciences

The University of Texas Southwestern Medical Center at Dallas

In Partial Fulfillment of the Requirements

For the Degree of

DOCTOR OF PHILOSOPHY / MASTER OF SCIENCE / MASTER OF ARTS

The University of Texas Southwestern Medical Center at Dallas

Dallas, Texas

December, 2014

ANALYSIS OF VIBRIO PARAHAEMOLYTICUS VIRULENCE SYSTEMS

THOMAS JAMES CALDER, Ph. D.

The University of Texas Southwestern Medical Center at Dallas, 2014

Supervising Professor: KIM ORTH, Ph.D.

Vibrio parahaemolyticus is a Gram-negative halophilic bacterium and one of the leading causes of food-borne gastroenteritis from the consumption of raw or undercooked seafood. The pathogenicity of *V. parahaemolyticus* is attributed to several virulence factors, including two hemolysins and two type III secretion systems (T3SS1 and T3SS2). Herein, we compare the virulence of *V. parahaemolyticus* POR strains, which harbor a mutation in the T3SS needle apparatus, to the *V. parahaemolyticus* CAB strains, which contain mutations in transcriptional regulators for the T3SSs. Additionally, we characterize a novel T3SS2 effector termed VPA1380.

From this study, we demonstrate that each structural or regulatory mutant of T3SS1 or T3SS2 alters the pathogenicity of the bacterium in a different manner. POR and CAB

strains exhibited differences in biofilm growth, but shared similar levels of swarming motility and effector production/secretion. Additionally, while the cytotoxicity of these strains was similar, the CAB2 (T3SS1 regulatory mutant) strain was strikingly more invasive than the comparable POR2 (T3SS1 structural mutant) strain. In summary, by creating structural or regulatory mutations in either T3SS1 or T3SS2, differential downstream effects on other virulence systems were observed.

Effector proteins secreted from T3SS2 have been previously shown to promote colonization of the intestinal epithelium, invasion of host cells, and destruction of the epithelial monolayer. In this study, we identify VPA1380, a T3SS2 effector protein that is toxic when expressed in yeast. Bioinformatic analyses revealed that VPA1380 is highly similar to the inositol hexakisphosphate (IP6)-inducible cysteine protease domain of several large bacterial toxins. Mutations of conserved catalytic residues and of residues in the putative IP6-binding pocket abolished toxicity in yeast. Furthermore, VPA1380 was not toxic in yeast cells deficient for the production of IP6. Therefore, our findings suggest that VPA1380 is a cysteine protease that requires IP6 as an activator. Additionally, VPA1380 appeared to disrupt trafficking of dextran and transferrin, which may be due to VPA1380's potential interaction with important retrograde factors. Elucidating the host targets and cellular effects of VPA1380 is important for understanding the pathogenic nature of *V. parahaemolyticus* for diagnostic and treatment and purposes.

TABLE OF CONTENTS

PRIOR PUBLICATIONS

Calder TJ, Santos MS, Attah V, Klimko J, Krachler AM, Orth K. Structural and regulatory mutations in *Vibrio parahaemolyticus* type III secretion systems display variable effects on virulence. Manuscript in preparation.

Calder TJ, Kinch LN, Fernandez J, Salomon D, Grishin NV, Orth K. *Vibrio* type III effector VPA1380 is related to the cysteine protease domain of large bacterial toxins. *PLoS One*. (2014) August; 9(8): e104387.

Broberg CA*****, **Calder TJ*,** and Orth K. *Vibrio parahaemolyticus* cell biology and pathogenicity determinants. *Microbes Infect.* (2011) November; 13(12-13): 992–1001. Review. (*Authors contributed equally)

LIST OF FIGURES

LIST OF TABLES

LIST OF ABBREVIATIONS

(In alphabetical order)

2xYT	2 times Yeast tryptone
AD	Activation domain
Amp	Ampicillin
AMP	Adenosine monophosphate
ATP	Adenosine triphosphate
BLAST	Basic local alignment search tool
BPD	phosphoinositide-binding domain
BSA	Bovine serum albumin
C-di-GMP	Cyclic diguanylate
cAMP	Cyclic adenosine monophosphate
CFP	Cyan fluorescent protein
CGT	Clostridial glucosylating toxins
ChiRP	Chitin-regulated pilus
CPD	Cysteine protease domain
CyaA	Adenylate cyclase
DMEM	Dulbecco’s modified Eagle's medium
DMSO	Dimethyl sulfoxide
DNA BD	DNA Binding domain
ER	Endoplasmic reticulum

ERGIC	ER Golgi intermediate compartment
Fic	Filamentation induced by cyclic AMP
GFP	Green fluorescent protein
HHPRED	Homology detection & structure prediction by HMM-HMM comparison
HI	Heart infusion
IP6	Inositol hexakisphosphate
IPTG	Isopropyl β-D-1-thiogalactopyranoside
IVT	*In vitro* translate/transcribe
Kan	Kanamycin
KP	Kanagawa Phenomenon
LB	Luria Bertani
LDH	Lactate dehydrogenase
MBP	Mannose-binding protein
MLB	Marine LB
MMM	Minimal marine media
MOI	Multiplicity of infection
MSHA	Mannose-sensitive hemagglutinin
Ndel1	Nuclear distribution element like 1
PAGE	Polyacrylamide gel electrophoresis
PAMPs	Pathogen-associated molecular patterns
PBS	Phosphate buffered saline
PCR	Polymerase chain reaction

PSG	Penicillin, streptomycin, L-glutamine
PtdIns(4,5)P2	Phosphotidyl-inositol 4,5-bisphosphate
RE	Restriction Enzyme
RT-PCR	Reverse transcriptase polymerase chain reaction
SD	Synthetic Drop-out
SDS	Sodium dodecyl sulfate
SM	Serum free media
STxB	Shiga toxin b-subunit
T3SS	Type III Secretion System
T6SS	Type VI secretion systems
TDH	Thermodirect-hemolysin
Tfn	Transferrin
TGN	Trans-Golgi network
TLH	Thermolabile hemolysin
TRH	TDH-related hemolysin
Vop	*Vibrio* outer protein
Vps52	Vacuolar protein sorting 52
VSVG	Vesicular stomatitis virus glycoprotein
X-α-gal	5-bromo-4-chloro-3-indolyl α -D-galactopyranoside
X-gal	5-bromo-4-chloro-3-indolyl-β-D-galactopyranoside
YPD	Yeast-extract Peptone, Dextrose

CHAPTER ONE
Introduction and Literature Review

PATHOGENESIS OF *VIBRIO PARAHAEMOLYTICUS*

Vibrio parahaemolyticus

In 1950, a small disease outbreak occurred in the suburb of Osaka, Japan that afflicted 272 patients and caused 20 fatalities. Patients suffered from symptoms of acute gastroenteritis, which included severe stomach pain, nausea, and diarrhea. The source of this outbreak was determined to be contaminated dried sardines that harbored a novel pathogenic bacterium that microbiologists eventually named *V. parahaemolyticus* [1,2]. This bacterium is a gram-negative halophile that thrives in marine and estuarine environments and commonly associates with shellfish and other sea creatures [3]. Since its initial discovery in 1950, *V. parahaemolyticus* has disseminated to coastal regions around the world and is currently the leading cause of seafood-derived gastroenteritis in the United States [4-6] **(Figure 1)**. Cases of gastroenteritis are mostly derived from the consumption of raw or undercooked shellfish [7]. Additionally, in the last decade, *V. parahaemolyticus* has devastated the global shrimp farm industry by causing a lethal hepatopancreatic disease in shrimp [8]. As a result, Asian shrimp markets have lost approximately 1 billion USD [9]. Due to the global dissemination of this human pathogen and its economic impact on the shrimp farm industry, understanding the pathogenic determinants of *V. parahaemolyticus* is crucial for diagnostic and treatment purposes.

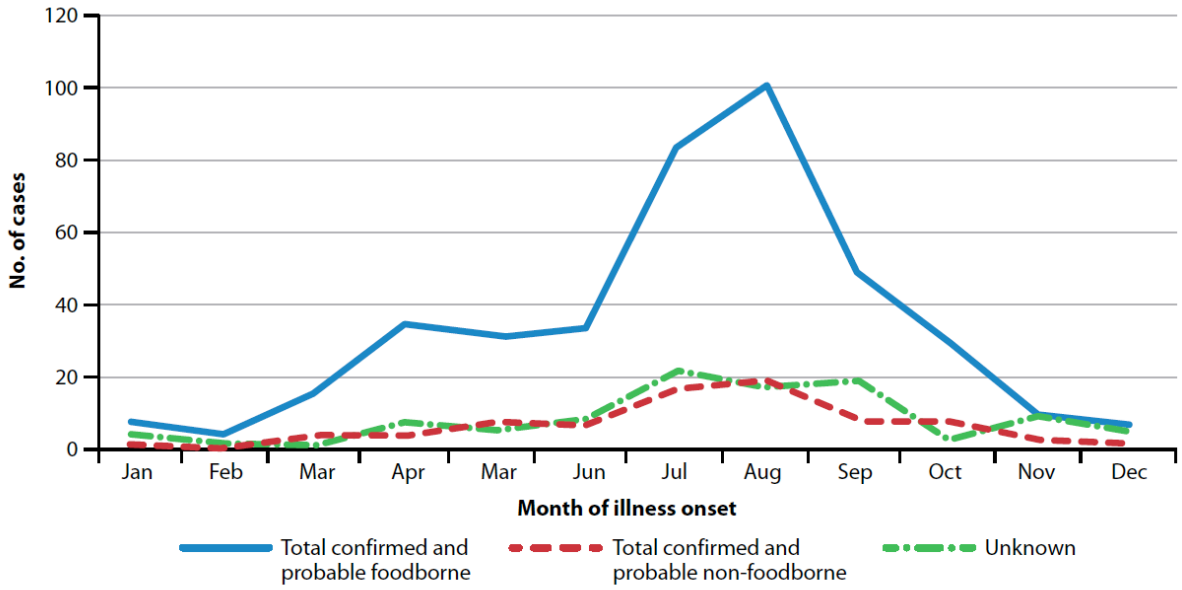

Figure 1. Cases of *Vibrio* infections in the United States in 2011. Illness associated with Vibriosis acquired in the United States throughout 2011. While this graph includes at least 10 different *Vibrio* species, *V. parahaemolyticus* was the most common cause of infection (38% of total cases). Figure reproduced from [10].

Environmental factors and serotype

V. parahaemolyticus is a halophilic, rod-shaped bacterium with a straight or single curved shape [11]. The bacterium thrives in brackish water environments with salinity levels between 0.8% and 3% and grows optimally at temperatures between 35°C and 39°C, but can still replicate in aqueous environments as cold as 16°C [3]. Within sea-habitats *V. parahaemolyticus* is found free-swimming or attached to sediments and other abiotic underwater surfaces. The bacterium also associates with various sea organisms such as shellfish, zooplankton, corals, and sponges [12]. Sediments and zooplankton are thought to

act as a reservoir for *V. parahaemolyticus* during colder months [13], and zooplankton may even act as a vehicle to transport the bacteria across the oceans to new coastal regions [12]. Strains of *V. parahaemolyticus* are classified into serotypes based on the bacterium's somatic (O) and capsular (K) antigens. Currently, 11 O-antigens and 71 K-antigens are known. While some serotypes of *V. parahaemolyticus* are strictly environmental, many serotypes are pathogenic to humans. The serotype O3:K6 is one of the most notorious strains because it has spread globally and causes an acute gastroenteritis disease that has led to higher rates of hospitalization [5]. Different pathogenic serotypes have been detected in most warm coastal areas around the world, but due to global warming, many pathogenic serotypes have also been detected in areas that were once thought to be too cold to harbor *V.* parahaemolyticus such as the coast of Alaska and southern Chile [14,15].

Disease and Prevention

V. parahaemolyticus is a foodborne pathogen that is acquired from consuming raw or undercooked shellfish. Disease symptoms of *Vibrio*-associated gastroenteritis occur rapidly within 2 to 6 hours after exposure and include acute abdominal pain, watery diarrhea, nausea, vomiting, headache, low fever and chills [1,7]. Infections are normally self-limiting but may lead to septicemia and death in patients with underlying medical conditions such as cancer, liver disease, and immune disorders [3]. In rare situations, *V. parahaemolyticus* can cause wound infections, which can be fatal [7]. For example, in the aftermath of Hurricane Katrina in 2005, two out of three infected patients died after suffering from severe wound infections caused by exposure to *V. parahaemolyticus* in the flood water [16].

V. parahaemolyticus is a mesophilic bacterium and thus replicates to high numbers in summer months. Therefore, health officials recommend avoid eating raw oysters and other shellfish during the warmest months of the year. One method to reduce *V. parahaemolyticus* infections during warmer months is to insure fisheries immediately store shellfish at cooler temperatures after harvest [17]. This technique is critical because *V. parahaemolyticus* replicates in less than 20 minutes when exposed to warm temperatures. Additionally, contaminated seafood can be treated to eliminate viable bacteria through short exposure to temperatures around 55°C, mild pasteurization, high-pressure treatment, and irradiation [3].

Cell Biology

To swim through liquid environments *V. parahaemolyticus* contains a single polar flagellum **(Figure 2A)** that moves in a spiral motion to propel the bacteria up to speeds of 60μm per second [18]. The flagella filament is encased in a membrane sheath and powered at the base by a rotary motor within the cell envelope. This motor functions by harnessing the Na^+ motor force as Na^+ ions traverse the cell membrane [19]. *V. parahaemolyticus* harbors approximately 50 polar flagella genes that are regulated by the σ^{54}-dependent activators FlaK and LafK [18,20].

To travel through viscous liquid, *V. parahaemolyticus* develops into an elongated cell and produces numerous lateral flagella **(Figure 2B)** [21,22]. Unlike the polar flagellum, the lateral flagella are unsheathed, driven by the H^+ motor force, and propel the bacteria at a slower speed of 25μm per second [19]. *V. parahaemolyticus* harbors approximately 40 lateral flagella genes that are regulated by LafK [20]. Expression of these genes is enhanced by low

iron levels and the disruption of polar flagellum movement, which signals viscosity or surface sensing conditions [21].

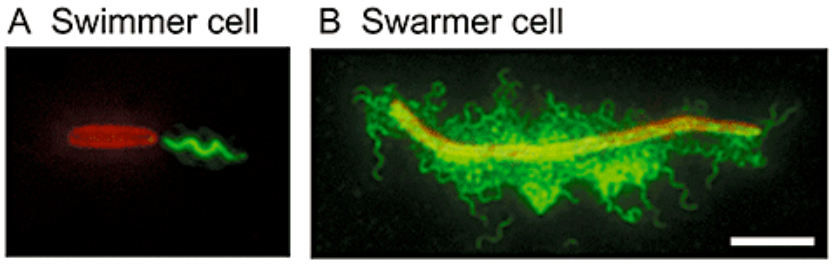

Figure 2. ***V. parahaemolyticus*** **flagella systems. (A)** Swimmer cell grown in liquid exhibiting a single polar flagellum. **(B)** Swarmer cell grown on a surface exhibiting numerous lateral flagella with an elongated cell shape. Cells were stained with FM 4-64 membrane dye (red) and flagella were immunostained with anti-flagellin antibody (green). Figure reproduced from [21].

V. parahaemolyticus produces biofilms to promote survival in various environments. These biofilms can exhibit an opaque or translucent phenotype depending on the polysaccharides that comprise the biofilm matrix [23]. Polar flagella mutants are incapable of forming biofilms, which suggests bacterial movement is crucial for biofilm development [24]. Additionally, to form robust biofilms, *V. parahaemolyticus* requires pili structures for attachment to surfaces and other cells [25]. Two different pili, mannose-sensitive hemagglutinin typeIV pili (MSHA) and chitin-regulated pili (ChiRP), have been shown to be critical for this process [24,26]. Biofilm genes are organized within two capsular polysaccharide loci that are controlled by quorum sensing regulators and cyclic di-GMP levels in an inverse relationship with swarming gene regulation [25].

Attachment to host cells is a vital initial stage of infection for many pathogenic bacteria. The bacterial protein, multivalent adhesion molecule 7 (MAM7), was shown to mediate this attachment by binding to both fibronectin and phosphatidic acid on the host membrane. MAM7 is conserved among many Gram-negative pathogenic bacteria and consists of 7 mammalian cell entry (mce) domains that are necessary for high affinity binding. *V. parahaemolyticus* requires MAM7 for type III secretion-mediated cytotoxicity in several cell types and for pathogenicity in the nematode *Caenorhabditis elegans* infection model. Interestingly, a non-pathogenic BL-21 *E. coli* strain that heterologously expressed MAM7 was able to compete with *V. parahaemolyticus* for cell binding during a co-infection experiment of tissue culture cells. This experiment suggests inhibitors of MAM7 can be utilized as a therapeutic tool to block *V. parahaemolyticus* and other pathogenic bacteria from establishing binding at an initial infection site [27].

Bacterial Cell Signaling

Bacteria utilize quorum sensing to measure population density. Each bacteria secretes autoinducer molecules that are sensed by signaling networks and act to inhibit or induce expression of various genes [28]. In *V. parahaemolyticus*, the high-cell density regulator OpaR enhances expression of capsular polysaccharide genes and represses swarming and virulence genes [29]. Interestingly, an *opaR* mutant strain can still produce biofilms but exclusively forms biofilms with a translucent phenotype, as opposed to opaque [30]. The low-cell density regulator AphA acts conversely to inhibit biofilm formation and promotes the production of swarming and virulence systems. As expected, the *aphA* mutant strain is non-virulent [31].

The cyclic-di-GMP second messenger molecule controls many molecular networks in bacteria to induce biofilm growth and repress motility and virulence systems. Proteins with diguanylate cyclase GGDEF domains are responsible for producing the molecule c-di-GMP, which can be broken down by phosphodiesterases with an EAL domain [32]. *V. parahaemolyticus* expresses many proteins with these domains. One protein, ScrG, contains both domains but appears to have phosphodiesterase activity since it was shown to limit c-di-GMP production, induce expression of swarming genes, and inhibit expression of capsular polysaccharide genes [33]. Another protein, ScrC, contains both domains and is able to produce and degrade c-di-GMP and was shown to inversely regulate swarming and biofilm production. However, ScrC was recently found to switch to a phosphodiesterase state by a quorum-sensing signal at low cell density [34,35]. Therefore, cell density can regulate

virulence traits in *V. parahaemolyticus* through quorum sensing networks and c-di-GMP signaling.

Virulence factors

In 1996, an O3:K6 strain of *V. parahaemolyticus* was isolated from a Japanese traveler suffering from diarrhea. This pathogenic isolate was termed RIMD 2210633 and its genome was sequenced in 2003 [36]. The genomic sequence revealed several toxins and virulence systems including genes encoding: two thermodirect-hemolysins (TDH), a thermolabile hemolysin (TLH), two type III secretion systems (T3SS), T3SS1 and T3SS2 **(Figure 3)**, and two type VI secretion systems (T6SS), T6SS1 and T6SS2 [37]. Analysis of the G+C content of the *tdhs* and T3SS2 genes suggests these genes were recently acquired by the bacterium [36], which likely coincides with the bacterium's recent emergence as a human pathogen.

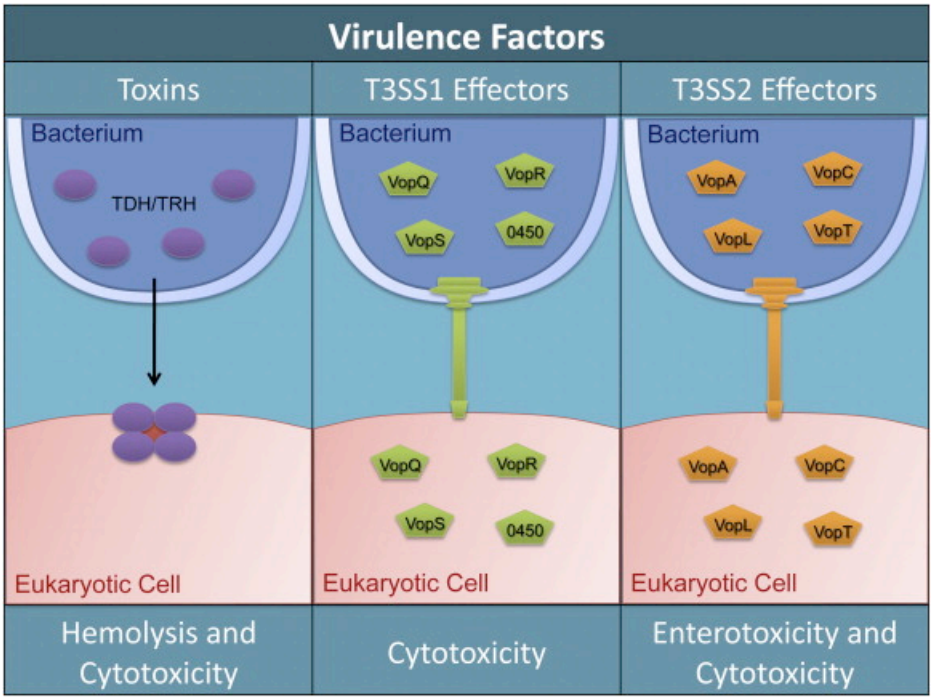

Figure 3. Three major virulence systems of *V. parahaemolyticus*. TDH and TRH are toxins secreted as monomers and form a tetrameric pore in the eukaryotic membrane to cause lysis of certain cell types. T3SS1 effector proteins are secreted through a needle apparatus into eukaryotic cells to cause cytotoxicity. T3SS2 effectors are secreted into eukaryotic cells through a different needle apparatus to cause cytotoxicity and enterotoxicity. Figure reproduced from [37].

Hemolysins

TDH was first characterized in the 1980s, and was found to be the toxin responsible for causing hemolysis when *V. parahaemolyticus* was grown on Wagatsuma blood agar plates. This hemolysis activity was termed the Kanagawa Phenomenon (KP) [38]. Originally, TDH was believed to be the major virulence factor of *V. parahaemolyticus* because clinical strains were typically "KP positive" and most environmental strains were "KP negative" [39]. Mutant strains lacking TDH still caused gastroenteritis in an infant rabbit model though and exhibited only a minor reduction of toxicity in a rabbit ileal loop model [40-42]. This suggested other virulence factors are essential for the gastroenteritis disease that was later associated with T3SS2.

TDH is a pore-forming toxin that is secreted as a monomer but organizes into a tetrameric complex in the host membrane. While the exact function of TDH is unknown, the crystal structure of the tetrameric complex revealed a large 23Å central pore that is thought to permit permeabilization of ions with low selectivity [43]. TDH may favor association with lipid rafts on cell membranes because treating cells with a raft-disrupting agent prevented TDH cytotoxicity. However, this association was independent of hemolysis [44]. Another *V. parahaemolyticus* toxin, termed TDH-related hemolysin (TRH), shares high sequence homology (68%) with TDH and is found in both TDH positive and negative strains [39]. This toxin was similarly shown to form a tetrameric pore and cause hemolysis [45].

The RIMD 2210633 clinical isolate contains two *tdh* genes, termed *tdhA* and *tdhS*. These genes are located in a pathogenicity island containing T3SS2 genes [36]. All *V. parahaemolyticus* strains also contained the putative thermolabile hemolysin (TLH) [39] that

is induced in the presence of bile salts; the same chemical inducer that transcriptionally activates T3SS2 and is a mimic for the intestinal environment [46]. The function and mechanism of TLH is currently unknown.

Type III Secretion Systems

T3SSs are produced by many gram-negative bacteria and are used to secrete bacterial effector proteins directly into host cells. These systems consist of a 3.5-megadalton (MDa) needle-like apparatus that is evolutionarily related to flagellum and comprised of more than 20 structural proteins. The T3SS needle contains a basal structure that spans the inner and outer membrane of the bacterium as well as a long conduit tube with a tip that penetrates the host membrane. The channel of the needle is only ~28Å in diameter which can only accommodate passage of effector proteins in an unfolded state [47-49].

Although most pathogenic bacterium with a T3SS contain a unique repertoire of effector proteins, the mechanism of effector protein secretion is thought to be similar between bacterial species. The first 20-30 amino acids of all effectors consists of a secretion signal, that is uncleaved, and often contains further functions within the host cell such as effector-localization [48]. Also within the N-terminal portion of effector proteins is a chaperone-binding domain. Bacteria utilize ATP-independent chaperones to prime the effector proteins for unfolding by an ATPase at the base of the needle apparatus [50]. Chaperones may also promote the ordered sorting of effector proteins prior to secretion [51]. Once effector proteins are unfolded and injected into the host cell, they refold and target different host machinery to benefit the bacteria during infection [48].

T3SS1

T3SS1 is found in both environmental and clinical strains of *V. parahaemolyticus* and causes cytotoxicity. Genes for this system are regulated by the ExsACDE cascade that is induced by low calcium Ca^{2+} levels and host-cell contact. A similar ExsACDE cascade is found in *Pseudomonas aeruginosa*, which also induces the expression of T3SS genes in low Ca^{2+} environments [52]. In fact, the genes *exsA*, *exsD*, and *exsC* were first identified in *V. parahaemolyticus* due to their high sequence homology to the characterized genes in *P. aeruginosa* [53,54]. The *exsE* gene from *V. parahaemolyticus* shares no homology to genes found in *P. aeruginosa*, but it was discovered due to its close proximity to *exsC*. The regulatory mechanism of this cascade in *P. aeruginosa* is relatively simple. ExsE binds to ExsC to block its function, and ExsD binds to ExsA to inhibit its ability to initiate T3SS gene expression. During low Ca^{2+} conditions or host cell contact, ExsE is secreted from the bacterium, which allows ExsC to sequester ExsD [55]. Once ExsA is free, it promotes the expression of all T3SS genes, including the *exsACDE* genes **(discussed in more detail in Chapter 3 and Figure 7)** [56,57].

While T3SS1 is not implicated in the gastroenteritis symptoms observed in animal models, T3SS1 effector proteins are able to cause lysis of tissue culture cells in less than three hours when the bacteria containing this system are induced with low calcium DMEM. The infection process begins with high levels of autophagy and blebbing of the outer membrane, and proceeds with cell rounding and finally cell lysis [58]. The effectors known to be involved in this process are VopQ, VPA0450, and VopS, respectively **(Figure 4)** [59-

61]. *V. parahaemolyticus* can also inhibit the pathogen sensor NLRC4 from triggering inflammasome activation, which is a cellular immune response against pathogen-associated molecular patterns (PAMPs). VopQ and VopS are necessary for this inhibition [62]. In addition to these characterized effectors, a novel T3SS1 effector termed VopR was recently shown to cause cell rounding as well [63].

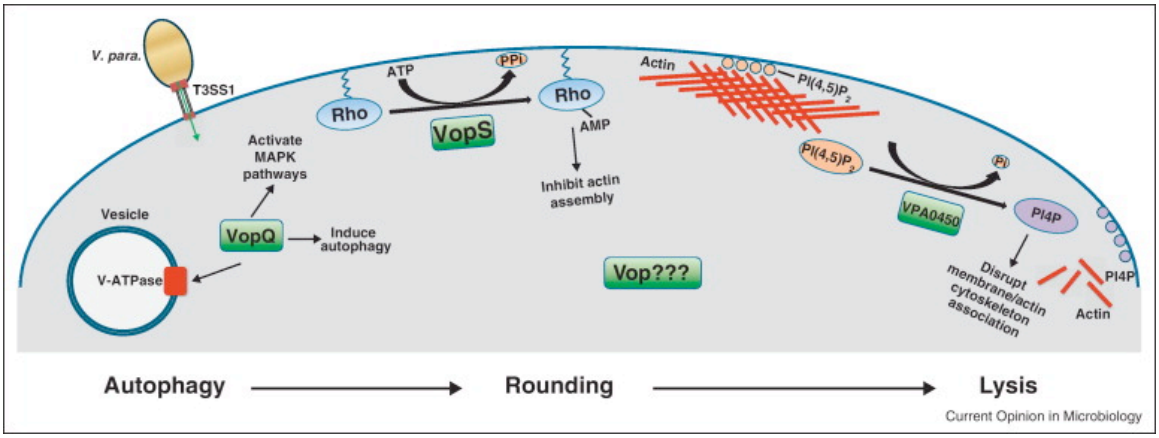

Figure 4. T3SS1 effectors and their functions during *V. parahaemolyticus* infection. VopQ forms a gated pore on lysosomal membranes that leads to high levels of autophagy and the downstream effect of MAPK activation. VopS AMPylates Rho family GTPases to sterically block their binding to downstream effector protein, which disrupts actin assembly and causes cell rounding. VPA0450 dephosphoylates the D5 phosphate from phosphotidyl-inositol 4,5-bisphosphate [PtdIns(4,5)P_2] to block the binding of actin adaptor proteins to the cell membrane and thus causes membrane blebbling. After 2-3 hours of infection, cells will undergo lysis. Figure reproduced from [64].

VopQ is necessary and sufficient to induce autophagy as demonstrated during *V. parahaemolyticus* infections and with microinjection assays using purified recombinant VopQ. Autophagy levels were verified by examining LC3-I to LC3-II conversion, a standard readout of autophagy, and by observing autophagic vesicles with electron microscopy [65]. Interestingly, VopQ-dependent autophagy is not due to the promotion of new autophagic vesicles, but instead is due to the inhibition of autophagic turnover. VopQ forms a gated channel within lysosomal membranes that allows for the release of molecules smaller than 18Å as confirmed by liposome release assays and electrophysiology assays. During *in vitro* experiments, VopQ binds to liposome membranes through an electrostatic interaction, but inside cells VopQ specifically targets lysosomes by binding to the V_o subunit of the V-ATPase proton pump enriched on lysosomal membranes. Thus, VopQ forms a targeted pore that deacidifies lysosomes, which in turn prevents autophagosome-lysosome fusion and leads to the build-up of autophagic vesicles [59]. Autophagy is thought to aid the bacteria by sequestering membrane machinery normally used for phagocytosis of the bacterium by phagocytic cells [65].

VPA0450 causes membrane blebbing in the plasma membrane of the host cell during infection. This phenotype was discovered by observing residual membrane blebs filled with actin cytoskeleton filaments along the interior side of the plasma membrane. Bioinformatic analysis of VPA0450 revealed homology to a family of eukaryotic inositol polyphosphate 5-phosphatases (IPP5C) [60]. Similar to synaptojanin, a *Schizosaccharomyces pombe* enyzyme belonging to this family [66], VPA0450 was shown to specifically dephosphorylate the D5 phosphate from phosphotidyl-inositol 4,5-bisphosphate [PtdIns(4,5)P_2]. A catalytic inactive

mutant of VPA0450 was verified to eliminate this phosphatase activity in vitro and significantly reduced the blebbing phenotype when transfected in tissue culture cells [60]. PtdIns(4,5)P_2 acts as a docking site for the actin cytoskeleton through intermediary adaptor proteins, which normally bind to PtdIns(4,5)P_2 with a conserved phospholipase-Cδ1 domain [67]. By removing the binding site for these adaptor proteins, VPA0450 causes the actin cytoskeleton to detach from the membrane and thus cause membrane blebbing [60].

VopS is necessary for cell rounding during infection by functionally collapsing the actin cytoskeleton network. This phenotype is due to the inactivation of the Rho family GTPases: Rac, Rho, and Cdc42 that normally interact with downstream effectors under activated conditions to alter actin dynamics [68]. With the use of mass spectrometry, VopS was found to cause inactivation of these GTPases by enzymatically adding the adenosine 5'monophosphate (AMP) portion of ATP to the effector binding switch I region of Rho family GTPases to sterically hinder effector binding. This transferase reaction was termed AMPylation and is mediated by the VopS Fic domain [61]. Furthermore, structural and kinetic studies revealed that the AMPylation reaction involves a "ping-pong" mechanism that necessitates the formation of a Fic-AMP intermediate before the AMP molecule is transferred to the GTPases [69]. Interestingly, the Fic domain was found in genes throughout many prokaryotic and eukaryotic organisms, including humans. Understanding the mechanism of the Fic domain will likely shed new light on the role of these genes.

VopR was recently shown to contain a conserved phosphoinositide-binding domain (BPD) that binds phosphatidylinositol-(4,5)-bisphosphate and causes VopR to localize to the host cell membrane. This interaction was shown by *in vitro* NMR experiments to mediate

stable folding of VopR, which suggests the phosphoinositide interaction may help VopR refold upon secretion into the host cell. VopR also causes cell rounding but the mechanistic details of this effect are unknown [63].

T3SS2

T3SS2 is primarily found in clinical *V. parahaemolyticus* strains and is thought to be the major virulence factor of the gastroenteritis disease. Expression of T3SS2 genes is controlled by the master regulator VtrA, which is activated by bile salts and temperatures near 37°C [46]. These conditions mimic the physiological conditions of the intestines. Once activated, VtrA promotes the expression of the transcription factor VtrB, which in turn promotes the expression of T3SS2 genes **(discussed in more detail in Chapter 3 and Figure 7)** [70]. The most active components of bile salts are taurodeoxycholate and glycodeoxycholate but an intermediate level of activation is induced by deoxycholate, taurochenodeoxycholate, glycochenodeoxycholate, taurocholate, and glycocholate [46].

The role of T3SS2 during intestinal infection has been studied with several animal models. The rabbit ileal loop model is commonly used to examine intestinal infections outside of a live animal and is performed by injecting bacteria into a ligated rabbit ileal loop followed by measuring fluid accumulation. *V. parahaemolyticus* causes high levels of fluid accumulation approximately 18 hours after injection, and was confirmed to be dependent on T3SS2 [41]. Another model involves oragastrically infecting 2-day old piglets. Infected piglets presented characteristic symptoms of vomiting and watery diarrhea in a T3SS2 dependent-manner but histological examination of the colon presented only minimal swelling

of the submucosa and serosa with no damage to the epithelial layer [71]. This minimal effect contrasts the noticeable epithelial disruptions seen in clinical samples from human patients [72]. To overcome this limitation, another model was developed that involves oragastrically infecting infant rabbits pre-treated with cimetidine to reduce stomach acidity. *V. parahaemolyticus* colonized the small and large intestines but the distal small intestines was determined to be the primary infection site, as determined by bacterial counts and levels of epithelial damage. Within early time points, *V. parahaemolyticus* formed confined colonies along the epithelial layer of the distal small intestines **(Figure 5A)**. After 20 hours, the infected rabbits developed yellow watery diarrhea and examination of the distal small intestines showed severe damage and permeabilization of the epithelial layer. In this model, T3SS2 was shown to be necessary for bacterial colonization and epithelial damage **(Figure 5B)** [72]. Several T3SS2 effectors that are known to play a role within this infection process include VopC, VopA/P, VopZ, VopL, VopV, and VopT **(Figure 6)**.

A

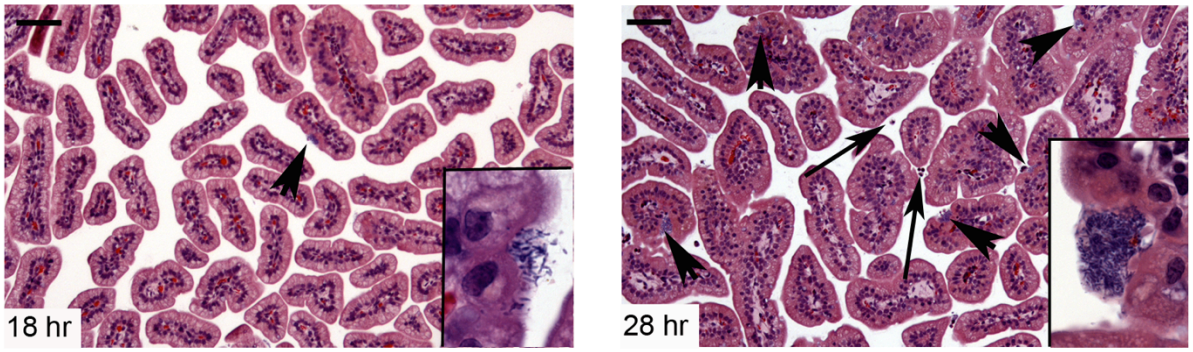

B

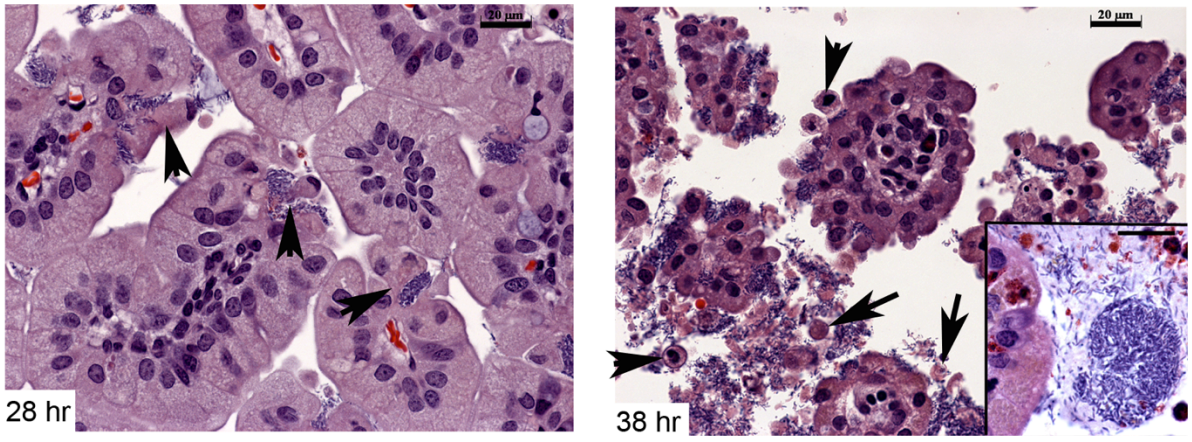

Figure 5. ***V. parahaemolyticus*** **infection of rabbit distal small intestines.** Hematoxylin and eosin (H&E) staining of tissue sections from distal small intestines. Infant rabbits were oragastrically infected and tissue sections were examined **(A)** 18 hr and 28 hr post infection with scale bar at 100um and **(B)** 28 hr and 38 hr post infection with scale bar at 20um. Short arrows point to bacterial microcolonies and long arrows point to heterophil immune cells. Images reproduced from [42].

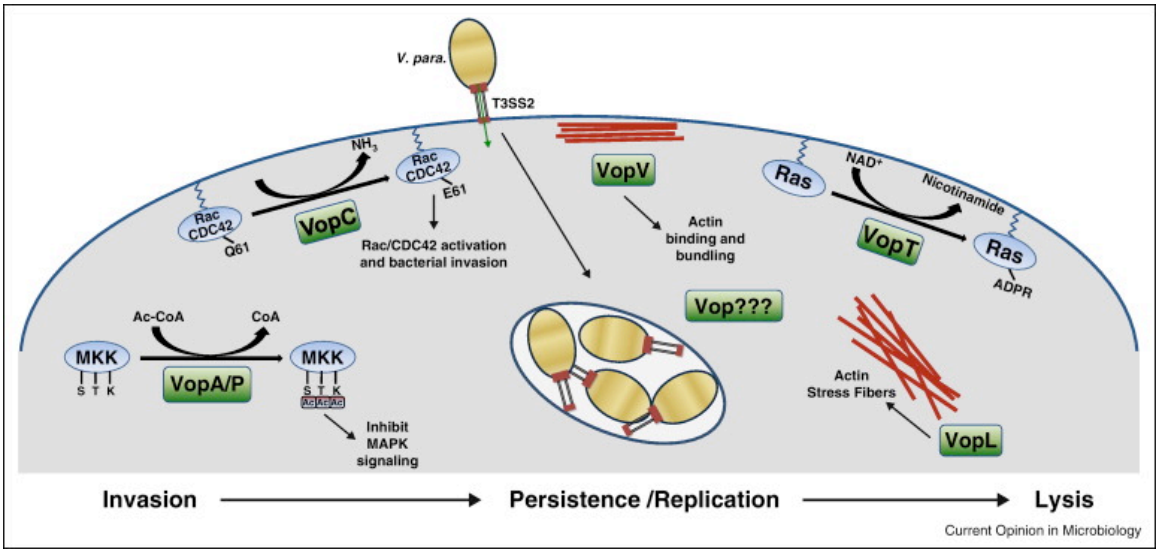

Figure 6. T3SS2 effectors and their functions during *V. parahaemolyticus* infection. VopC mediates bacterial invasion into non-phagocytic cells by Deamidating Rac and CDC42 to alter actin dynamics at the site of infection. VopA/P acetylates MAPKK's to block signaling and activation of the MAPK immune pathway. VopL nucleates actin to cause stress fibers and VopV bundles actin. VopT ADP-ribosylates RAS but the cellular effects of this modification are unknown. During infection, bacteria are thought to replicate inside the host cell and eventually cause cell lysis. Figure reproduced from [64].

VopC was recently discovered to promote bacterial invasion into non-phagocytic cells, which changed the previous dogma that *V. parahaemolyticus* is exclusively an extracellular pathogen [73]. The initial idea of bacterial invasion was explored because VopC is homologous to the catalytic region of the cytotoxic necrotizing factor (CNF) toxin that promotes bacterial invasion of other bacterial species through deamidation of Rho family GTPases [74]. Similarly, VopC deamidates the Rho family GTPases, Cdc42 and Rac [73], but only modification of Cdc42 promotes invasion. From one study, invasion was not necessary for gastroenteritis phenotypes examined in the infant rabbit infection model at 38 hours post infection [75]. Further animal model experiments with more experimental

parameters are required to examine how invasion contributes to *V. parahaemolyticus* infection of the intestines.

VopA/P inhibits the innate immunity MAPK pathway [76]. This inhibition was first characterized from studies of the VopA/P homolog YopJ from *Yersinia*, which blocks MAPK kinases (MKKs) by acetylating serine and threonine residues on the protein's activation loop. From *in vitro* signaling assays and mass spectrometry analysis, VopA/P was found to inhibit MKK activity differently by acetylating a conserved lysine residue on the kinase catalytic loop. This modification inhibits the kinase by blocking ATP binding, but not ADP binding [77]. In further contrast to YopJ, VopA/P does not inhibit the pro-survival NFκB pathway [76], which suggests *V. parahaemolyticus* favors host survival. This is likely important if the bacterium has an intracellular lifestyle. Recently a novel effector termed VopZ was shown to inhibit the MAPK pathway by blocking the activation of TAK1, a kinase directly upstream of MKKs [78]. Future studies are required to understand this redundancy and to differentiate the roles of VopA/P and VopZ.

VopL causes actin stress-fiber formation and VopV causes actin bundling. Bioinformatic analysis of VopL revealed three copies of the eukaryotic domains, Wiskott-Aldrich Homology 2 (WH2) and proline-rich motif (PRM). These domains are implicated in actin assembly, so an *in vitro* actin assembly assay was utilized to test VopL's activity. Interestingly, VopL was found to nucleate actin independent of eukaryotic factors [79]. Subsequent structural experiments found that the WH2 domains bind to actin monomers and the C-terminal region organizes the actin monomers into filaments [80]. VopV was determined by pull-down assays to directly bind to F-actin filaments. Sedimentation

experiments revealed VopV also aggregates F-actin filaments, and these aggregates were visualized by transmission electron microscopy to be shaped into bundles of parallel filaments. The role of VopL and VopV during infection is still unknown but VopV was found to be completely necessary for enterotoxicity in a rabbit ileal loop model [81].

VopT is necessary for full cytotoxicity during infection of Caco-2 gut epithelial cells. Bioinformatic analysis revealed an ADP-ribosyltransferase domain that is also found in the *Pseudomonas aeruginosa* effectors, ExoS and ExoT. Similar to these toxins, VopT was found to ADP-ribosylate the GTPase Ras and to require the 14-3-3 family protein FAS for enzyme activity. Ras is known to regulate cell growth, differentiation, and apoptosis, but the effect of ADP-ribosylation is unknown [82].

Aim of thesis

In this work we further explore the virulence phenotypes regulated by the master regulators, ExsA and VtrA, which regulate expression of T3SS1 and T3SS2 genes, respectively [53,70]. Micro-array and RNA-sequencing studies have revealed that these regulators control gene expression outside the T3SS1 and T3SS2 genes [46,70,83], which suggests these regulators control expression of other virulence related systems. To test this hypothesis, we compare T3SS needle mutants to ExsA and VtrA mutants in several virulence-related assays including: effector production/secretion, swarming, biofilm growth, cytotoxicity, and invasion.

Additionally, we identify and characterize a novel T3SS2 effector with the gene name *vpa1380*. Bioinformatic analyses revealed VPA1380 is homologous to the *Shigella flexneri*

effector OspB, but little is known about the mechanism and cellular effects of OspB [84,85]. To identify the mechanism of VPA1380 we further analyzed the protein using bioinformatics analysis and examined the protein's cytotoxicity in the yeast strain *Saccharomyces cerevisiae*. To identify VPA1380's host target, we performed a yeast two-hybrid screen and tested the resulting interaction partners *in vitro* and in HeLa cells. Additionally, we examined VPA1380's localization in HeLa cells to elucidate a cellular phenotype and determine the cellular compartment that VPA1380 may act upon. Understanding the role of VPA1380 during infection is important for understanding the pathogenicity of *V. parahaemolyticus*.

CHAPTER TWO
MATERIALS AND METHODS

Vibrio strains and growth conditions

The genotypes of the strains used in this study are listed in **Table 1**. All strains were derived from the parental RIMD 2210633 strain, which was generously donated by Dr. Tetsuya Iida and Dr. Takeshi Honda [40]. *V. parahaemolyticus* strains were routinely grown in marine LB (MLB) media (1% tryptone, 0.5% yeast extract, 3% NaCl) or on minimal marine media (MMM) agar plates (77mM K_2HPO_4, 35mM KH_2PO_4, 20mM NH_4Cl, 5mM K_2SO_4, 2% NaCl, 0.4% galactose, and 1.5% agar) at 30°C. Selection for the pBAD/Myc-His vector (Invitrogen) was maintained with 200 μg/ml kanamycin.

HeLa cell culture conditions

HeLa cells (ATCC) were cultured in DMEM (Invitrogen), containing 4.5g/L glucose, and supplemented with PSG [1mM sodium pyruvate, 100U/mL penicillin, 100μg/mL streptomycin, 2mM L-glutamine (Invitrogen)] and 10% heat-inactivated fetal bovine serum (Sigma). Cells were incubated at 37°C in 5% CO_2. During infections, cells were cultured in DMEM solution lacking PSG.

Cloning of genes

Genes for constructs (**Table 2**) were PCR amplified with Vent DNA polymerase (NEB) and designed primers (Sigma) (**Table 3**). PCR product was purified and digested, along with the target vector, with digestion enzymes (NEB or Thermo Scientific Fermentas).

DNA was run on an agarose gel and extracted using Gel-extraction kit (Biobasic Inc). Digestion products were then ligated with T4 DNA Ligase (NEB) and then transformed into the *E. coli* DH5α strain. DH5α bacteria were grown on Luria Bertani (LB) media agar (1% tryptone, 0.5% yeast extract, 1% NaCl, and 1.5% agar) or in 2xYT liquid broth (1.6% tryptone, 1% yeast extract, 0.5% NaCl) with selective antibiotics at 37°C. The cloned plasmid was purified using a mini-prep kit (Invitrogen or BioBasic Inc) and the gene insertion was confirmed by colony PCR and sequencing.

Yeast growth conditions

The yeast strain BY4741 (MATa his3Δ0 leu2Δ0 met15Δ0 ura3Δ0) was grown on YPD agar (10g/L yeast extract, 20g/L peptone, 2% glucose, 2% agar) at 30°C. Yeast containing plasmids were selected on SD agar media (6.7g/L yeast nitrogen base without amino acids, 1.4g/L yeast synthetic drop out medium supplement without selective amino acids, 2.5mM NaOH, 2% glucose, 2% agar). To induce protein expression from plasmid, glucose in SD media was replaced with 2% galactose and 1% raffinose. Yeast were also grown in 3ml liquid cultures in similar media lacking agar [86]. The yeast strain BY4741Δ*ipk1* was obtained from a yeast knock out library (OpenBioSystems).

Yeast transformation

Overnight cultures were spun down briefly (10k rpm for 5 sec) and the pellet was resuspended in 1mL resuspension buffer (10% TE solution, 10% 1M LiAc). For each transformation, 100μL resuspended yeast were mixed with 5 μL single stranded salmon

sperm DNA (10 mg/mL) and 250-500 ng plasmid DNA, with medium-level vortexing. Next 650µL of transformation solution (10% TE solution, 10% LiAc solution, 80% PEG) was added with medium-level vortexing, and then put on a nutator for 30 min at 30°C. Next, 70µl DMSO was added and mixed by inverting tubes 10 times, and then tubes were incubated in 42°C water bath for 15 min. Tubes were then placed on ice for 2 min and then spun down at 800g for 5 min. Pellet was resuspended with 100µl water and spotted on SD media agar plate. Yeast were spread on plate with sterile glass hockey stick.

Yeast 2-hybrid screen

Yeast 2-hybrid screen performed according to manufacturer's instructions (Clontech Matchmaker Gold Yeast Two-Hybrid System). Briefly, VPA1380 C/A was cloned in a pGBKT7 vector, with DNA binding domain (DNA-BD) fusion, and transformed in *Saccharomyces cerevisiae* Gold strain provided by manufacturer. DNA-BD-VPA1380 C/A was first shown to not autoactivate by screening yeast on SD agar without histadine and SD agar containing 5-bromo-4-chloro-3-indolyl α -D-galactopyranoside (x-α-gal). Next, yeast containing pDNA-BD-VPA1380 C/A were transformed with library of genes from mouse embryo library within pACT2 vector, with activation domain (AD). Positive clones were initially chosen by growth on SD agar without histadine, and further confirmed by testing positive clones on SD agar containing x-α-gal. The pACT2 was obtained from yeast through phenol-chloroform DNA extraction, and positive clones were identified by sequencing with manufacturer primer.

To test Ndel1 fragments within the yeast 2-hybrid system, VPA1380Δ50 C/A was cloned into pLexAde, with DNA-BD, and transformed in *S. cerevisiae* L40 yeast. These yeast were transformed with pVP16 containing Ndel1 fragments fused to the VP16 AD, and tested for activation on SD plates with 5-bromo-4-chloro-3-indolyl-β-D-galactopyranoside (x-gal).

T3SS1 and T3SS2 induction

To induce T3SS1 or T3SS2 gene expression, bacteria grown over-night in MLB were diluted to OD_{600}=0.3 in DMEM or marine LB with 0.05% bile salts, respectively. For induction of both systems, bacteria were then transferred to 37°C for 1.5 hours, or 3 hours for swarming experiments and effector secretion assays.

Growth curve

POR and CAB strains were grown over-night and diluted to OD_{600}=0.1 in 30mL MLB in triplicate at 30°C. OD_{600} was measured every 30 min for each strain.

Swarming motility assay

For swarming motility assays, bacteria were grown over-night and normalized to OD_{600}=1. After T3SS1, or no induction, 2µl of diluted culture was spotted in triplicate onto heart infusion (HI) plates containing 2% NaCl and 1.5% agar. Swarming plates were incubated at 30°C for 24 hours and then swarming diameter was measured.

Biofilm growth

V. parahaemolyticus cultures were grown over-night and diluted to OD_{600}=0.1 in triplicate in MLB media, DMEM, or MLB media with 0.05% bile salts. Bacteria were grown aerobically in 96-well microtiter plate with lid at 37°C for 24 hours. Bacteria cultures were then removed, washed with water 3 times, and stained with 0.1% crystal violet for 15 minutes. Wells were then washed with water and dried overnight. The remaining crystal violet was resuspended in 30% acetic acid and the absorbance was measured at 595 nm [87].

Invasion assay

Invasion of *V. parahaemolyticus* strains was performed as described [73]. Briefly, pre-induced *V. parahaemolyticus* strains were added at an MOI of 10 to HeLa cells, and the plates were centrifuged at 1,000g for 5 min. After a 2 hour incubate at 37°C, 100 μg/ml gentamicin was added to kill extracellular bacteria. At the indicated time points, bacterial numbers were determined by serially diluting samples on marine minimal plates. Analysis was performed in triplicate.

Secretion assay

For induction of T3SS1 and T3SS2 genes, *V. parahaemolyticus* cultures were diluted to OD_{600}=0.3 in DMEM and LB media with 0.05% bile salts, respectively. To harvest the lystate fraction, bacterial pellets were resuspended and boiled in 2x Laemmli sample buffer for 5 min. The supernatant was filtered (22μm pore) and precipitated with deoxycholate (150 μg/ml) and trichloroacetic acid (10%) on ice overnight. The precipitated protein was

washed with acetone and resuspended in 2x Laemmli sample buffer and boiled for 5 min [63]. Samples were examined by western blot analysis using *Vibrio* effector antibodies: rabbit anti-VopQ [65], rabbit anti-VopS [61], rabbit anti-VopA, and rabbit anti-VopL [79], and also mouse anti-CyaA antibody (Invitrogen). Effector antibodies were generated by Strategic Biosolutions (Newark, DE) using recombinant proteins.

Translocation assay

V. parahaemolyticus strains were grown overnight and diluted to OD_{600}= 0.3 in LB supplemented with 0.05% bile salts. Cultures were pre-induced for 1 hour at 37°C and then added at an MOI of 10 to confluent HeLa cells in a 96 well plate. The cells were spun down at 1000g for 5 minutes and then incubated for 1 hour at 37°C. Intracellular cAMP levels were measured in triplicate with the cAMP Direct Biotrak EIA kit (GE Healthcare Life Sciences) according to the manufacturer's directions.

LDH release assay

Pre-induced *V. parahaemolyticus* strains were added at an MOI of 10 to confluent HeLa cells in DMEM containing no serum or phenol red. Plates were centrifuged at 1,000g for 5 min to synchronize infection, and then incubated at 37°C for set time points. Next, samples were collected and LDH activity in the medium was measured using a Cytotoxicity Detection kit (Takara). Percentage cytotoxicity is compared to total lysed cells in 0.5% Triton X-100. Each sample was calculated as an average of 3 replicates done in triplicate.

Transfection of HeLa cells

HeLa cells were seeded at $1.5x10^5$ cells/well on sterile glass coverslips in 6-well dishes and grown for 2 days. For transfection, 2µg of total DNA was vortexed with 100µl of OptiMEM media. Next, 2µl of X-tremeGENE (Roche) reagent was added and vortexed briefly. After a 30 min wait time, samples were added drop-wise to cells. Cells were then incubated at 37°C for 4 hours and then the media was replaced with fresh DMEM. Cells were then incubated at 37°C for 12-16 hours.

Cell lysate harvest and Western blot analysis

While on ice, transfected HeLa cells were washed 2x with PBS and removed from plate with cell scraper. Cells were resuspended in PBS, pelleted, and resuspended in 200µL lysis buffer. Next, cells were put on a nutator for 15 min and then centrifuged at 14,000 rpm for 5 min. Supernatant was mixed with 40µL SDS sample buffer and boiled for 5 min. Samples were run on SDS-PAGE gel, transferred to a membrane, and analyzed by western blot analysis. Primary antibodies include: mouse anti-V5 (Invitrogen), mouse anti-GFP (Clontech), mouse anti-HA (Cell Signaling), and mouse anti-Tubulin (Sigma).

Immunohistochemistry and confocal preparation

Cells were fixed in 3.2% paraformaldehyde and then permeabilized with 0.5% Triton X-100. Cells that required immune-staining were then blocked in PBS with 1% BSA for 30 min. Next, 150µl of primary antibody solution (PBS, 0.5% BSA, 0.25% Tween) was

carefully incubated on top of coverslip for 1 hr. Cells were washed 3 times with PBS and then incubated with 150µl of secondary antibody solution (PBS, 0.5% BSA, 0.25% Tween) for 1 hr. The nuclei were stained with Hoescht (Sigma) and the actin was stained with Rhodamine-phalloidin (Molecular probes), with 10 min incubation in PBS. Images were taken by a Zeiss LSM 510 scanning confocal microscope.

Primary antibodies include mouse anti-calnexin (Abcam) for ER staining, mouse anti-TGN97 (Invitrogen) for trans-Golgi straining, rabbit Anti-p58 (Invitrogen) for ERGIC staining, mouse anti-EEA1 (BD Biosciences) for early endosome staining, and rabbit anti-Rab11 (Cell Signaling) for recycling endosomes. For lysotracker staining, cells were incubated with Lysotracker Red DND-99 (Invitrogen) (1µl stock solution in 10 mL DMEM) for 20 min at 37°C prior to fixation.

VSVG Trafficking

pVSVG-CFP was co-transfected peGFP-effector plasmids for 16 hrs, with each sample repeated in 3x 6-well plates. All plates were transferred to 40°C for 3 hrs to keep VSVG-CFP in the ER. Next, 1 plate was prepared for microscopy as described above in "Immunohistochemistry and confocal preparation" and 2 plates were transferred to 32°C for 30 min to promote VSVG-CFP trafficking to the Golgi apparatus. Another plate was prepared for microscopy as described above in "Immunohistochemistry and confocal preparation", and 1 plate was incubated at 32°C for an additional 30 min to promote VSVG-CFP trafficking to recycling endosomes. This plate was then prepared for miscroscopy as described above in "Immunohistochemistry and confocal preparation."

Dextran and Transferrin Uptake

Dextran and transferrin uptake assays were performed after 16 hours of transfection or after 1 hour of infection with *Yersinia pseudotuberculosis* strain YP37. For dextran uptake assays, DMEM and Texas red dextran (1mg/ml) + 0.1% Filters BSA was incubated with cells for 3 hours, followed by 3x quick washes with PBS. Cells were then prepared for microscopy. For transferrin (Tfn) uptake assays, cells were incubated with 2 ml SM (serum free media) DMEM at 37°C for 1 hour to remove endogenous transferrin. Cells were then washed 2x with plain DMEM and put on ice for 15 min. Next, cells were incubated with 1 ml cold Internalization Media (SM + 0.1% filter sterilized BSA + Alexa 680-Transferrin (40μg/ml)) on ice for 30 min to allow transferrin to bind to the receptor. Plate was then added to 37°C for 30 min to promote transferrin uptake. Next cells were put on ice and were washed 2x with cold PBS followed by one rapid wash with stripping media (0.2M acetic acid and 0.5M NaCl) to remove receptor bound transferrin. Cells were prepared for microscopy as described above in "Immunohistochemistry and confocal preparation."

Yersinia pseudotuberculosis infection model

YP37 strains with pMMB67HE plasmid were diluted to OD_{600} = 0.3 and induced in LB induction media (25mM NaOx and 20m MgCl2) at RT for 30 min. After the addition of 0.4 mM Isopropyl β-D-1-thiogalactopyranoside (IPTG), cells were incubated at 37°C for 1 hr. Bacteria were then added to HeLa cells at an MOI of 10, and spun down at1000 rpm for 5 min.

Bioinformatics

VPA1380-related sequences were collected using default settings of BLAST [88] against the NR database with the sequence query (GI|28901235|). To identify the closest related structures, we queried the PDB70 database (April 10, 2014) with the same sequence using the HHPRED server [89]. VPA1380-related sequences were aligned to the top identified structure sequences (3fzy A, 3pa8A, and 3ho6A) using PROMALS3D [90], with manual adjustments guided by secondary structure predictions for VPA1380 (JPRED server [91]), HHPRED alignments, and conserved hydrophobicity patterns. The resulting alignment extended the initial HHPRED alignment to include the VPA1380 C-terminus, but is lacking a portion of the N-terminus (starts at residue 116).

Yeast growth assays

Spotting assays were performed as described [86]. Briefly, BY4741 strains were grown overnight in SD media. Yeast were then normalized to OD_{600}=1.0 and 5-fold dilutions were spotted (10µl) on SD agar plates under non-inducing conditions (2% glucose) or inducing conditions (2% galactose and 1% raffinose) with and without 0.5 M NaCl. Production of effector protein was detected with mouse anti-GFP (Clontech) antibody as previously described [86].

Protein purification

VPA1380Δ50 (WT and C/A) were cloned into pET28b vector, containing an N-terminal mannose-binding protein (MBP) and His-tag, and transformed into BL-21 *E. coli*. A single colony was grown to OD_{600}=0.6-0.8 in 2xYT media at 37°C and protein expression was induced with 0.4 mM IPTG for 16 hrs at room temperature. Bacteria were pelleted and resuspended in lysis buffer (20mM Tris pH 7.4, 250mM NaCl, 10mM Imidazole) and lysed by a cell disruptor (Avestin Emulsiflex-C3). Protein was purified using Ni^{2+} beads (Invitrogen), washed 3x with lysis buffer, and eluted with elution buffer (20mM Tris pH 7.4, 250mM NaCl, 250mM Imidazole). Protein was exchanged into buffer (50mM Tris pH7.4, 150mM NaCl) using concentrator column (Amicon).

***In vitro* protease reaction**

Nde1 (1-191) and Ndel1 (1-192) were cloned into pET23a and *in vitro* translated/transcribed (IVT) with TnT Quick Coupled Transcription/Translation System (Promega) in the presence of ^{35}S. Reaction was performed in 25µL volume (20µL Tnt Mix, 1µL ^{35}S, 250ng plasmid DNA and DNAse free water) and incubated in 30°C water bath for 1 hr. From this reaction, 1µL was incubated with 1µg MBP/His-VPA1380 Δ50 protein and 100µM IP6 in 20µL reaction with reaction buffer (20mM Tris pH7.4 and 150mM NaCl) in 30°C water bath for 1 hr. Reaction was stopped by addition of 20µL SDS sample buffer, boiled for 5 min, and run on SDS-PAGE gel. After transfer, membranes were exposed on film.

Table 1. Bacteria and yeast strains

Bacteria strains	**Genotype**	**Reference**
RIMD 2210633	Wild Type *V. parahaemolyticus*	[36]
POR1	RIMD 2210633 Δ*tdhA/S*	[40]
POR2	POR1Δ*tdhA/S* Δ*vcrD1*	[92]
POR3	POR1Δ*tdhA/S* Δ*vcrD2*	[92]
POR4	POR1Δ*tdhA/S* Δ*vcrD1/vcrD2*	[92]
CAB2	POR1Δ*tdhA/S* Δ*exsA*	[73]
CAB3	POR1Δ*tdhA/S* Δ*vtrA*	[73]
CAB4	POR1Δ*tdhA/S* Δ*exsA/vtrA*	[73]
POR1Δ*hns*	POR1Δ*tdhA/S* Δ*hns*	[93]
POR1Δ*lafK*	POR1Δ*tdhA/S* Δ*lafK*	[93]
YP37	Effectorless *Y. pseudotuberculosis*	[94]
YP37 + Vector	pMMB67HE	This study
YP37 + VPA1380	pMMB67HE VPA1380-Flag tag	This study
YP37 + VPA1380 C/A	pMMB67HE VPA1380(C/A)-Flag tag	This study
DH5α	F-*φ80lacZΔM15* Δ(*lacZYA*-argF)U169 *recA1 endA1 hsdR17*(rk-,mk+) *phoA supE44thi-1 gvrA96 relA1λ-*	Invitrogen
BL21	F-*ompT hsdSB*(rB-, mB-) *gal dcm* (DE3)	Novagen

***S. cerevisiae* Yeast strains**	**Genotype**	**Reference**
BY4741	*MATa his3Δ0 leu2Δ0 met15Δ0 ura3Δ0*	Research Genetics
BY4741Δ*ipk1*	Δ*ipk1*	OpenBio-Systems
BY4741Δ*ipk1* + Ipk1	Δ*ipk1* pAML10 Ipk1	This study
Y2HGold	*ATa, trp1-901, leu2-3, 112, ura3-52, his3-200, gal4Δ, gal80Δ, LYS2::GAL1$_{UAS}$–Gal1$_{TATA}$–His3, GAL2$_{UAS}$–Gal2$_{TATA}$–Ade2, URA3::MEL1$_{UAS}$–Mel1$_{TATA}$ AUR1-C MEL1*	Clontech
L40	*MATa his3Δ200 trp1-901 leu2-3112 ade2 LYS::(4lexAop-HIS3) URA3::(8lexAop-LacZ)GAL4*	[95]

Table 2. Plasmids and constructs

Plasmid	Description	Primers	Reference
pBad/Myc-His	*V. parahaemolyticus* expression vector, Kan^r		[73]
pBad/Myc-His VPA1380-CyaA	-1kb of *vpa1380* and *vpa1380* cloned into SacI and PstI, catalytic region of cyaA, cloned into PstI and EcoRI	TC084 TC223 TC442 TC003	This study
pDGFP	Yeast expression vector, gal-promoter, C-terminal GFP and Myc tag, Amp^r, Ura		[63]
pDGFP VPA1380-GFP/Myc	*vpa1380* cloned into XbaI and SacI	TC097 TC215	This study
pDGFP VPA1380 H^{154}A-GFP/Myc	Mutagenesis reaction with pDGFP VPA1380-GFP/Myc	TC353 TC354	This study
pDGFP VPA1380 C^{195}A-GFP/Myc	Mutagenesis reaction with pDGFP VPA1380-GFP/Myc	TC095 TC096	This study
pDGFP VPA1380 K^{148}N-GFP/Myc	Mutagenesis reaction with pDGFP VPA1380-GFP/Myc	TC464 TC465	This study
pDGFP VPA1380 Y^{150}A-GFP/Myc	Mutagenesis reaction with pDGFP VPA1380-GFP/Myc	TC494 TC495	This study
pDGFP VPA1380 R^{191}Q-GFP/Myc	Mutagenesis reaction with pDGFP VPA1380-GFP/Myc	TC496 TC497	This study
pDGFP VPA1380 Y^{253}A-GFP/Myc	Mutagenesis reaction with pDGFP VPA1380-GFP/Myc	TC498 TC499	This study
pDGFP VPA1380 R^{271}Q-GFP/Myc	Mutagenesis reaction with pDGFP VPA1380-GFP/Myc	TC466 TC467	This study
pDGFP VPA1380 R^{283}Q-GFP/Myc	Mutagenesis reaction with pDGFP VPA1380-GFP/Myc	TC470 TC471	This study
pDGFP VPA1380Δ50 GFP/Myc	*vpa1380Δ50* cloned into XbaI and SacI	TC141 TC215	This study
pDGFP VPA1380Δ50 C^{195}A-GFP/Myc	Mutagenesis reaction with pDGFP VPA1380Δ50-GFP/Myc	TC095 TC096	This study
pGBKT7 DNA-BD-VPA1380Δ50	Yeast 2-Hybrid (DNA-BD), *vpa1380* C/A cloned into EcoRI and SalI, Kan^r, Trp	TC106 TC080	This study
pLexAde DNA-BD-VPA1380Δ50 C/A	Yeast 2-Hybrid (DNA-BD), *vpa1380Δ50* C/A cloned into EcoRI and SalI, Amp^r Trp	TC176 TC080	This study
pACT2 AD-Ndel1	Yeast 2-Hybrid (AD), Ndel1 (from screen), Within EcoRI and XhoI, Amp^r, Leu		This study

pACT2 AD-Vps52 (428-724)	Yeast 2-Hybrid (AD), Vps52 (428-724)(from screen), within EcoRI and XhoI, Amp^r, Leu		This study
pVP16 AD-Ndel1 (1-157)	Yeast 2-Hybrid (AD), Ndel1 (1-157), cloned into BamHI and EcoRI, Amp^r, Leu	TC185 TC186	This study
pVP16 AD-Ndel1 (1-99)	Yeast 2-Hybrid (AD), Ndel1 (1-99), cloned into BamHI and EcoRI, Amp^r, Leu	TC185 TC244	This study
pVP16 AD-Ndel1 (33-143)	Yeast 2-Hybrid (AD), Ndel1 (33-143), cloned into BamHI and EcoRI, Amp^r, Leu	TC187 TC188	This study
pVP16 AD-Ndel1 (61-157)	Yeast 2-Hybrid (AD), Ndel1 (61-157), cloned into BamHI and EcoRI, Amp^r, Leu	TC245 TC186	This study
pET28b MBP/His-VPA1380 Δ50	Protein expression, N-terminal MBP/His, *vpa1380Δ50* cloned into BamHI and SalI, Kan^r	TC160 TC080	This study
pET28b MBP/His-VPA1380 Δ50 C/A	Protein expression, N-terminal MBP/His, *vpa1380Δ50 C/A* cloned into BamHI and SalI, Kan^r	TC160 TC080	This study
pET23a His-Nde1 (1-191)	Protein expression (IVT), N-terminal His, *nde1* (1-191) cloned into EcoRI and XhoI, Amp^r	TC193 TC396	This study
pET23a His-Ndel1 (1-192)	Protein expression (IVT), N-terminal His, *ndel1* (1-192) cloned into EcoRI and XhoI, Amp^r	TC195 TC397	This study
pSurf	Eukaryotic expression vector, N-terminal eGFP, C-terminal V5-tag, Amp^r		Gift from Dr. Alto Lab
pSurf eGFP-VPA1380-V5	*vpa1380* cloned into NotI and ApaI, Amp^r	TC349 TC350	This study
pSurf eGFP-VPA1380 (C/A)-V5	*vpa1380 C/A* cloned into NotI and ApaI, Amp^r	TC349 TC350	This study
pSFFV HA-Nde1-Flag	*ha-nde1-flag* cloned into HindIII and NotI	TC411 TC212	This study
pSFFV HA-Ndel1-Flag	*ha-ndel1-flag* cloned into NotI and ApaI	TC412 TC214	This study
pMMB67HE	*Y. pseudotuberculosis* expression vector, IPTG inducible, Amp^r		[77]
pMMB67HE VPA1380-Flag	*vpa1380* cloned into XbaI and EcoRI	TC097 TC083	This study

pMMB67HE VPA1380 C/A-Flag	*vpa1380 C/A* cloned into XbaI and EcoRI	TC097 TC083	This study
pEF-V5-His Vps52-V5/His	Eukaryotic expression vector, C-terminal V5/His tag, Amp^r		Gift from Dr. Bonifacino

Table 3. Primers

Primer Code	Description	RE Site	Sequence
TC003	(R) *cyaA* (with stop codon)	EcoRI	G ATC GAA TTC TTA GCG TTC CAC TGC GCC CAG
TC080	(R) *vpa1380*	SalI	G ATC GTC GAC TTA ATC TAA ATC AGA TTC TAA GG
TC083	(R) *vpa1380-flag*	EcoRI	G ATC GAA TTC TTA CTTGTCATCGTCGTCCTTGTAGTC ATC TAA ATC AGA TTC TAA GG
TC084	(F) -1kb of *vpa1380*	SacI	G ATC GAG CTC GTA AGC TAC TGA CTG GCT G
TC095	(F) VPA1380 $C^{195}A$ mutagenesis		AAAGACATAAGACTTACCTGCGCT AATTCAGCTGATAAAAGAGAA
TC096	(R) VPA1380 $H^{195}A$ mutagenesis		TTCTCTTTTATCAGCTGAATTAGCG CAGGTAAGTCTTATGTCTTT
TC097	(F) *vpa1380*	XbaI	G ATC TCT AGA ATG GTT GTG TGT TTT TTG GCC
TC097	(F) *vpa1380-flag*	XbaI	G ATC TCT AGA ATG GTT GTG TGT TTT TTG GCC
TC106	(F) *vpa1380*	EcoRI	G ATC GAA TTC ATG GTT GTG TGT TTT TTG GCC
TC141	(F) *vpa1380Δ50*	XbaI	G ATC TCT AGA ATG GAA AAA GTC GGG GCA ATT TTA G
TC160	(F) *vpa1380Δ50*	BamHI	A TCG GGA TCC ATG GAA AAA GTC GGG GCA ATT TTA G
TC176	(F) *vpa1380Δ50*	EcoRI	G ATC GAA TTC ATG GAA AAA GTC GGG GCA ATT TTA G
TC185	(F) *ndel1*	BamHI	A TCG GGA TCC CC GCT TTC TTG ATC ATG GAT GG
TC186	(R) *ndel1* (1-157) (with stop)	EcoRI	A TCG GAA TTC TTA CTC GCT TTC TAA GAA TGC ATT TC
TC187	(F) *ndel1* (33-143)	BamHI	A TCG GGA TCC CC GCT CGG GAT GAG CTA GTT G
TC188	(R) *ndel1* (33-143) (with stop)	EcoRI	A TCG GAA TTC TTA TAG CCT TTG TTC AAA GTC TTC C
TC193	(F) *nde1*	EcoRI	A TCG GAA TTC ATG GAG GAC TCG GGA AAG AC
TC195	(F) *ndel1*	EcoRI	A TCG GAA TTC ATG GAT GGT GAA GAT ATA CCG

TC212	(R) *ha-nde1-flag*	NotI	G ATC ATC GCG GCC GC TCA CTTGTCATCGTCGTCCTTGTAGTC GGG AAG GGA TCC TTT ATC GC
TC214	(R) *ha-ndel1-flag*	ApaI	A TCG GGG CCC TCA CTTGTCATCGTCGTCCTTGTAGTC CAC ACT GAG AGG CAG CAT AC
TC215	(R) *vpa1380* (no stop codon)	SacI	A TCG GAG CTC GG ATC TAA ATC AGA TTC TAA GGT AAC
TC223	(R) *vpa1380* (no stop codon)	PstI	A TCG CTG CAG A ATC TAA ATC AGA TTC TAA GGT AAC
TC244	(R) *ndel1* (1-99) (with stop)	EcoRI	A TCG GAA TTC TTA TGA GAC CTG CTT GTA GCT C
TC245	(F) *ndel1* (61-157)	BamHI	A TCG GGA TCC CC GTG TTA GAA GAT GAT TTA AGT C
TC349	(F) *vpa1380*	NotI	G ATC ATC GC GGC CGC ATG GTT GTG TGT TTT TTG GCC
TC350	(R) *vpa1380* (no stop codon)	ApaI	G ATC GGG CCC TC ATC TAA ATC AGA TTC TAA GGT AAC
TC353	(F) VPA1380 $H^{154}A$ mutagenesis		CGTAAAATATATATTACAGGCGCT GGTTCATCAGGAATGCCTTAT
TC354	(R) VPA1380 $H^{154}A$ mutagenesis		ATAAGGCATTCCTGATGAACCAGC GCCTGTAATATATATTTTACG
TC396	(F) *nde1* (1-191)	XhoI	G ATC CTC GAG TCA TGT CCG GGG CTT GTC TTG
TC397	(F) *ndel1* (1-192)	XhoI	G ATC CTC GAG TCA GCG GGT CAC TTC CTG TTG T
TC411	(F) *ha-nde1-flag*	HindIII	A TCG AAG CTT ATG TACCCATACGATGTTCCAGATTACG CT GAG GAC TCG GGA AAG ACC
TC412	(F) *ha-ndel1-flag*	NotI	G ATC ATC GCG GCC GC ATG TACCCATACGATGTTCCAGATTACG CT GAT GGT GAA GAT ATA CCG
TC442	(F) *cyaA*	PstI	G ATC CTG CAG ATG CAG CAA TCG CAT CAG GCT G
TC464	(F) VPA1380 $K^{148}N$ mutagenesis		CAAATTAGAATCTTTTCGTAACATA TATATTACAGGCCATGGT
TC465	(R) VPA1380 $K^{148}N$ mutagenesis		ACCATGGCCTGTAATATATATGTTA CGAAAAGATTCTAATTTG
TC466	(F) VPA1380 $R^{271}Q$ mutagenesis		TGTTGCAGGAATTGTAGAACTTTGC AAATGGGTAAGTGGAAGTTC
TC467	(R) VPA1380 $R^{271}Q$ mutagenesis		TCCTGCAACAGAGACAGTAAACCG TAAATACCTTAGAGTTACC

TC470	(F) VPA1380 $R^{283}Q$ mutagenesis		CTGCAACAGAGACAGTAAAACAGA AATACCTTAGAGTTACCTTAG
TC471	(R) VPA1380 $R^{283}Q$ mutagenesis		CTAAGGTAACTCTAAGGTATTTCTG TTTTACTGTCTCTGTTGCAG
TC494	(F) VPA1380 $Y^{150}A$ mutagenesis		TTAGAATCTTTTCGTAAAATAGCTA TTACAGGCCATGGTTCATC
TC495	(R) VPA1380 $Y^{150}A$ mutagenesis		GATGAACCATGGCCTGTAATAGCT ATTTTACGAAAAGATTCTAA
TC496	(F) VPA1380 $R^{191}Q$ mutagenesis		TTAGATAATATTAAAGACATACAA CTTACCTGCTGTAATTCAGC
TC497	(R) VPA1380 $R^{191}Q$ mutagenesis		GCTGAATTACAGCAGGTAAGTTGT ATGTCTTTAATATTATCTAA
TC498	(F) VPA1380 $Y^{253}A$ mutagenesis		ACAGATGTGCGAATTACAGGTGCC CATGGAAAAGGCGTTTTCTA
TC499	(R) VPA1380 $Y^{253}A$ mutagenesis		TAGAAAACGCCTTTTCCATGGGCA CCTGTAATTCGCACATCTGT

CHAPTER THREE
Structural and regulatory mutations in *Vibrio parahaemolyticus* type III secretion systems display variable effects on virulence

Introduction

Virulent strains of the Gram-negative halophilic bacterium, *V. parahaemolyticus*, are emerging in coastal regions throughout the world [5]. *V. parahaemolyticus* thrives in warm brackish waters, and is one of the leading causes of seafood-derived food poisoning due to the consumption of raw or undercooked shellfish. Infection of this pathogen can lead to acute gastroenteritis and even septicemia [37]. Additionally, strains of *V. parahaemolyticus* have recently been associated with lethal infection of shrimp, resulting in the devastation of shrimp farms [8]. The global dissemination of *V. parahaemolyticus*, which is linked to rising water temperatures, underscores the need for better understanding of the bacterium's virulence traits [96].

Principle to the pathogenicity of *V. parahaemolyticus* are thermostable direct hemolysins (TdhA/S) and two type III secretion systems (T3SS1 and T3SS2) [37]. The T3SSs form a needle-like apparatus to translocate effector proteins directly into the host cytoplasm to manipulate host cell machinery **(Figure 7A)**. T3SS1 contains several effectors that systematically kill host cells by causing autophagy, membrane blebbing, cell-rounding, and finally lysis [58-61]. T3SS2 is necessary for the enterotoxicity seen in a rabbit ileal loop model, and piglet and infant rabbit models [41,42,59,71]. Effectors from T3SS2 promote bacterial invasion, inactivation of the host immune pathway, and disruption of the gut epithelial barrier [41,42,73,78].

The two T3SSs of *V. parahaemolyticus* are regulated by separate transcriptional networks. Low calcium levels induce T3SS1 gene expression, which is regulated by the ExsACDE cascade **(Figure 7B)** [54]. ExsA is an AraC family transcription factor that binds to the promoter region of T3SS1 genes to promote their expression [53]. DMEM with low calcium is often used to prime bacteria for T3SS1-mediated infection [58]. T3SS2 genes are induced by bile salts through activation of the transcription factors VtrA and VtrB **(Figure 7C)** [46]. Both of these transcription factors are positive regulators that work in a sequential fashion to promote expression of T3SS2 genes [70].

Mutations in these transcriptional networks can have unexpected consequences that must be evaluated for proper interpretation of experimental results. For example, ExsA and VtrA have been shown by microarray and RNAseq analysis to affect gene expression outside the pathogenicity island of T3SS1 and T3SS2 [21,46,70,83]. In this study we compare the different virulence-related aspects of strains with a mutation in a T3SS transcriptional regulator gene as opposed to a mutation in a T3SS structural gene. We examine effector production and secretion, swarming, biofilm formation, cytotoxicity, and invasion. From our experiments, we found that biofilm growth is inversely regulated with T3SS2 and that a T3SS2 regulatory mutant invades host cells with an efficacy over 10 fold higher than that of a T3SS2 structural mutant in the needle apparatus. Analysis of these traits helps to elucidate the phenotypic differences between the T3SS mutant strains and highlights the impact of a regulatory versus structural manipulation of T3SSs on the overall virulence ability of *V. parahaemolyticus*.

Results

Creating regulatory and structural T3SS mutant strains

Two sets of strains, PORs and CABs, were created with mutations in either a T3SS needle apparatus component or a transcriptional regulator, respectively **(Table 4)**. These strains are derived from the POR1 strain, which was originally derived from the virulent O3:K6 serotype RimD 2210633 by deleting the *tdhA/S* toxins [92]. Therefore, the POR and CAB strains carry mutations in two toxin genes, *tdhA* and *tdhS*, to eliminate the toxic effects of these hemolysins on host cells [41]. POR2 (POR1Δ*vcrD1*) and POR3 (POR1Δ*vcrD2*) contain a deletion in a gene that encodes the inner membrane ring of the needle apparatus belonging to either T3SS1 or T3SS2, respectively **(Figure 7A)**. POR4 contains mutations in both T3SS1 and T3SS2 needles, and therefore lacks the ability to secrete all T3SS effector proteins. Importantly, all the POR strains are capable of producing effectors from both systems, but cannot secrete effectors through the crippled system [37]. In contrast, the CAB strains contain mutations that disrupt gene expression. CAB2(POR1Δ*exsA*) and CAB3(POR1Δ*vtrA*) contain a deletion of a master regulator responsible for controlling expression of either T3SS1 or T3SS2, respectively **(Figure 7B and 7C)**. CAB4 contains both deletions, and is entirely deficient in T3SS1 and T3SS2 gene expression [73].

Table 4. Effector production and secretion from POR and CAB strains.

	Produce T3SS1 Effectors	Secrete T3SS1 Effectors	Produce T3SS2 Effectors	Secrete T3SS2 Effectors
POR1	+	+	+	+
POR2	+	-	+	+
POR3	+	+	+	-
POR4	+	-	+	-
CAB2	-	-	+	+
CAB3	+	+	-	-
CAB4	-	-	-	-

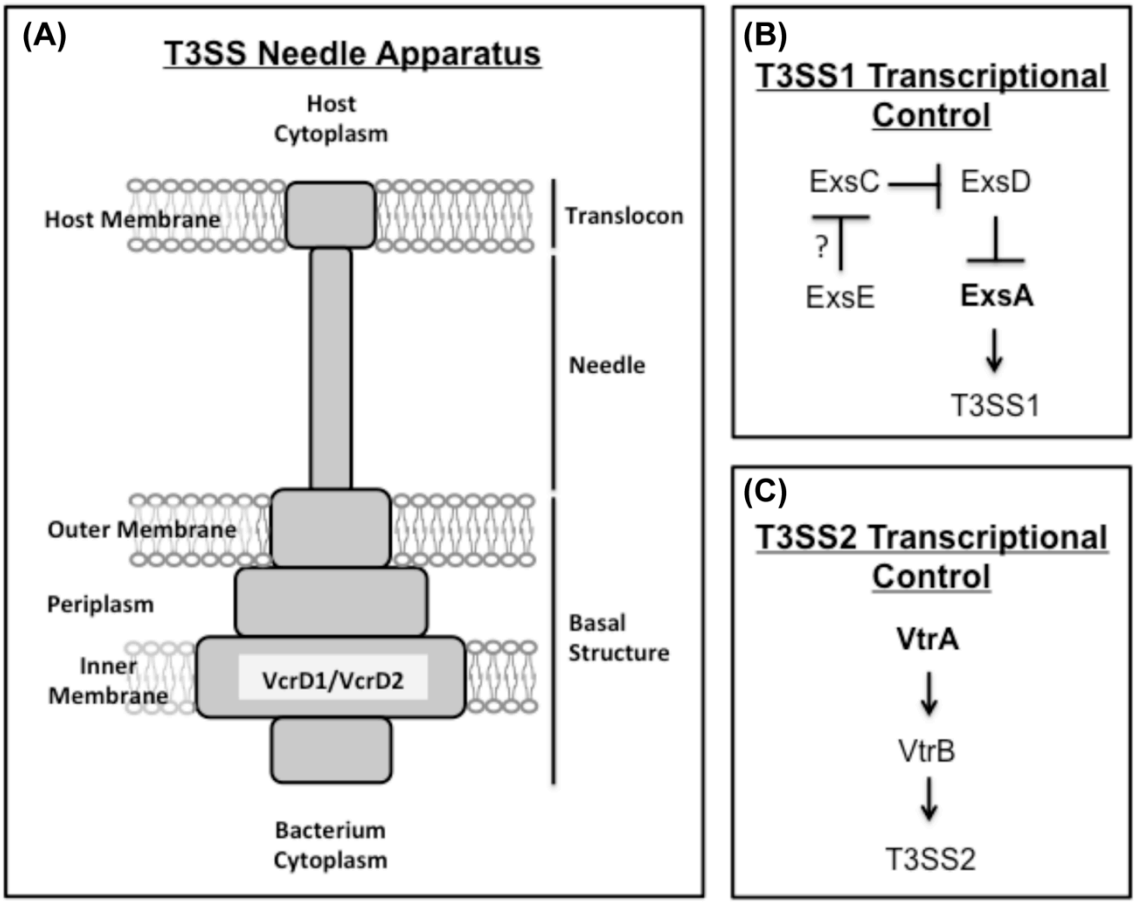

Figure 7. Schematic of T3SS needle apparatus and the transcriptional networks controlling T3SS1 and T3SS2 gene expression. (A) The T3SS is composed of a needle that spans the inner and outer membranes of the bacterium, and injects effector proteins directly into the host cytoplasm. The POR strains contain mutations in the vcrD1 and vcrD2 genes that are an essential component of the inner membrane ring of the needle's basal structure in T3SS1 and T3SS2, respectively. **(B)** T3SS1 gene expression is controlled by the ExsACDE cascade. The exsA gene was removed in the CAB2 strain to prevent induction of T3SS1 genes. **(C)** T3SS2 gene expression is controlled by the sequential activation of the transcriptional regulators VtrA and VtrB. The vtrA gene was removed in the CAB3 strain to prevent induction of T3SS2 genes.

To assess differences in virulence traits of mutant strains lacking a T3SS needle apparatus component or transcriptional regulator, we compared the virulence phenotypes of the POR and CAB strains. Importantly, the T3SS mutations did not affect the bacteria's growth rate **(Figure 8)** and, therefore, the differences seen in this study are independent of this factor. Additionally, since we used POR1 as the parental strain in this study, instead of RIMD 2210633, we examined if POR1 and RIMD 2210633 exhibit similar levels of growth, swarming, and biofilm production. From these assays, POR1 and RIMD 2210633 behaved similarly **(Figure 9)**, which suggests POR1 that is deleted for the hemolysins can be used as the parental strain. In these experiments, the negative control *lafk* and *hns* mutant strains are known to be deficient in swarming gene expression and biofilm production, respectively [29,97].

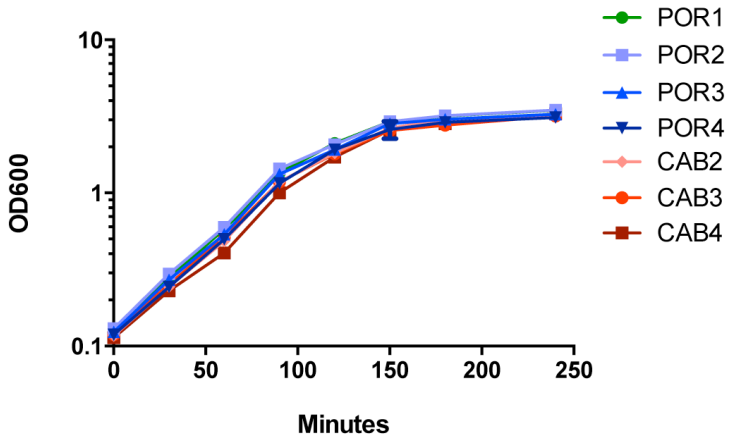

Figure 8. POR and CAB strains grow at similar rates. Growth of bacteria in MLB media at 30°C. Bacteria were quantified by measuring the OD600 of each sample every 30 minutes.

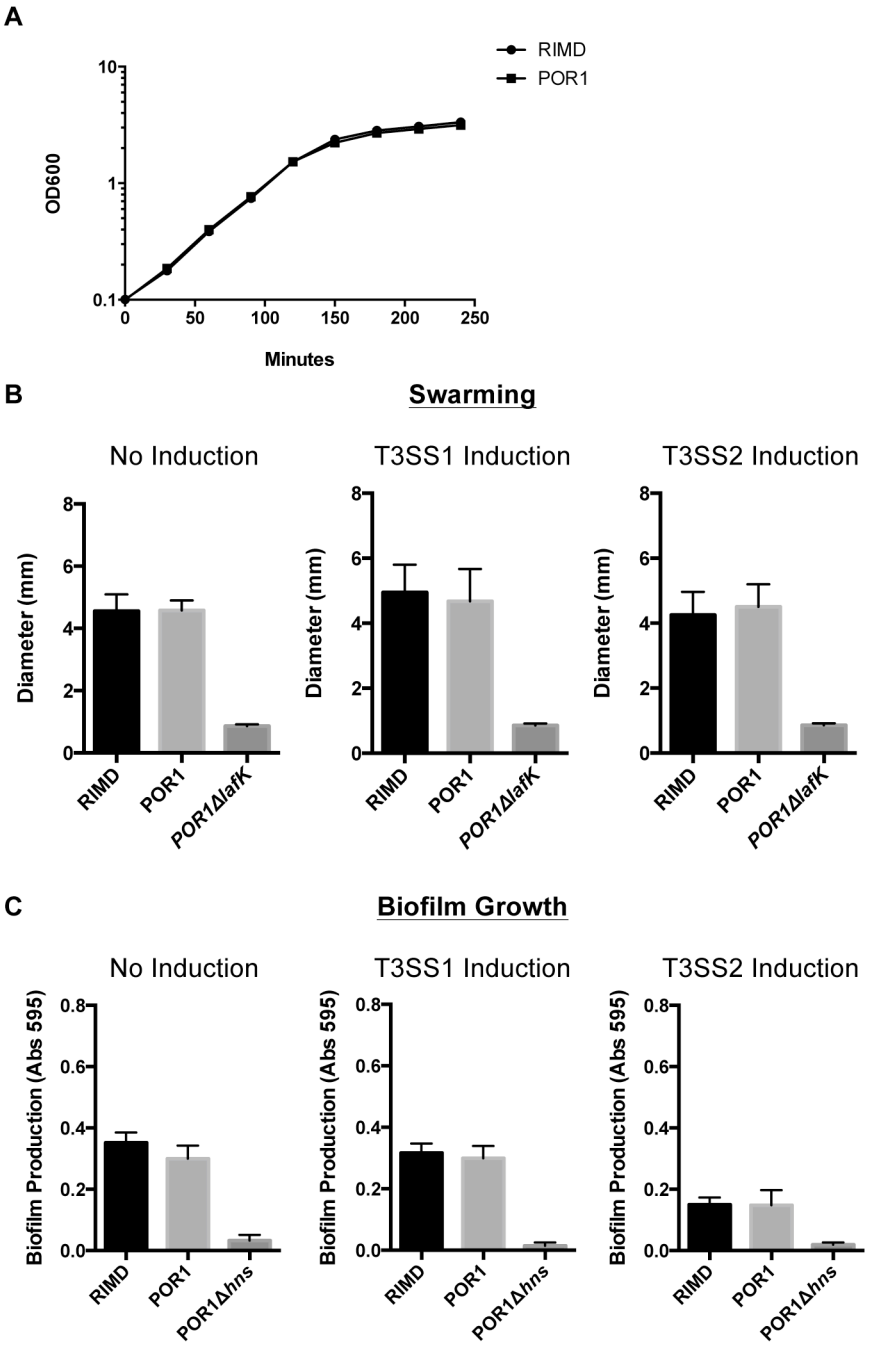

Figure 9. POR1 and RIMD 2210633 show similar levels of growth, swarming, and biofilm production. (A) Growth of bacteria in MLB media at 30°C. Bacteria were quantified by measuring the OD600 of each sample every 30 minutes. **(B)** Swarming diameter of bacteria pre-incubated in not inducing (MLB) media, T3SS1 inducing (DMEM) media, and T3SS2 inducing (MLB with 0.05% bile salts) media, and spotted on HI swarm plates (n=4). **(C)** Levels of biofilm growth from bacteria grown statically in non-inducing (MLB) media,

T3SS1 inducing (DMEM) media, and T3SS2 inducing (MLB + 0.05% bile salts) media. Resulting biomass was stained with 0.1% crystal violet and measured at absorbance 595nm (n=8).

POR and CAB strains express and secrete effectors at a similar level

Next, we examined if POR and CAB strains produce and secrete similar levels of effector proteins. To test this, we induced each T3SS for 3 hours and detected effector levels in bacterial lysates and culture supernatants. When T3SS1 was induced, the T3SS1 effectors VopQ and VopS were produced and secreted at similar levels between POR and CAB strains **(Figure 10A)**. Interestingly, there was a difference in effector production within POR strains, which supports the hypothesis that T3SS1 needle construction is necessary for optimal effector production. Additionally, when T3SS2 was induced, the T3SS2 effectors VopA and VopL were produced and secreted at similar levels in all strains **(Figure 10B)**. In contrast to T3SS1, no decrease in effector production was observed in the POR strains with a structural mutation in the T3SS2. Overall, mutational differences in each T3SS have no effect on the relative amount of effector proteins secreted by either T3SS1 or T3SS2.

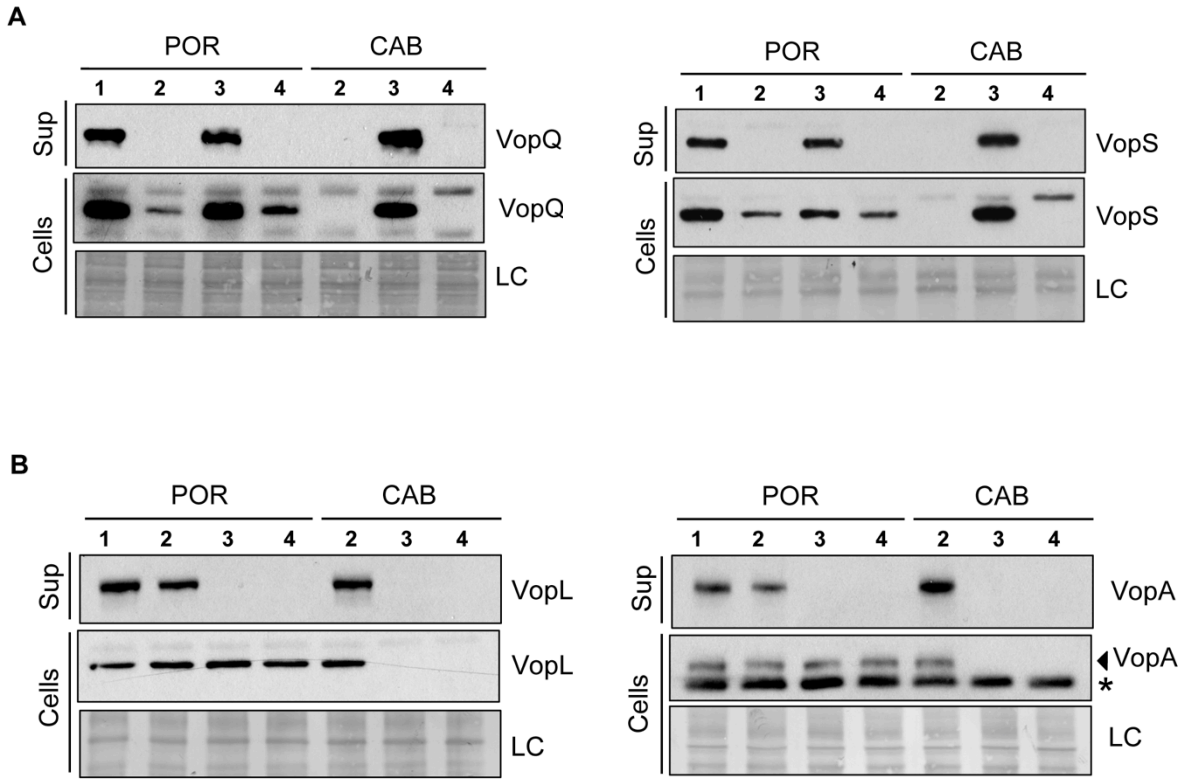

Figure 10. T3SS1 and T3SS2 effectors are produced and secreted at similar levels by POR and CAB strains. (A) Secretion of T3SS1 effectors, VopQ and VopS, from T3SS1-induced strains grown in DMEM for 3 hours at 37°C. **(B)** Secretion of T3SS2 effectors, VopA and VopL, from T3SS2-induced strains grown in MLB with 0.05% bile salts for 3 hours at 37°C. Protein from bacterial lysate or TCA-precipitated media detected by western blot analysis using anti-VopQ, anti-VopS, anti-VopA, and anti-VopL antibodies. (*) Non-specific band recognized by antibody.

Swarming is similar for POR and CAB strains

Lateral flagella are produced by *V.* parahaemolyticus to transport the bacterium through viscous environments and along surfaces [98]. Swarming is important during infection and is similarly co-regulated with T3SS1 genes by surface contact, quorum sensing, and levels of calcium and iron [21,29,99]. We tested the swarming abilities of POR and CAB strains on HI swarming agar for 24 hours, and found no differences in migration **(Figure 11A)**. As a negative control, we mutated the gene *lafK* encoding an essential regulator of swarming genes [97]. We then induced T3SS1 and T3SS2 prior to spotting the bacteria on the swarming agar. Again, no difference was observed in bacterial migration upon T3SS1 induction **(Figure 11B)** or T3SS2 induction **(Figure 11C)**, supporting the proposal that the mutations within the POR and CAB strains have no effect on the regulation of swarming.

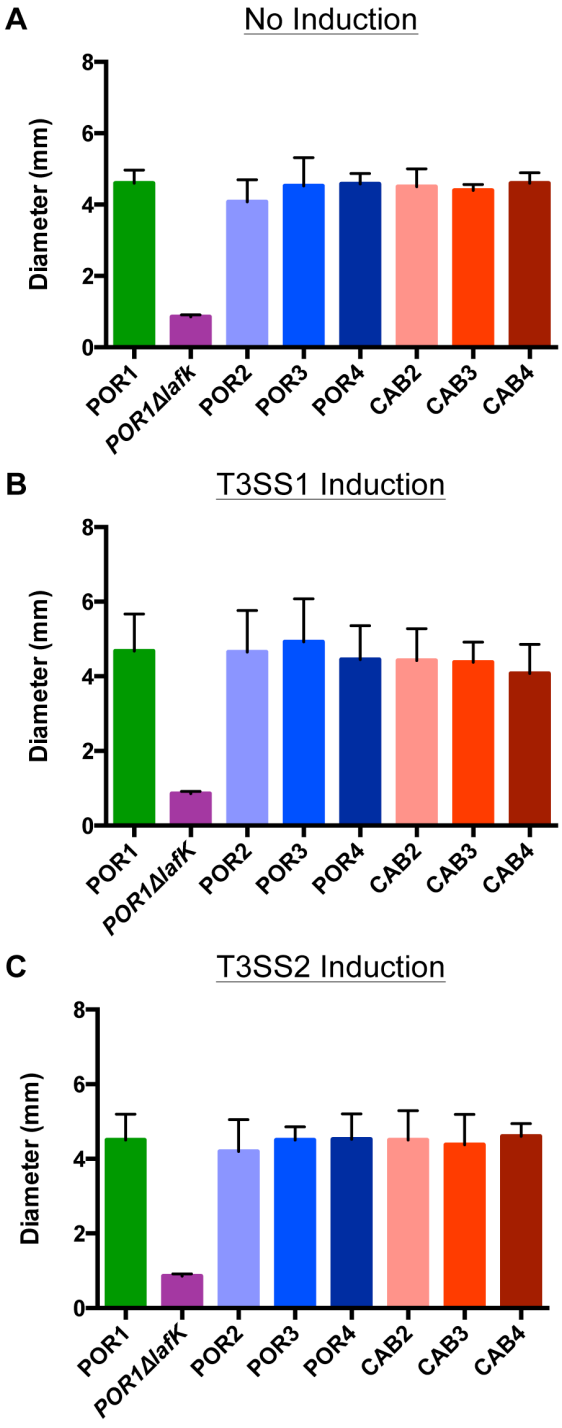

Figure 11. POR and CAB strains exhibit similar levels of swarming. Swarming diameter of POR and CAB strains pre-incubated in **(A)** not inducing (MLB) media, **(B)** T3SS1 inducing (DMEM) media, and **(C)** T3SS2 inducing (MLB with 0.05% bile salts) media, and spotted on HI swarm plates. (n=4)

Variable biofilm production observed with bile salts

Biofilm production is important for bacteria survival in different environments and shares an inverse relationship with swarming and T3SS1 gene induction in *V. parahaemolyticus* [29,33,100]. To assess biofilm production, we grew the POR and CAB strains statically in microtiter plates for 24 hours and stained the resulting biomass with crystal violet. A mutant lacking the *hns* gene served as a negative control in this assay, since this strain does not exhibit biofilm growth [29]. Growing the bacteria in non-inducing or T3SS1-inducing conditions caused no variation in biofilm production between POR and CAB strains **(Figure 12A and 12B)**. However, when grown in T3SS2 inducing conditions, CAB3 and CAB4 produced almost 2 fold higher amounts of biomass when compared to the POR strains or CAB2 strain **(Figure 12C)**, which also produced less biomass than non-induced strains **(Figure 12A)**. Since biofilm production is optimal when T3SS2 proteins are not expressed, these experiments support the idea that biofilm production is inversely regulated with T3SS2 gene expression.

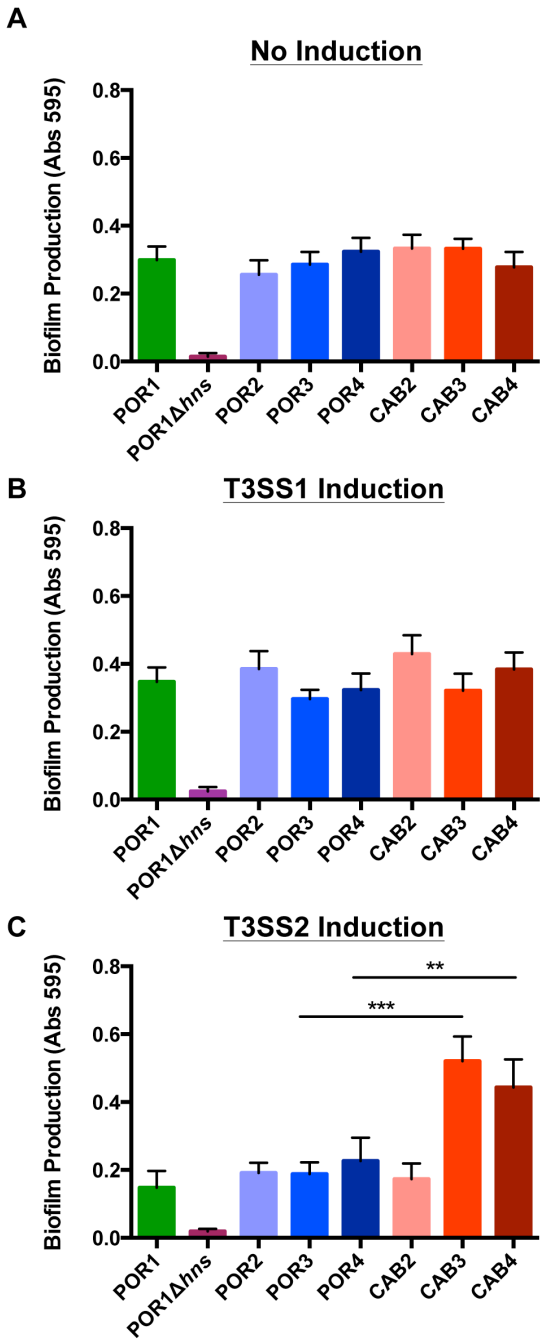

Figure 12. Bile salts reduce biofilm formation through VtrA. Levels of biofilm growth from strains grown statically in **(A)** non-inducing (MLB) media, **(B)** T3SS1 inducing (DMEM) media, and **(C)** T3SS2 inducing (MLB + 0.05% bile salts) media. Resulting biomass was stained with 0.1% crystal violet and measured at absorbance 595nm. (n=8) Asterisks indicate statistical significant differences using two-tailed t-test (** $p < 0.005$, *** $p < 0.0005$).

Cytotoxicity is similar between POR and CAB strains under T3SS1 inducing conditions.

We next assessed whether the POR3 and CAB3 strains exhibit different levels of T3SS1-dependent cytotoxicity towards HeLa cells. After pre-inducing T3SS1, we infected HeLa cells and measured LDH release every 30 minutes. Both POR3 and CAB3 caused host cell lysis within 2 hours at a similar rate similar to that of the POR1 parental strain. As expected, POR4 and CAB4 were not cytotoxic **(Figure 13)**. In addition to cell lysis, we examined the ability of POR3 and CAB3 to cause T3SS1-dependent cell rounding, which is a well-documented phenotype resulting from VopS-mediated actin cytoskeleton collapse [58,61]. In accordance with the LDH release assay, POR3 and CAB3 caused rounding at a rate similar to that of the POR1 parental strain. The negative control strains, POR4 and CAB4, did not cause any noticeable alteration in the actin cytoskeleton **(Figure 14)**. These results show that POR and CAB strains exhibit comparable levels of cytotoxicity with T3SS1 induction and are consistent with the similar levels of effector secretion **(Figure 10)**.

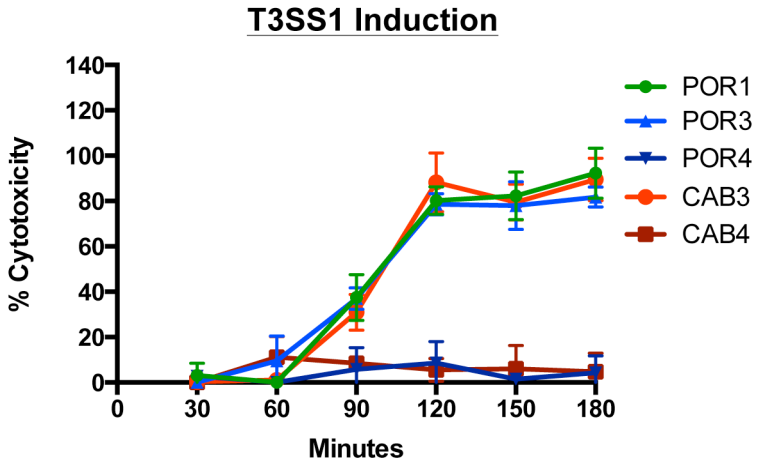

Figure 13. POR3 and CAB3 exhibit similar rates of cytotoxicity with T3SS1 induction. Cytotoxicity of HeLa cells infected with POR and CAB strains pre-induced in T3SS1 inducing (DMEM) media. Cytotoxicity measured by LDH release with detection kit.

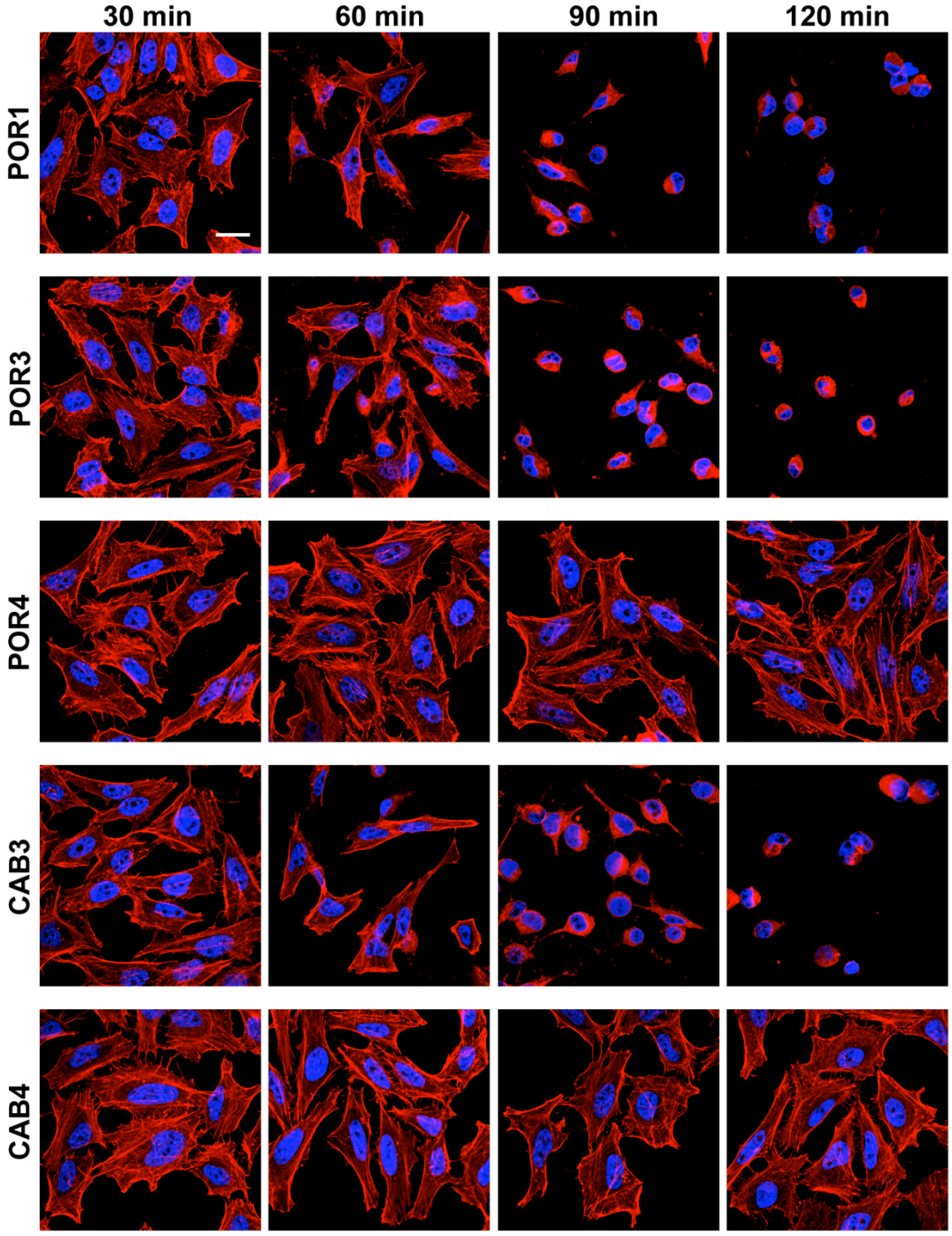

Figure 14. POR2 and CAB2 cause similar rates of actin rearrangement in HeLa cells. Confocal images of HeLa cells incubated with POR and CAB strains pre-induced in T3SS1 inducing (DMEM) media. The HeLa nuclei were stained with Hoescht and the actin cytoskeleton was stained with Rhodamine-phalloidin. Scale bar represents 100μm.

Cytotoxicity is similar between POR and CAB strains under T3SS1 inducting conditions.

We next examined the cytotoxicity rates of POR2 and CAB2 upon T3SS2 induction. POR1 was omitted from these experiments since this strain contains an active T3SS1, which is epistatic to T3SS2 in regards to cytotoxicity. After pre-inducing T3SS2, we infected HeLa cells with relevant POR and CAB strains and measured LDH release every hour. We found that POR2 and CAB2 caused 100% cytotoxicity at a similar rate within 4 hours. POR4 and CAB4 started causing detectable lysis at 6 hours **(Figure 15)**, but this was likely due to overgrowth of the bacteria (data not shown).

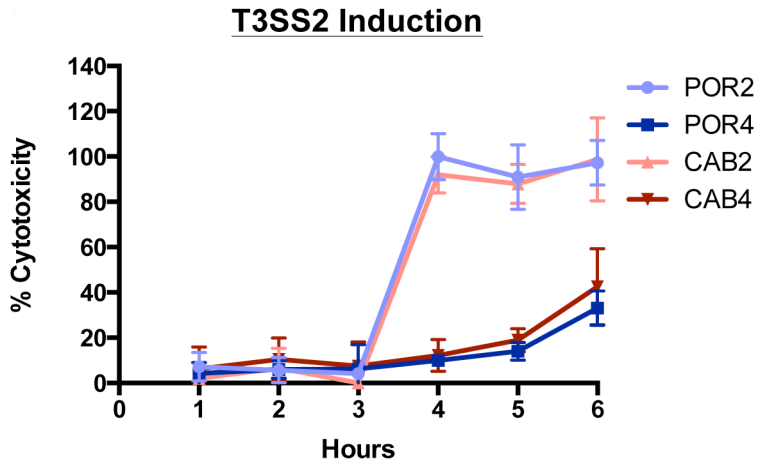

Figure 15. POR2 and CAB2 exhibit similar rates of cytotoxicity with T3SS2 induction. Cytotoxicity of HeLa cells infected with POR and CAB strains pre-induced in T3SS2 inducing (MLB + 0.05% Bile Salts) media. Cytotoxicity measured by LDH release with detection kit.

POR and CAB strains differ in T3SS2-mediated invasion efficiency.

Recently, it was shown that *V. parahaemolyticus* invades host cells in a T3SS2-dependent manner [73]. Therefore, we tested the ability of POR2 and CAB2 strains to invade HeLa cells over the course of an infection. Prior to the first time point, the HeLa cells were incubated with T3SS2-induced bacteria for 2 hours and then inoculated with gentamicin. This antibiotic is non-permeable to host cell membranes and will only kill extracellular bacteria [73]. At each time point after gentamicin addition, bacteria were recovered. CAB2 exhibited over 10-fold higher levels of invasion compared to the POR2 strain, and this difference was maintained throughout the course of the infection. The negative control strains, POR4 and CAB4, exhibited very low levels of invasion **(Figure 16)**.

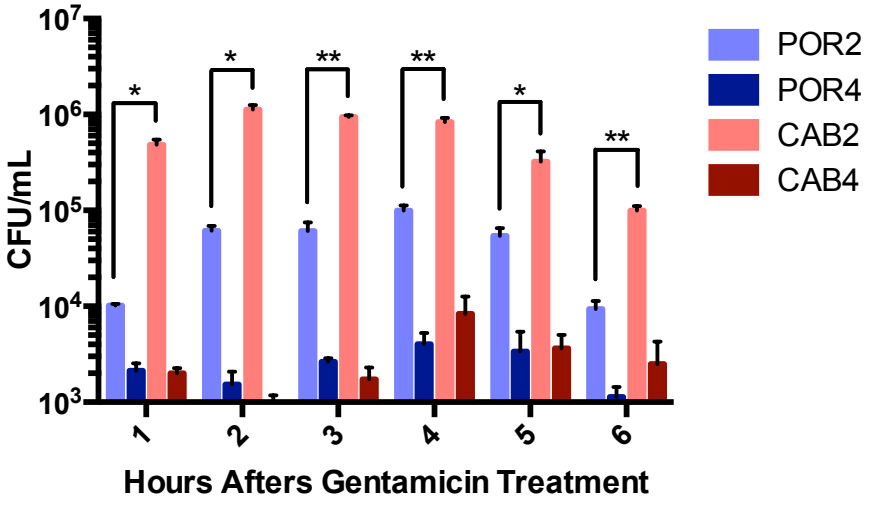

Figure 16. CAB2 is more invasive than POR2. HeLa cell invasion with POR and CAB strains. Cells were incubated with bacteria 2 hours prior to inoculation with 100 µg/ml gentamicin to kill extracellular bacteria. Asterisks indicate statistical significant differences using two-tailed t-test (* $p < 0.05$, ** $p < 0.005$).

Discussion

In this study, we investigated the virulence differences between structural and regulatory mutants of the *V. parahaemolyticus* T3SSs. Previous studies of *V. parahaemolyticus* reported that swarming and T3SS1 gene expression are both induced by similar stimuli but the mechanistic relationship between swarming and T3SS1 gene activation is unknown [21,29,99]. Additionally, one study found that overexpressing *exsA* down-regulates swarming genes and inhibits the swarming phenotype on heart infusion swarm plates. These results suggest the two systems might operate in a negative feedback loop [99]. Yet, despite this connection, we found no variation in swarming between the T3SS mutants under a variety of induction conditions. One possibility for this discrepancy is that swarming gene regulation could be strain dependent since prior studies were mostly performed with environmental strains and this study was performed with strains derived from a clinical isolate. Additionally, studies have shown that biofilm production is inversely regulated with swarming and T3SS1 induction [35,101]. While we did not find a difference in biofilm growth during T3SS1 induction, we found that T3SS2 regulatory mutants could produce larger biofilms than other mutants during T3SS2 induction. Furthermore, these other strains produced less biofilm mass than similar strains in non-induced conditions. From these observations, there appears to be no link between the regulation of swarming and T3SS1 or T3SS2 induction, but biofilm formation appears to be down-regulated in at VtrA-dependent manner under T3SS2 inducing conditions. This inverse relation between biofilm formation and T3SS2 provides insight on the phenotypic traits of T3SS2-induced bacteria, but requires

further experimentation to better understand the relationship between these two virulence systems.

One interesting observation from this study was that POR1 and POR3, in which T3SS1 is active, exhibited higher levels of effector production than POR2 and POR4, in which T3SS1 is inactive, during T3SS1 induction. This result would support the hypothesis that a factor dependent on a functional needle apparatus alters the expression levels of T3SS1 genes. ExsE, a negative regulator of this system, is likely the factor responsible since it is secreted from the bacterium during induction of T3SS1 [54]. Therefore, the repressive role of ExsE is likely maintained in POR2 and POR4 strains as ExsE is accumulating inside the cell, and this could explain the low levels of T3SS1 effector production in these strains.

From the tissue culture infection data, POR3 and CAB3 caused cell rounding and host cell lysis at a similar rate. These strains cause actin cytoskeleton rearrangement by the T3SS1 effector VopS, an AMPylator of Rho family GTPases [61]. The lack of differences suggests the T3SS structural and regulatory mutations have no effect on T3SS1 dependent infection, but there may exist further differences that are more subtle and hard to distinguish during the 2-hour infection process.

Similarly, POR2 and CAB2 strains caused lysis of HeLa cells at the same rate in a T3SS2-dependent manner, but a striking result was observed when both strains were tested for invasion efficiency. CAB2 invaded HeLa cells with an efficacy over 10 fold higher than that of POR2. The T3SS2 effector, VopC, mediates invasion by constitutively activating Rac and CDC42 through deamidation [73,102]. However, POR2 and CAB2 appear to produce and secrete similar levels of effector proteins, which suggest the increased invasiveness is not

due to higher production levels of effector proteins. The possibility exists that CAB2 may replicate intracellularly faster than the POR2 strain. This hyperproliferative state has been observed for other bacterial pathogens [103].

In this study, we demonstrate that certain virulence traits differ between structural and regulatory T3SS mutants in *V. parahaemolyticus*. The importance of performing multiple assays to illuminate strain variation is exemplified in this study by our analysis of the differences observed with strains harboring a mutation in a structural component of the T3SS needle or a regulatory factor for expression of T3SS genes. This point is demonstrated clearly by observing phenotypes of strains containing mutations in *V. parahaemolyticus* T3SS2. While POR2 and CAB2 did not differ in cytotoxic ability, they differed greatly in invasion efficiency. Therefore, differences do exist between strains harboring structural or regulatory mutations, and these differences are only found by examining multiple aspects of infection. Future studies on the expression profiles of these various strains will help to elucidate candidate genes and their involvement during infection.

CHAPTER FOUR

Vibrio type III effector VPA1380 is related to the cysteine protease domain of large bacterial toxins

Introduction

Vibrio parahaemolyticus is a Gram-negative bacterium and one of the major etiological agents of acute gastroenteritis derived from eating raw or undercooked shellfish [37]. Disease symptoms include abdominal cramps, headache, nausea, vomiting, and mild to severe diarrhea [104]. If exposed to open wounds, the bacterium can cause wound infections and even septicemia [105]. In recent decades, *V. parahaemolyticus* has emerged as an important pathogen due to its dissemination to coastal regions throughout the world [5]. The bacterium's preference for warm temperatures and the rising of global water temperatures appear to be aiding with its spread [7].

The genome sequence of the *V. parahaemolyticus* RIMD 2210633 clinical isolate revealed several virulence factors in pathogenicity islands [36]. These pathogenicity islands include two type III secretion systems (T3SS), T3SS1 and T3SS2 [92], and two type VI secretion systems (T6SS), T6SS1 and T6SS2 [106]. Also within the T3SS2 pathogenicity island, are genes for two thermodirect-hemolysin (*tdh*) toxins. Importantly, the *V. parahaemolyticus* T3SS2 is induced by bile salts [46] and was shown to be required for intestinal colonization and enterotoxicity, as shown in several infection model organisms [42,71,78,92], albeit septicemia has yet to be observed in an animal model. In culture systems, the T3SS2 system was shown to mediate invasion [73]. The T3SS is a needle-like apparatus that delivers bacterial effector proteins into the host cell cytoplasm. Once inside the host cell, effector proteins target different host machinery to manipulate the immune

response and to promote a niche outside or within the host cell [48]. Six T3SS2 effector proteins have been identified and characterized to-date. VopA and VopZ both target cellular immunity by inhibiting different components of the MAPK pathway [76,78]. VopT ADP-ribosylates Ras, and the three other effectors, VopC, VopL, and VopV, alter actin dynamics [73,79,81]. Notably, VopC constitutively activates Cdc42 through a deamidation reaction to promote invasion of the bacterium into non-phagocytic cells [73,102]. This data suggests bacterial invasion may play a role during infection.

Previous work on T3SS2 in *V. parahaemolyticus* identified the protein VPA1380 as a T3SS2-dependent secreted protein [81]. In this work, we set out to determine whether VPA1380 is a T3SS2 effector and characterize its activity. To this end, we confirmed that VPA1380 is translocated into host cells by T3SS2. Bioinformatic analyses revealed that VPA1380 is similar to cysteine protease domains (CPDs) from several large bacterial toxins. Using yeast as a heterologous model, we found that VPA1380's toxicity is abolished when the putative catalytic residues of the protease domain are mutated. Furthermore, we show that like other CPDs found in bacterial toxins, VPA1380 requires IP6 as an activator. A yeast 2-hybrid screen was performed to identify a eukaryotic target and vesicle trafficking studies were performed which shows VPA1380 may alter vesicle trafficking. Thus our results suggest that VPA1380 is a T3SS2 effector with an IP6-dependent catalytic activity that is required for its effects on vesicle trafficking.

Results

VPA1380 is a T3SS2 Effector

While examining the genes within the T3SS2 pathogenicity island (*vpa1310-vpa1396*) we identified *vpa1380* as a putative T3SS2 effector. The *vpa1380* gene encodes for a 295 amino acid protein, which is homologous to the partially characterized OspB effector from *Shigella flexneri* (32% identity and 50% similarity) **(Figure 17)** [84,85].

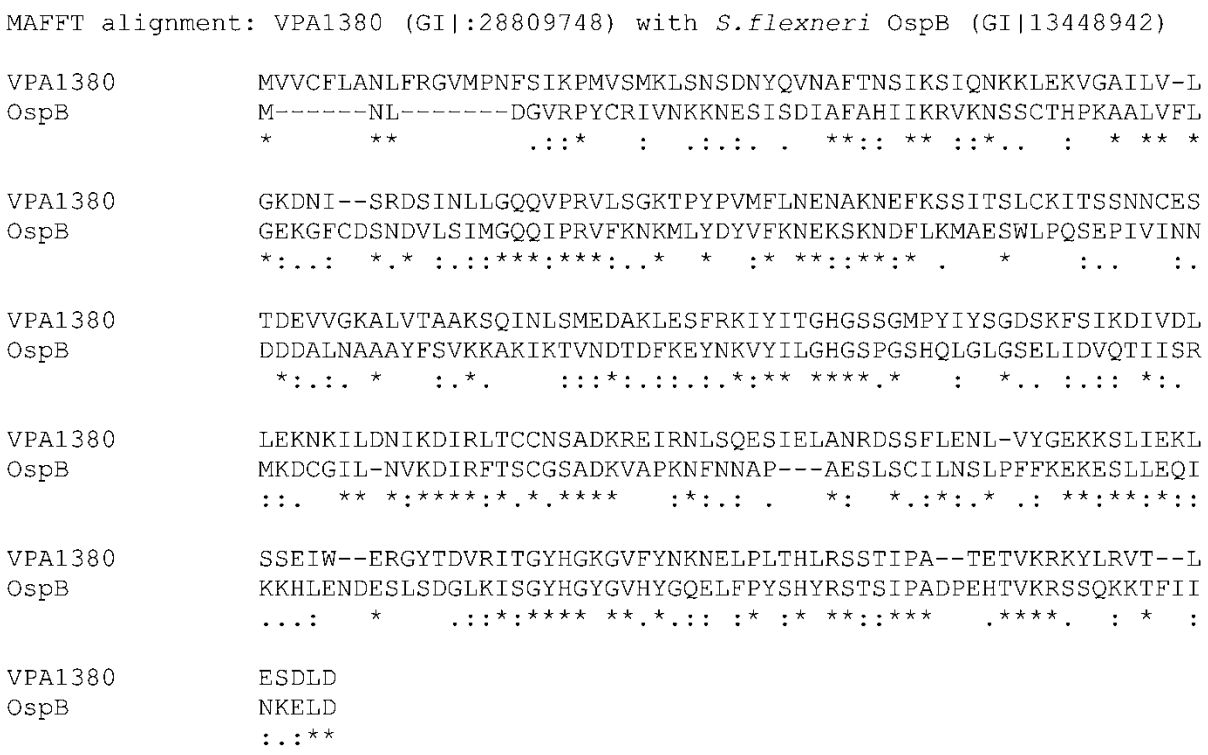

Figure 17. VPA1380 is homologous to OspB from *Shigella flexneri* Sequence homology of VPA1380 and *Shigella flexneri* effector OspB. The (*) represents identical amino acids, (:) represents conservative substitutions, and (.) represents semiconservative substitutions.

Recently, VPA1380 was shown to be secreted from *V. parahaemolyticus* via the T3SS2 [81]. To confirm VPA1380 is secreted from T3SS2, we transformed *V. parahaemolyticus* strains with a plasmid containing *vpa1380* fused to the catalytic region of the *cyaA* gene with *vpa1380's* endogenous promoter. The POR1 strain contains a functional T3SS1 and T3SS2, while the POR2 and POR3 strains harbor a mutation in the needle apparatus of T3SS1 and T3SS2, respectively **(Table 4)** [40]. Upon induction of T3SS2 with bile salts [46], we found VPA1380-CyaA was produced in all tested strains but only secreted from POR1 and POR2 strains that contain an active T3SS2 and not from the POR3 strain that contains an inactive T3SS2 **(Table 4 Figure 18A)**. These results confirm that VPA1380 is secreted through the T3SS2.

To determine if VPA1380 is *a bona fide* T3SS2 effector, we next determined whether VPA1380 is translocated into eukaryotic host cells in a T3SS2-dependent manner using the CyaA reporter system. *V. parahaemolyticus* strains expressing the VPA1380-CyaA fusion were used to infect HeLa cells, and production of cAMP was monitored. HeLa cells infected with POR1 and POR2 exhibited significantly higher levels of cAMP than cells infected with POR3 **(Figure 18B)**. Taken together, these results confirmed that VPA1380 is indeed a translocated T3SS2 effector.

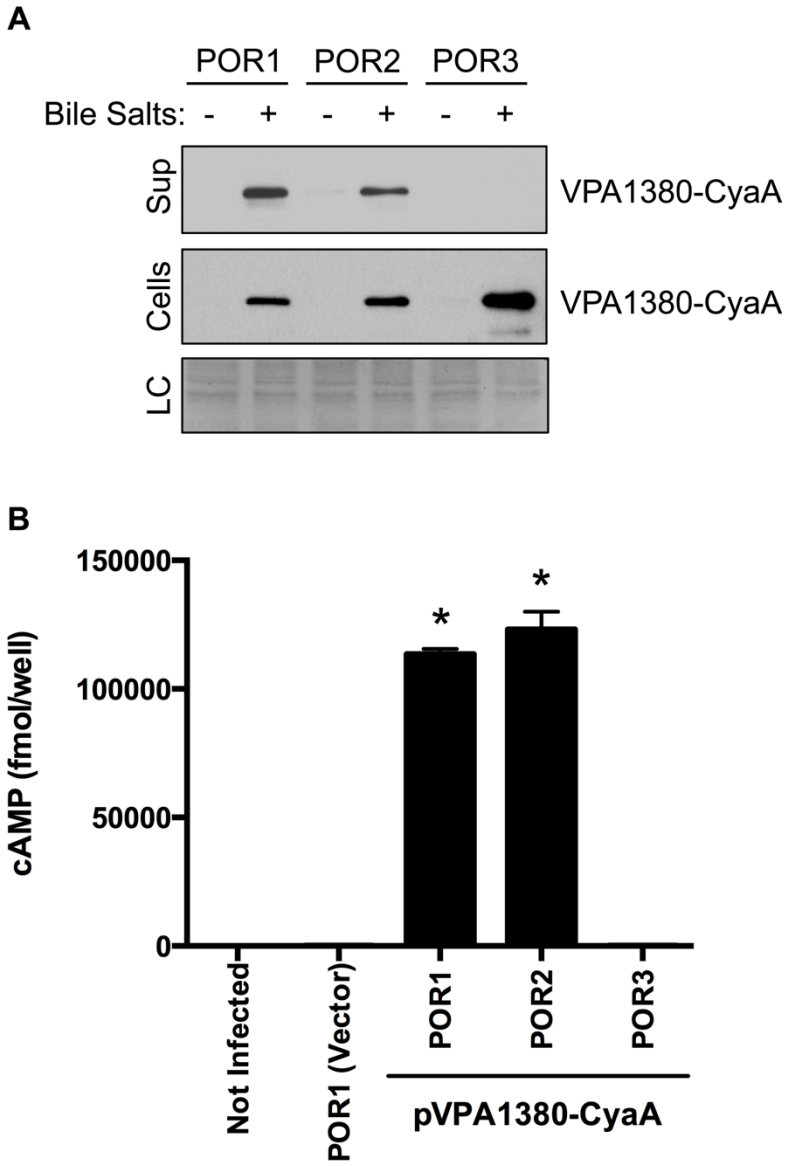

Figure 18. VPA1380 is a T3SS2 effector. (A) Secretion of VPA1380-CyaA from *Vibrio parahaemolyticus* strains POR1, POR2, and POR3 as detected by immunoblot analysis from bacterial cell lysate or TCA-precipitated media. Blots were probed with anti-CyaA antibody. Loading control (LC) is shown for total protein lysate. **(B)** Measurement of translocated VPA1380-CyaA after infection of HeLa cells with *V. parahaemolyticus* strains for 1 hour. Intracellular cAMP levels were quantified by ELISA system. Asterisks indicate statistical significant differences between POR1(VPA1380-CyaA) and POR3(VPA1380-CyaA) (P = 0.0001, n = 3) and between POR2(VPA1380-CyaA) and POR3(VPA1380-CyaA) (P = 0.001, n = 3), using two-tailed t-test.

VPA1380 is detrimental when expressed in yeast

To determine whether VPA1380 targets a conserved eukaryotic process, we used yeast as an alternative heterologous system. Yeast are commonly used to study T3SS effectors since the targets of T3SS effectors are often conserved across eukaryotic species [107-109]. VPA1380 inhibited yeast growth **(Figure 19A)** when expressed as an eGFP-fusion from a galactose-inducible promoter **(Figure 19B)**. Previous studies of bacterial T3SS effectors in yeast showed that effector–mediated toxicity can be revealed or exacerbated in the presence of stress conditions [107,108]. Interestingly, VPA1380-mediated yeast growth inhibition was exacerbated in the presence of osmotic stress by addition of 0.5 M NaCl to the medium **(Figure 19A)**. These results suggest that VPA1380 targets a conserved eukaryotic process found in yeast.

VPA1380 is similar to the cysteine protease domain of other bacterial toxins

Despite the fact that homologs of VPA1380 from various bacteria have been previously identified as T3SS effectors, their mechanism of action remains unknown. To shed light on the molecular function of VPA1380, we sought to identify related structures using a sensitive sequence detection method (HHPRED). Top hits to the VPA1380 sequence query include the CPD of multifunctional-autoprocessing RTX (MARTX) from *Vibrio cholera* and clostridial glucosylating toxins (CGTs), TcdB and TcdA, from *Clostridium difficile* (MARTX (3fzy A) with probability 97.9%, TcdB (3pa8 A) with probability 95.8%, and TcdA (3ho6 A) with probability 95.3%) **(Figure 20A)**.

A

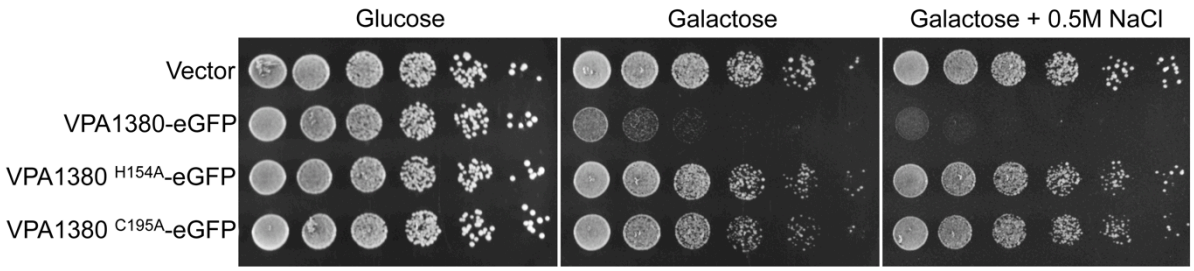

B

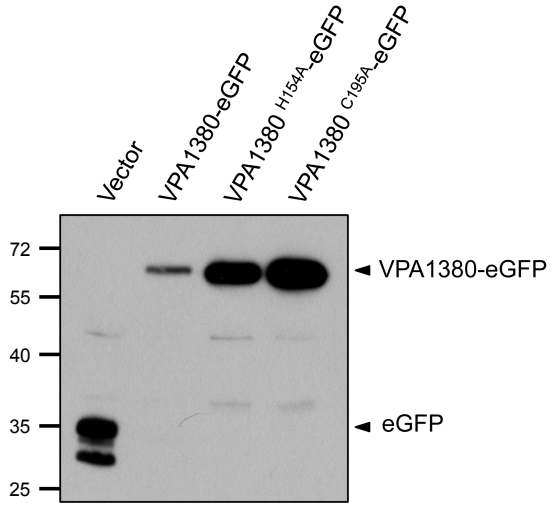

Figure 19. VPA1380 is toxic in yeast (A) Growth of yeast expressing VPA1380-eGFP and putative active site mutants. 5-fold serial dilutions of yeast were spotted on repressing (glucose) or inducing (galactose) medium. Additionally, yeast were spotted on inducing medium with osmotic stress (0.5M NaCl). **(B)** Detection of eGFP, VPA1380-eGFP, and VPA1380-eGFP point mutants by immunoblot analysis. Blots were probed with anti-GFP antibody.

These large bacterial toxins contain a CPD that requires the eukaryotic signaling molecule inositol hexakisphosphate (IP6) for activation. Studies to understand this process have been mainly focused on the CPD from the *V. cholerae* MARTX toxin and the *C. difficile* CGT toxins, TcdA and TcdB [110-112]. These multi-domain toxins gain access to the host cytosol by forming a pore in the host membrane, which allows their CPD to bind IP6 and initiate autoprocessing of the toxin. This autoprocessing event allows for the release of toxin effector domains, which function to alter different cellular processes [113]. The CPDs from MARTX and CGT toxins contain a catalytic dyad with a conserved histidine and cysteine, along with a conserved IP6 binding pocket comprised mostly of positive charged residues. IP6 is thought to activate the CPD by initiating conformational folding of the catalytic site [111,114].

Resulting HHPRED alignments map to the C-terminal region of VPA1380 (residues 116-268) and encompass the conserved Cys-His active site residues **(Figure 20A and 20B)**. Interestingly, several conserved VPA1380 positions map to residues that mediate binding to IP6 **(Figure 20A and 20C)**, including several invariant residues (K148, Y150, R191 and Y253) and several conserved residues (R271 and R283) that are capable of forming similar interactions **(Figure 20C)**.

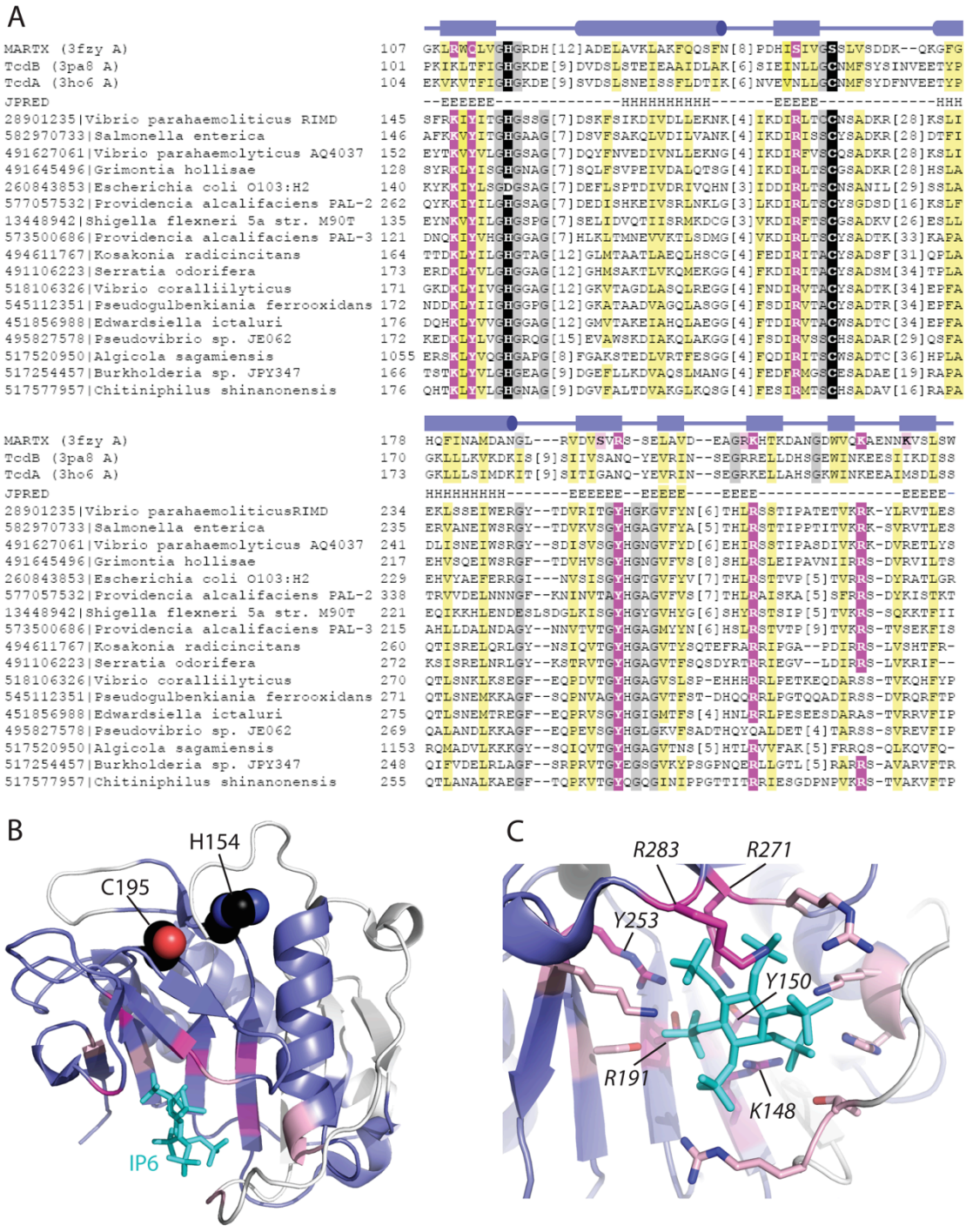

Figure 20. VPA1380 is related to the IP6-activated cysteine protease domain of MARTX and CGT toxins. (A) Multiple sequence alignment (missing first mapped helix) of

IP6-binding MARTX and CGT toxin CPD structures (top, labeled to the left according to gene name and PDB ID) with representative VPA1380-related sequences (bottom, labeled to the left according to NCBI GI and species) highlights conserved active site (black highlights) and IP6 binding residues (magenta and pink highlighted). The observed MARTX secondary structures (boxes for strands and cylinders for helices above the alignment) correspond to the VPA1380 predicted secondary structures (E for strands and H for helices), and the hydrophobicity patterns match (mainly hydrophobic positions highlighted yellow, and mainly small positions highlighted gray). **(B)** A ribbon representation of the *Vibrio cholera* MARTX cysteine protease domain (PDB 3fxy) depicts the region of the structure that confidently aligns to VPA1380 (colored slate, with unaligned region in white). The aligned region encompasses the Cys-His active site (black spheres), and a majority of the IP6 (cyan stick) binding site (magenta and pink). **(C)** A zoom of the IP6 binding site highlights MARTX residues that form hydrogen bonds to IP6 and map to conserved VPA1380 positions (magenta sticks, labeled in italics according to VPA1380 residues). Several MARTX residues that form the IP6 binding pocket were either mapped to the unaligned N-terminus or were not mutated (pink sticks).

While VPA1380 retains all of the active site residues common to the CPDs of MARTX and CGT toxins, the sequence diverges at the N-terminus (Figure 20 alignment starts with residue 145). In fact, the N-terminal portion of the VPA1380 CPD more closely resembles a more distantly related cysteine protease (VPA1380 residues 52-202 maps to 4m9r with HHPRED probability 75.34). This relationship extends the coverage of the VPA1380 sequence to include the complete CPD fold. We found VPA1380Δ50-eGFP, lacking the far N-terminal region (aa 1-50), still reduced yeast growth **(Figure 21A and 21B)**, which demonstrates only the CPD region is necessary for VPA1380's toxicity in yeast.

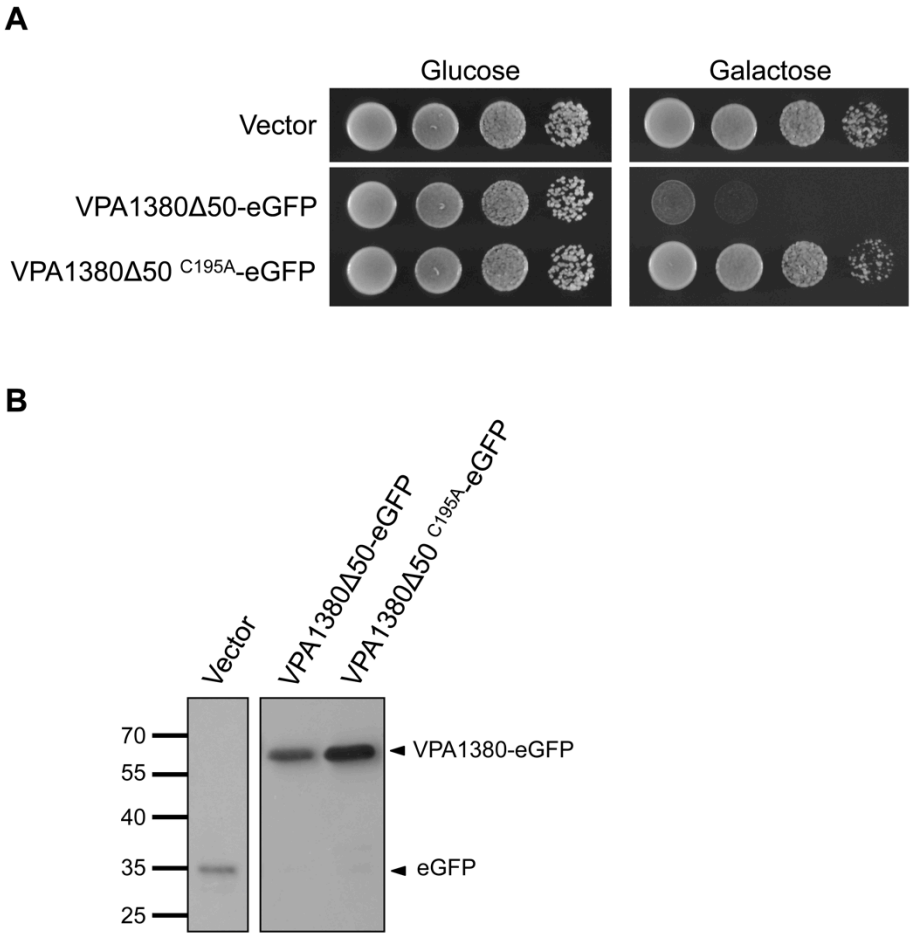

Figure 21. VPA1380's CPD is sufficient for toxicity in yeast. (A) Growth of yeast expressing VPA1380Δ50-eGFP, which encodes the CPD region, and putative active site mutant. 10-fold serial dilutions of yeast were spotted on repressing (glucose) or inducing (galactose) medium. **(B)** Detection of eGFP, VPA1380Δ50-eGFP, and VPA1380Δ50-eGFP by immunoblot analysis. Blots were probed with anti-GFP antibody.

Putative active site residues are required for VPA1380's toxicity in yeast

To examine whether the putative Cys-His catalytic dyad that we identified is required for VPA1380's activity, we examined the effects of corresponding point mutations on VPA1380's toxicity in yeast. Whereas galactose-inducible expression of VPA1380-eGFP greatly reduced yeast growth, the toxic effects were abolished when the putative active site residues (H154 and C195) were mutated to an alanine **(Figure 19A)**. Moreover, no growth inhibition was observed when VPA1380^{H154A}-eGFP and VPA1380^{C195A}-eGFP were expressed in yeast in the presence of osmotic stress **(Figure 19A)**. Importantly, all of the mutated forms of VPA1380 and the wild-type effector were expressed **(Figure 19B)**. Therefore, these conserved residues appear to be critical for VPA1380's toxicity.

VPA1380's toxicity is dependent on IP6 and putative IP6 binding residues

As the cysteine proteases similar to VPA1380 are known to use IP6 as an activator, we next set out to determine whether VPA1380 requires IP6 to cause yeast growth inhibition. In yeast, the kinase Ipk1 is responsible for converting IP5 to IP6 [115]. The *ipk1* deletion strain of *Saccharomyces cerevisiae* is unable to make IP6 and yet is still viable, which allowed us to examine the IP6-dependency of VPA1380. Interestingly, deletion of *ipk1* greatly suppressed the VPA1380-mediated yeast growth inhibition. The inhibition was restored when expression of Ipk1 was complemented from a plasmid in the *ipk1* deletion strain **(Figure 22A)**. Importantly, VPA1380-eGFP was expressed in the Δ*ipk1* strain and the reconstituted strain **(Figure 23A)**. Therefore, IP6 is required for the VPA1380-mediated toxicity in yeast.

Since IP6 is required for the activity of VPA1380, we next sought to verify the importance of the six putative IP6-binding residues, which we identified in VPA1380 **(Figure 20A, and 20C)**. The positively charged residues (K148, R191, R271, and R283) were mutated to similar sized residues, asparagine and glutamine, respectively, without a charge to mitigate the effects on protein structure, while still removing the specific hydrogen-bonding ability of the residues. Additionally, the tyrosine residues (Y150 and Y253) were mutated to an alanine to also eliminate possible hydrogen-bonding interactions. All six point mutants were significantly less toxic when expressed in yeast, though the Y150A mutation appeared to have an intermediate effect **(Figure 22B)**. Importantly, all the mutant constructs were expressed **(Figure 23B)**. To better visualize the difference in yeast inhibition, we also tested the effect of these mutants in the presence of osmotic stress (0.5M NaCl), which exacerbates the VPA1380-mediated growth inhibition **(Figure 19A)**. Indeed, the toxicity differences described above were more apparent under the stress condition **(Figure 22B)**. Taken together, the dependence of VPA1380 on IP6 and the six conserved residues that contribute to the putative IP6 binding pocket in VPA1380 support our hypothesis that IP6 is likely required for VPA1380's activity.

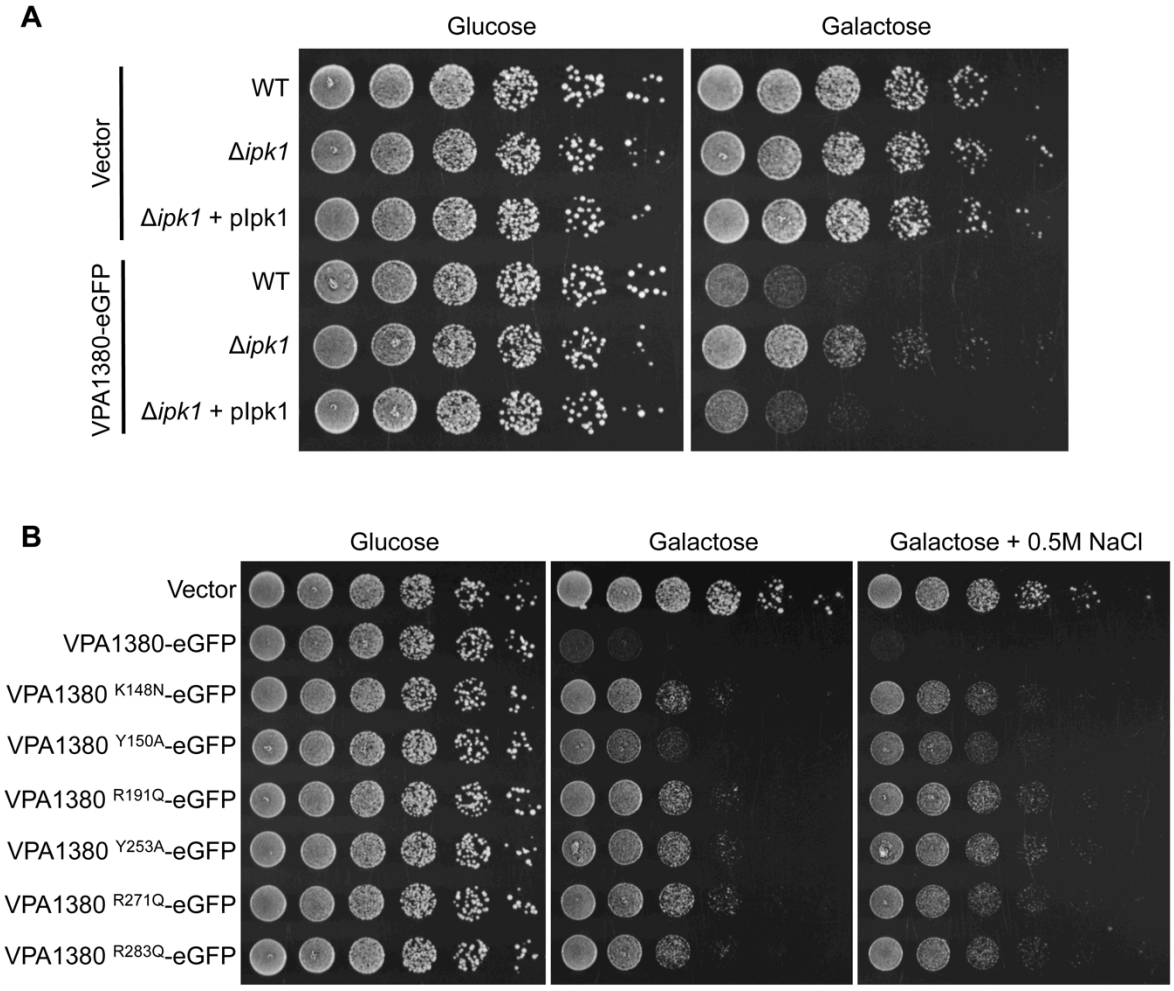

Figure 22. VPA1380 requires IP6 and putative IP6 binding residues for toxicity in yeast. (A) Growth of yeast strains: wt, Δ*ipk1* IP6-deficient, and Δ*ipk1* + pIpk1 complemented yeast, expressing eGFP or VPA1380-eGFP. 5-fold serial dilutions of yeast were spotted on repressing (glucose) or inducing (galactose) plates. **(B)** Growth of Yeast expressing VPA1380-eGFP or putative IP6-binding mutants. Additionally, yeast were grown on inducing plates with osmotic stress (0.5M NaCl).

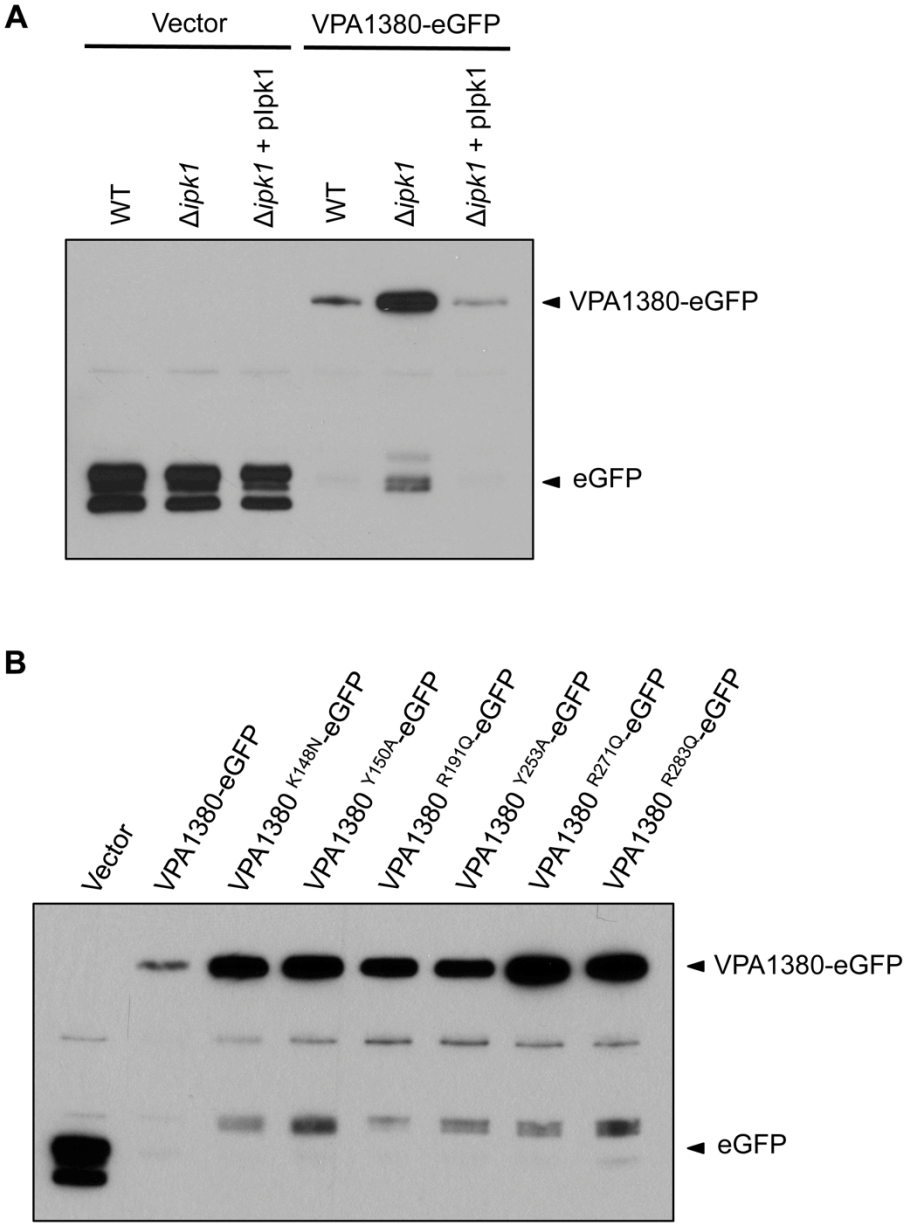

Figure 23. Verifying protein production in yeast spotting assays examining VPA1380's dependence on IP6. Detection of eGFP, VPA1380-eGFP, and VPA1380-eGFP point mutants by immunoblot analysis from strains examined in **(A)** Figure 4A and **(B)** Figure 4B. Blots were probed with anti-GFP antibody.

VPA1380 interacts with Ndel1 and Vps52

To determine the eukaryotic target of VPA1380, we performed a yeast 2-hybrid screen. VPA1380 was fused to a Gal4 DNA binding domain (DNA-BD) and screened against a mouse embryo library of genes fused to a Gal4 activation domain (AD). Within this yeast 2-hybrid system, interaction of DNA-BD-VPA1380 with an AD-protein allows for the AD to be brought to the promoter region of genes that are required for a certain response on selective media. Positives interactions cause the AD to induce expression of the α-galactosidase gene *mel1*, and cause yeast to appear blue when grown in the presence of x-α-Gal. Additionally, positive interactions cause the AD to induce expression of the *his3* gene and allows yeast to grow on media lacking histidine. For a positive control, we tested the interaction between DNA-BD-p53 and AD-SV40, which are known to interact [116]. For a negative control, we tested DNA-BD-Lamin with AD-SV40, which do not interact **(Figure 24)** [117]. Our screen yielded 13 positive interactions, which included 12 full-length clones of Ndel1 (Nuclear distribution element – like 1) and 1 C-terminal (aa 428-724) clone of Vps52 (Vacuolar protein sorting 52). To verify these positive clones in the yeast 2-hybrid system, we re-transformed yeast with plasmids encoding DNA-BD-VPA1380 and either AD-Ndel1 or AD-Vps52(428-724), and confirmed that both Ndel1 and Vps52(428-724) interact with VPA1380 because they caused yeast to appear blue on agar containing x-α-Gal and promoted yeast growth on agar lacking histidine **(Figure 24)**.

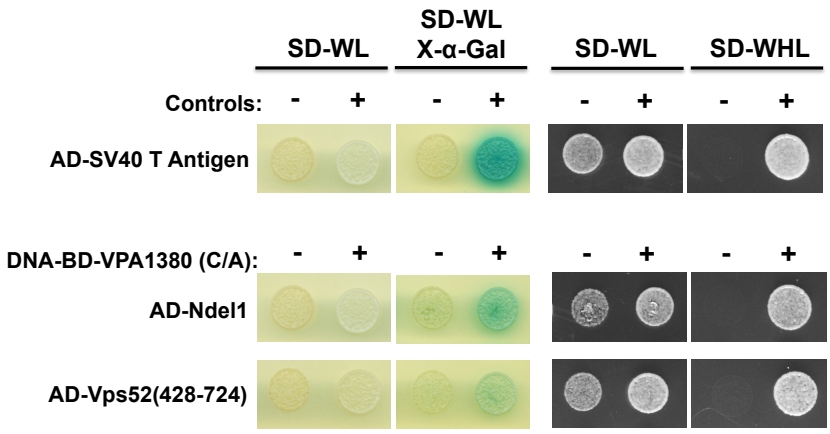

Figure 24. VPA1380Δ50 C/A interacts with Ndel1 and Vps52 within yeast 2-hybrid system. The yeast 2-hybrid hits, Ndel1 and Vps52, fused to the Activation Domain (AD) were tested for interaction with VPA1380 (C/A) fused to the DNA-binding domain (DNA-BD) by growing yeast on X-α-Gal (5-Bromo-4-Chloro-3-indolyl a-D-galactopyranoside) plates and histidine-minus agar. Negative control (-) is DNA-BD-Lamin and Positive control (+) is DNA-BD-p53.

VPA1380's activity towards Nde1 and Ndel1 is not observed during infection

Ndel1 is involved in the retrograde transport of vesicles [118]. Retrograde transport describes the directional movement of cargo towards the minus-end of microtubules, which terminates at the microtubule organizing complex. This complex is localized within the perinuclear region of most cell types. Notably, polarized cells, such as gut epithelial cells, have a reversed microtubule polarity that redirects retrograde movement outward. Dynein motors are responsible for moving cargo along microtubules in a retrograde direction [119]. These large motors are approximately 1.6 MDa in size and contain several adaptor proteins that bind to cargo and mediate efficient movement of the dynein motor [120]. Ndel1 is one of these adaptor proteins and is known to bind to both ends of the dynein motor with two dynein-binding domains and is also necessary for recruiting the Lis1 adaptor protein through

its Lis1-binding domain [118,121]. Both Ndel1 and Lis1 are essential for dynein motor movement in cells and for efficient movement *in vitro*, but the exact functional role of Ndel1 in this process is unknown [122,123]. Humans also encode a close homolog termed *nde1* that is thought to be interchangeable for *ndel1* in many roles. Disruption of either Nde1 or Ndel1 has been shown to cause Golgi dispersion and the exclusion of cargo from the perinuclear space [124]. Importantly, yeast encode a similar gene termed *ndl1*, which is important for transporting the nucleus into a newly budded cell during cell division [125].

To determine the portion of Ndel1 that interacts with VPA1380, we examined N-terminal fragments of Ndel1 in a similar yeast 2-hybrid system. In this system the Gal4 DNA-BD is replaced with the LexA DNA-BD. We tested DNA-BD-VPA1380Δ50 with four N-terminal fragments of Ndel1 **(Figure 25A)** fused to a VP16 AD in a blue/white assay. Each fragment containing a portion of the Lis1 binding domain caused activation, while the extreme N-terminal fragment lacking the Lis1 binding domain did not cause activation **(Figure 25B)**. From these results, the minimal region required for activation is Ndel1 (100-143), which is part of a coiled-coil region [126].

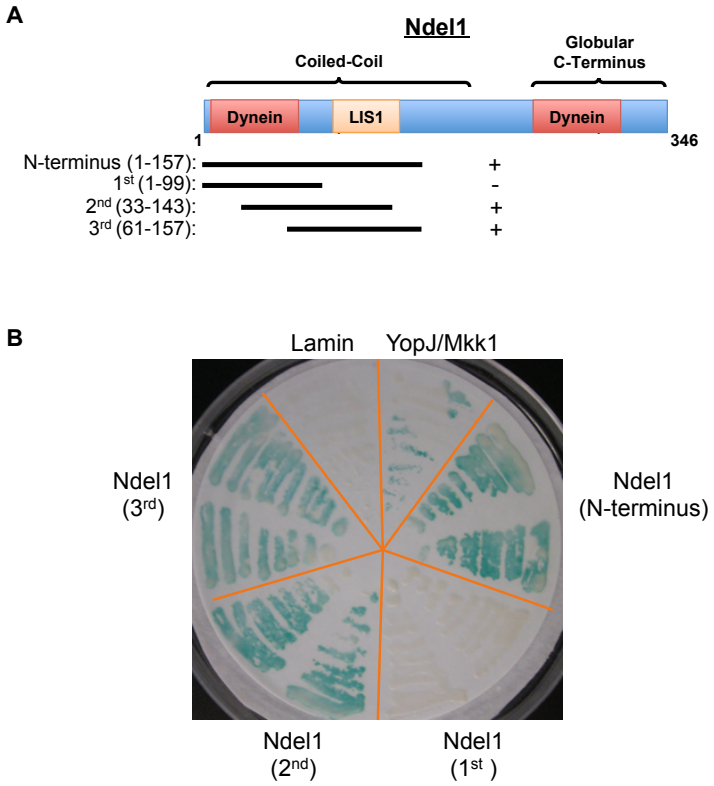

Figure 25. VPA1380Δ50 C/A interacts with the Lis1 binding domain of Ndel1. (A) Schematic showing the N-terminal fragments of Ndel1 examined within the yeast 2-hybrid system. **(B)** Interactions of the N-terminal fragments of Ndel1, fused to the activation domain (AD), with VPA1380 (C/A), fused to the DNA-binding domain (DNA-BD). Blue/white test was performed with X-Gal (5-Bromo-4-Chloro-3-indolyl β-D-galactopyranoside. Negative control is DNA-BD-Lamin and Positive control is DNA-BD-YopJ and AD-MKK1.

VPA1380 is a putative protease so we tested if VPA1380 could cleave Nde1 and Ndel1 *in vitro*. To create VPA1380 recombinantly, we replaced the non-conserved N-terminal region with MBP (mannose binding protein), which is known to provide greater stability to recombinant proteins. MBP/His-VPA1380Δ50 was stably produced in *E. coli* and extracted by affinity purification with nickel beads **(Figure 26A)**. We next created N-terminal fragments of His-Nde1 and His-Ndel1 through an *in vitro* transcription/translation

(IVT) reaction with ^{35}S labeling, and found [^{35}S]-Nde1 (1-191) and [^{35}S]-Ndel1 (1-192) **(Figure 26B)** to be more stable than the full-length proteins. To test for protease activity, MBP/His-VPA1380Δ50 was incubated with [^{35}S]-His-Nde1 or [^{35}S]-His-Ndel1, along with the activator IP6. A weak 16-17kDa band appeared that is a potential cleavage product, and was shown to be dependent on IP6 and the putative catalytic site of VPA1380 **(Figure 26C)**. Unfortunately, increasing the amount of enzyme, cofactor, or time of the reaction did not enhance cleavage of the substrate (data not shown).

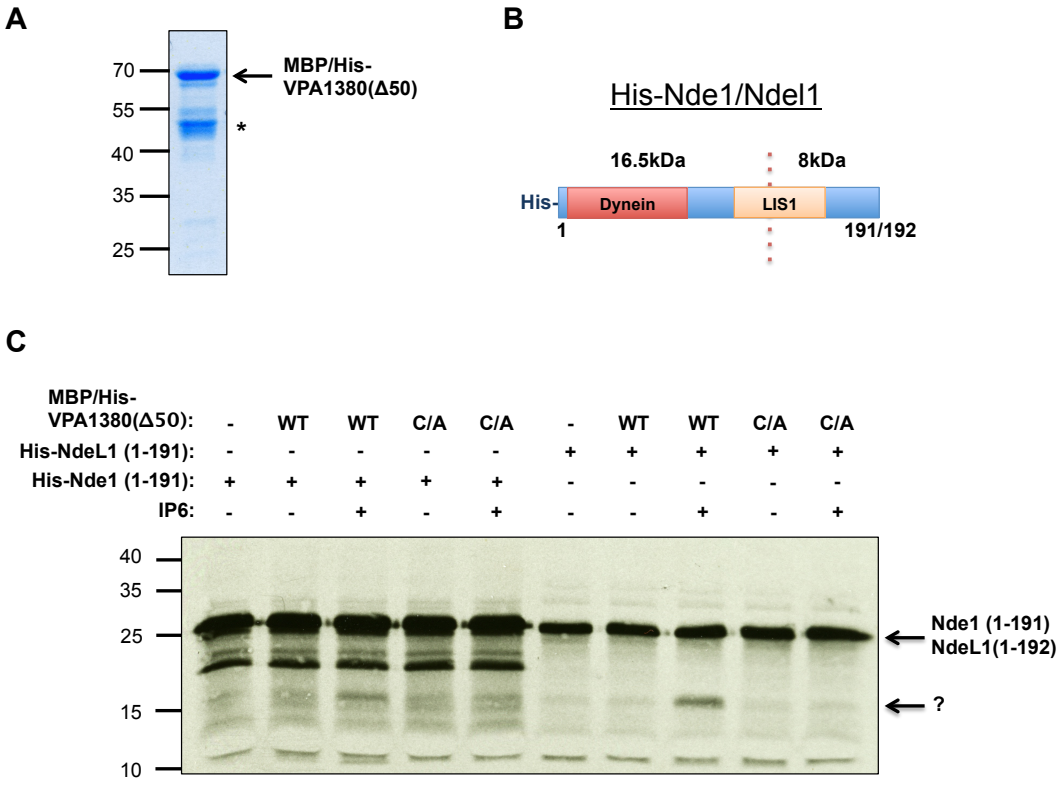

Figure 26. MBP/His-VPA1380Δ50 weakly cleaves His-Nde1 and His-Ndel1 *in vitro*. (A) Recominant MBP/His-VPA1380Δ50 stained with coomassie blue. The (*) represents degradation products or non-specific proteins. **(B)** Diagram showing the N-terminal fragment of Nde1 (1-191) and Ndel1 (1-192). The dotted red line represents a putative cleavage site. **(C)** MBP/His-VPA1380Δ50 incubated with 35S-labeled His-Nde1 (1-191) and His-Ndel1 (192), along with IP6, for 1 hour at 30°C.

VPA1380 may require more eukaryotic components besides IP6 for activity towards Nde1 and Ndel1 so we next examined VPA1380's activity in HeLa cells. We co-transfected HeLa cells with peGFP-VPA1380-V5 and either HA-Nde1-Flag or HA-Ndel1-Flag and found a significant reduction in Nde1 and Ndel1 protein levels that was dependent on VPA1380's putative catalytic site **(Figure 27)**. This effect was more drastic than effects seen *in vitro* **(Figure 26C)** but no cleavage product appeared—possibly due to degradation of the cleavage product inside cells. We next tested if this reduction/elimination of Nde1 and Ndel1 is seen during bacterial infection. The effectorless *Yersinia pseudotuberculosis* strain YP37 [94] was utilized as an infection model and delivery system. *Y. pseudotuberculosis* was able to produce and secrete VPA1380-Flag and VPA1380-Flag (C/A) protein in a T3SS-dependent manner **(Figure 28A)**. HeLa cells were first transfected with pHA-Nde1-Flag or pHA-Ndel1-Flag and then infected with *Y. pseudotuberculosis* strains induced for VPA1380-Flag secretion. There was no reduction in HA-Nde1 or HA-Ndel1 protein levels after 1.5 hours or 3 hours of infection **(Figure 28B and 28C)**, suggesting Nde1 and Ndel1 may not be actual targets during infection.

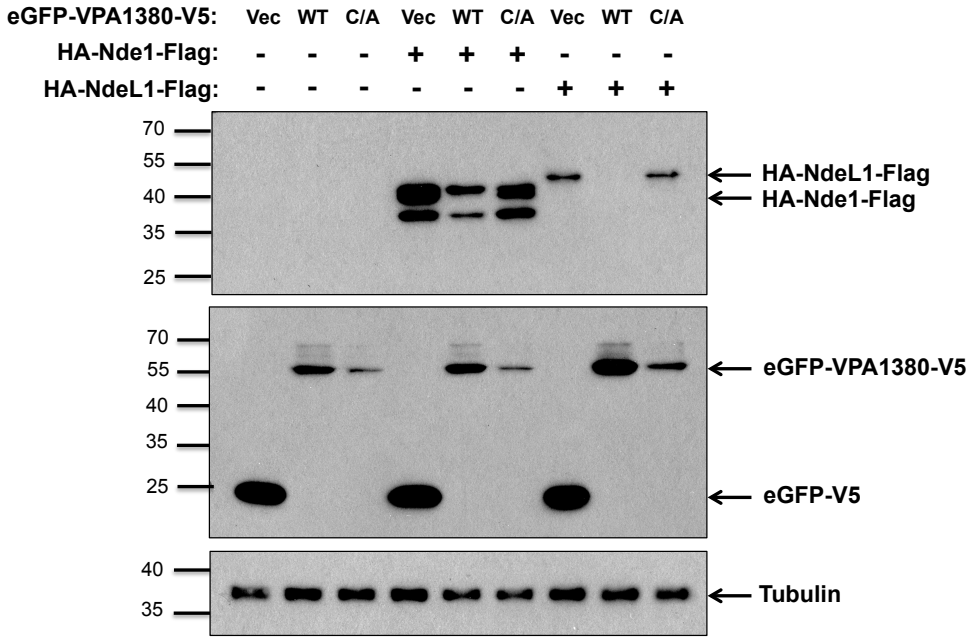

Figure 27. eGFP-VPA1380-V5 reduces HA-Nde1-Flag and HA-Ndel1-Flag protein levels in HeLa cells. HeLa cells co-transfected with mammalian expression vectors encoding *egfp* constructs and HA-Nde1/Ndel1. Proteins levels examined 16 hours after transfection by immunolot analysis with anti-HA, anti-V5, and Anti-Tubulin antibodies.

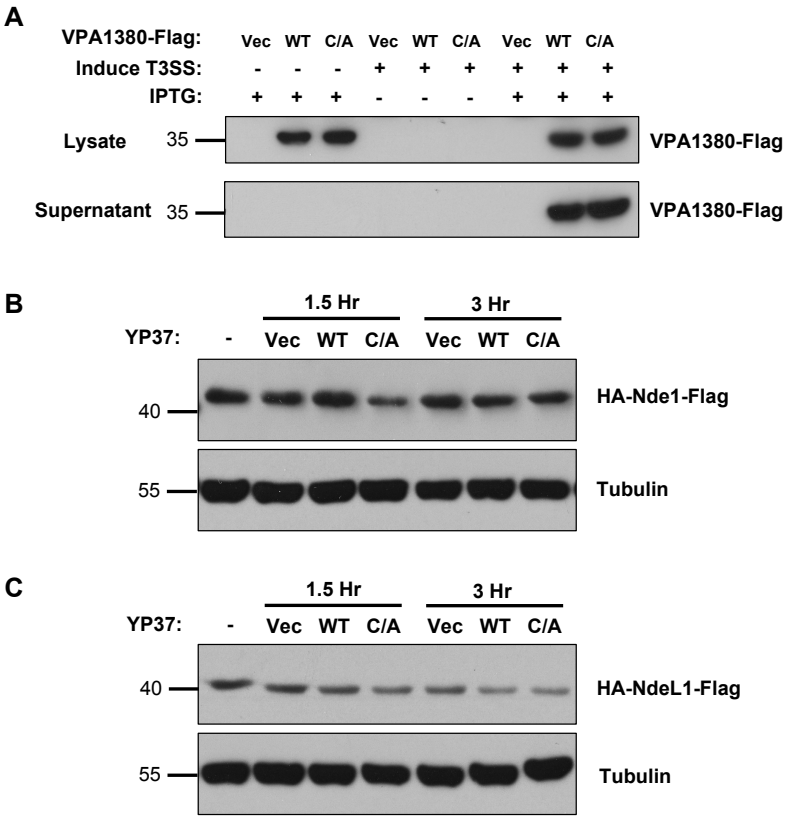

Figure 28. VPA1380-Flag secreted from *Yersinia pseudotuberculosis* does not affect HA-Nde1-Flag and HA-Ndel1-Flag protein levels during infection. (A) Detection of VPA1380-Flag from bacteria lysate and culture supernatant under IPTG-inducible and T3SS-inducible conditions. VPA1380-Flag detected by immunoblot analysis with anti-Flag antibody. HeLa cells transfected with mammalian expression vector harboring **(B)** *ha-nde1-flag* or **(C)** *ha-ndel1-flag* and infected with induced *Y. pseudotuberculosis* strains. Proteins detected by immunoblot analysis with anti-HA antibodies.

VPA1380 does not reduce Vps52 protein levels in HeLa cells

Vps52 is part of a multi-subunit tethering complex that helps to establish an initial linkage between the trans-Golgi network (TGN) and transport endosomes traveling in a retrograde direction. Disruption of the GARP complex causes a defect in retrograde trafficking of different cargo to the TGN [127]. A mutation in the yeast homolog of *vps52* is not lethal but does diminish yeast growth [128]. Similar to Ndel1, the C-terminal region of Vps52 (428-724 aa) that was shown to interact with AD-VPA1380 C/A in the yeast 2-hybrid system also contains a predicted coiled-coil region **(Figure 29A)** [127]. This suggests VPA1380 may interact with coiled-coil folds. To test if VPA1380 has protease activity towards Vps52, we co-transfected HeLa cells with peGFP-VPA1380-V5 and pVps52-V5 (full length). In these cells, eGFP-VPA1380-V5 did not appear to diminish Vps52 protein levels **(Figure 29B)**. More experiments are required to verify the interaction between VPA1380 and Vps52.

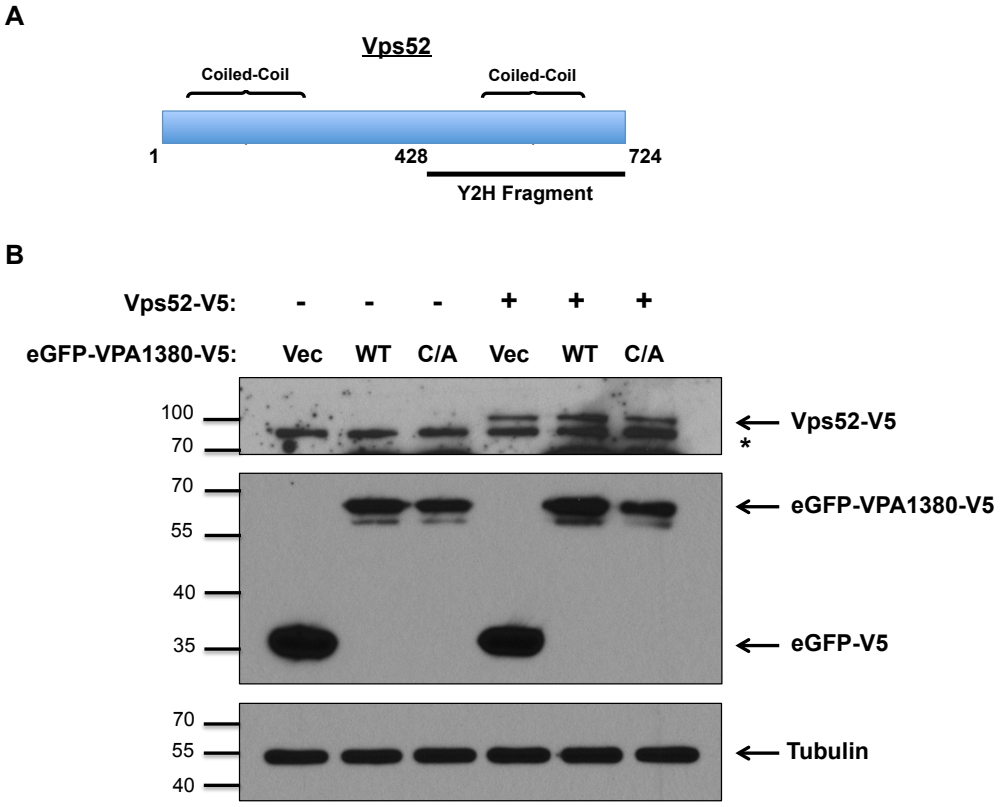

Figure 29. eGFP-VPA1380-V5 does not reduce Vps52-V5 protein levels in HeLa cells. (A) Diagram of the Vps52 fragment from yeast 2-hybrid screen **(B)** HeLa cells co-transfected with mammalian expression vectors encoding *egfp* constructs and *vps52-v5*. Proteins levels examined 16 hours after transfection by immunolot analysis with anti-GFP, anti-V5 (for Vps52-V5), and anti-Tubulin antibodies. (*) indicates non-specific protein band.

VPA1380 localization

To narrow down VPA1380's activity in the host cell, we examined the localization of GFP-VPA1380-V5 and the putative catalytic mutant GFP-VPA1380-V5 (C195A). Both proteins appeared as punctate structures with an endosome-like appearance, but GFP-VPA1380-V5 (C/A) was primarily found in a Golgi ribbon-like structure by the nucleus **(Figure 30)**. We thus hypothesized that VPA1380 is localized within the secretory/endosomal pathway. This pathway is a complex trafficking network of organelles and transport vesicles. Cargo that originates from the ER (endoplasmic reticulum) shuttles to the ERGIC (ER-Golgi intermediate compartment), and then travels through the Golgi and TGN (trans-Golgi network). From there, cargo is dispatched to different endosomes, which allows for secretion of the cargo or cargo-degradation in lysosomes. This pathway involves anterograde trafficking. Alternatively, cargo transported from early endosomes to recycling endosomes, late endosomes or the Golgi complex involves retrograde trafficking **(Figure 31)** [129,130]. Each of these organelles and endosome compartments has a distinct identity based on proteins found at the membrane. For example the protein EEA1 (early endosome antigen 1) is primarily found on early endosomes, while the protein p58 is found primarily on the ERGIC [131-133].

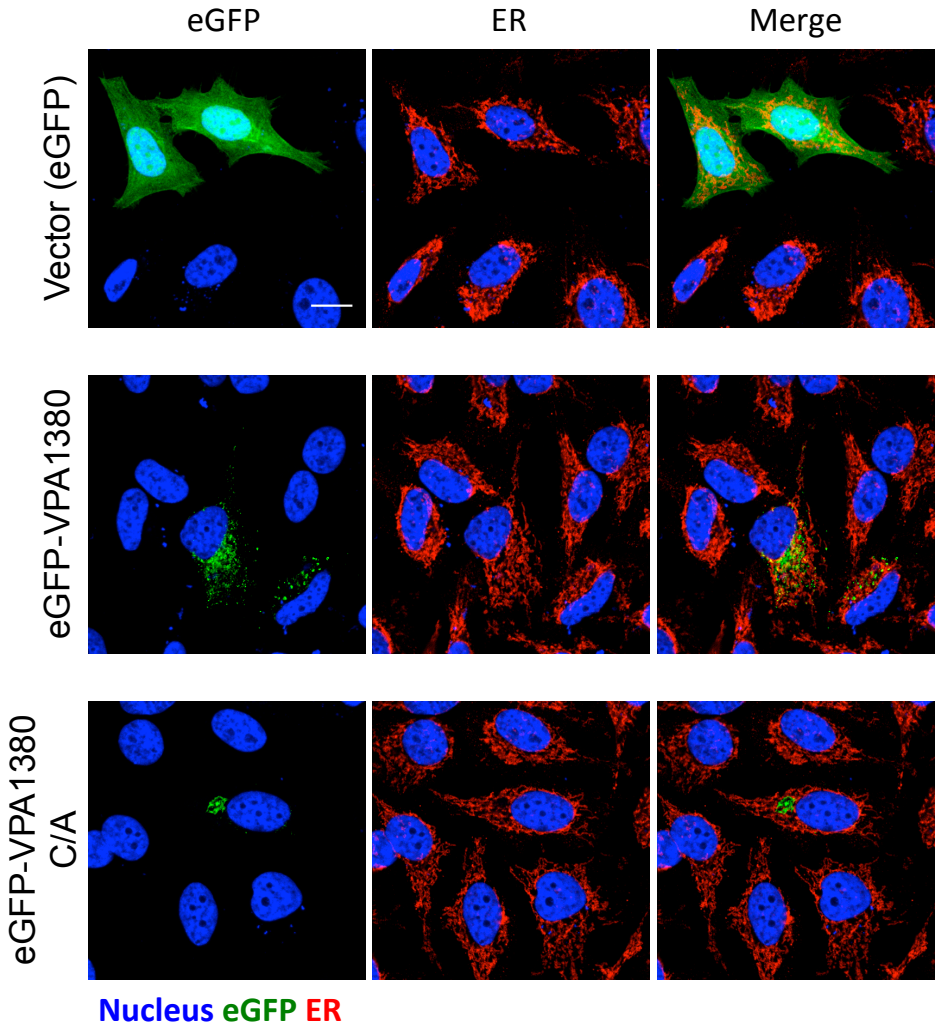

Figure 30. eGFP-VPA1380 does not co-localize with the ER. HeLa cells transfected with pSurf expression vector encoding *egfp*, *egfp-vpa1380,* and *egfp-vpa1380(C/A)*. Nucleus was stained with Hoescht and ER was immunostained with mouse anti-Calnexin antibody. Scale bar represents 20 μm.

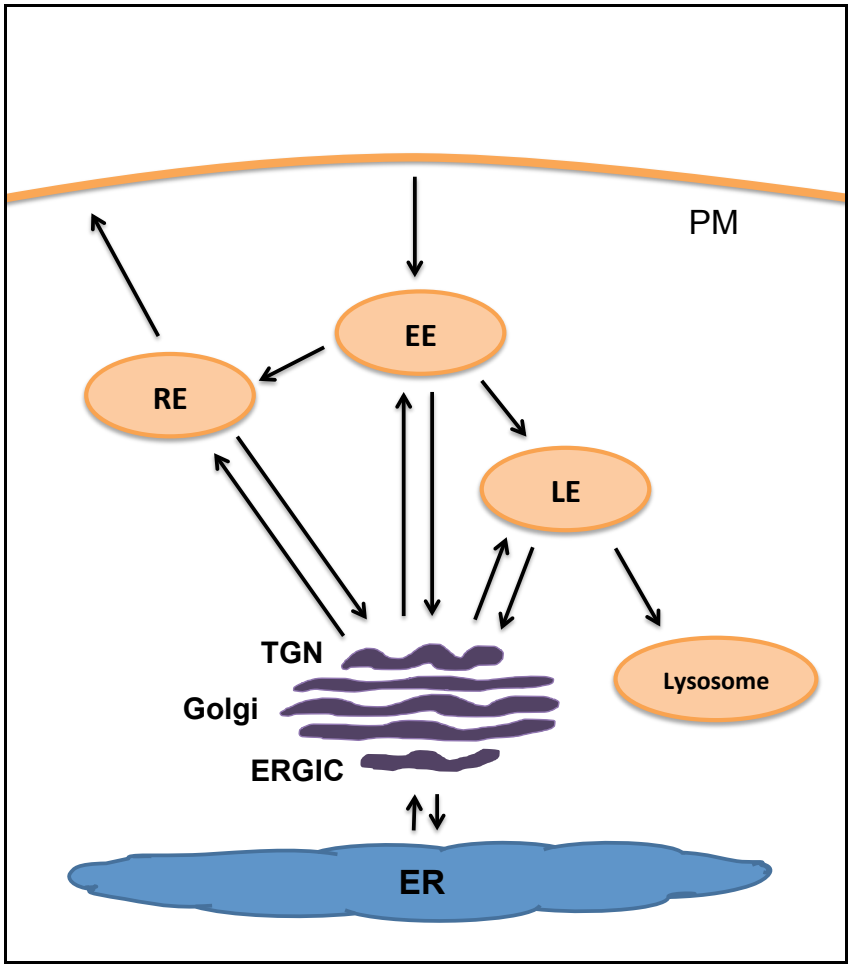

Figure 31. Secretory and endosomal pathway. Schematic of the cargo-transport network in cells. Cargo that originates in the ER (endoplasmic reticulum) is shuttled to the Golgi apparatus. Cargo is transported through the Golgi stacks by going through the ERGIC (ER-Golgi intermediate compartment), Golgi, and TGN (trans-Golgi network) in a sequential manner. Cargo can then be shuttled out of the cell in REs (recycling endosome), or degraded by traveling to LEs (late endosome) that mature into lysosomes. Cargo that originates outside the cell will enter EEs (early endosome) and travel to RE, LE, or the TGN. Transport to REs will secrete cargo back outside the cell and transport to LEs will lead to degradation of the cargo [129,130,132].

We compared the localization of GFP-VPA1380-V5 and GFP-VPA1380-V5 (C/A) to different components of the secretory/endosomal pathway to identify the site of VPA1380's activity. Neither protein appeared to localize with the ER **(Figure 30)**, suggesting VPA1380 works outside this organelle. GFP-VPA1380-V5 localized mostly outside the ERGIC, but GFP-VPA1380-V5 (C/A) almost completely co-localized with the ERGIC—except for the small vesicles that did not co-localize **(Figure 32)**. Similarly, only GFP-VPA1380-V5 (C/A) appeared to co-localize with the TGN **(Figure 33)**. This data suggests the putative catalytic activity of VPA1380 is necessary for its localization in spots outside the Golgi complex.

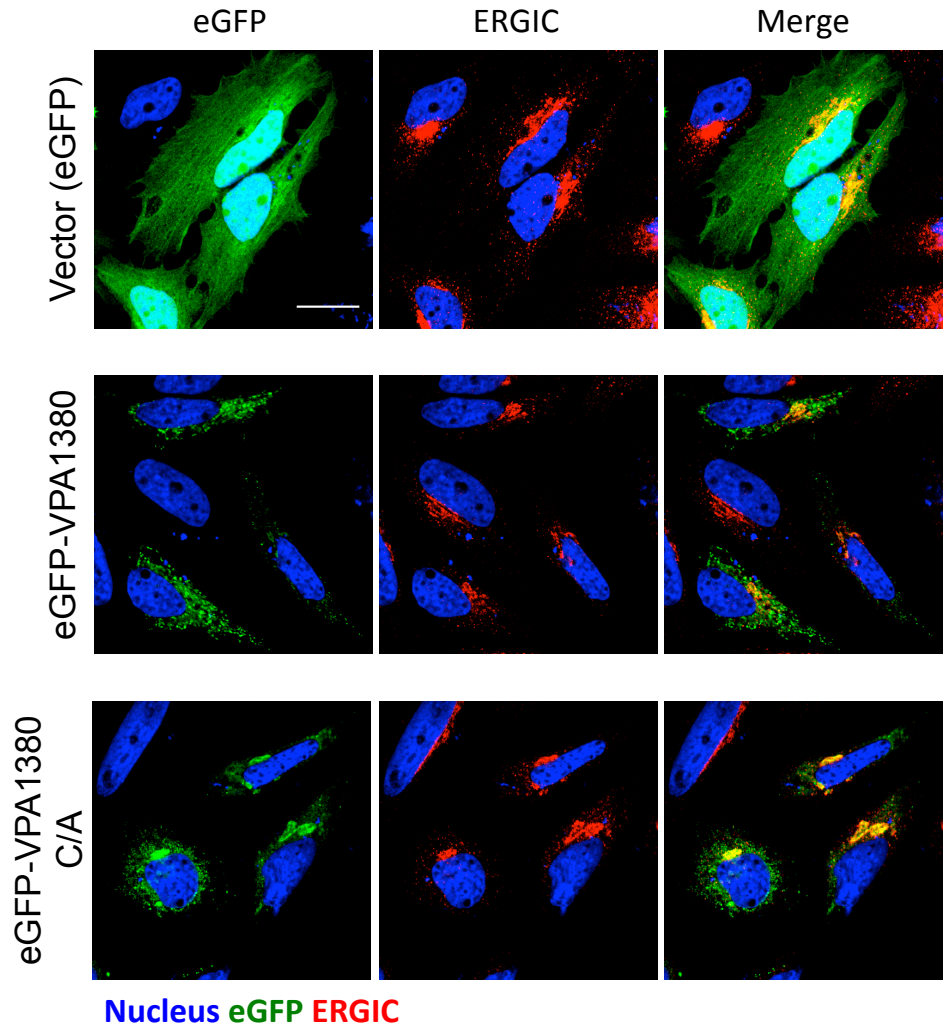

Figure 32. eGFP-VPA1380 (C/A) co-localizes with the ERGIC. HeLa cells transfected with pSurf expression vector encoding *egfp*, *egfp-vpa1380,* and *egfp-vpa1380(C/A)*. Nucleus was stained with Hoescht and ERGIC was immunostained with mouse anti-p58 antibody. Scale bar represents 20 μm.

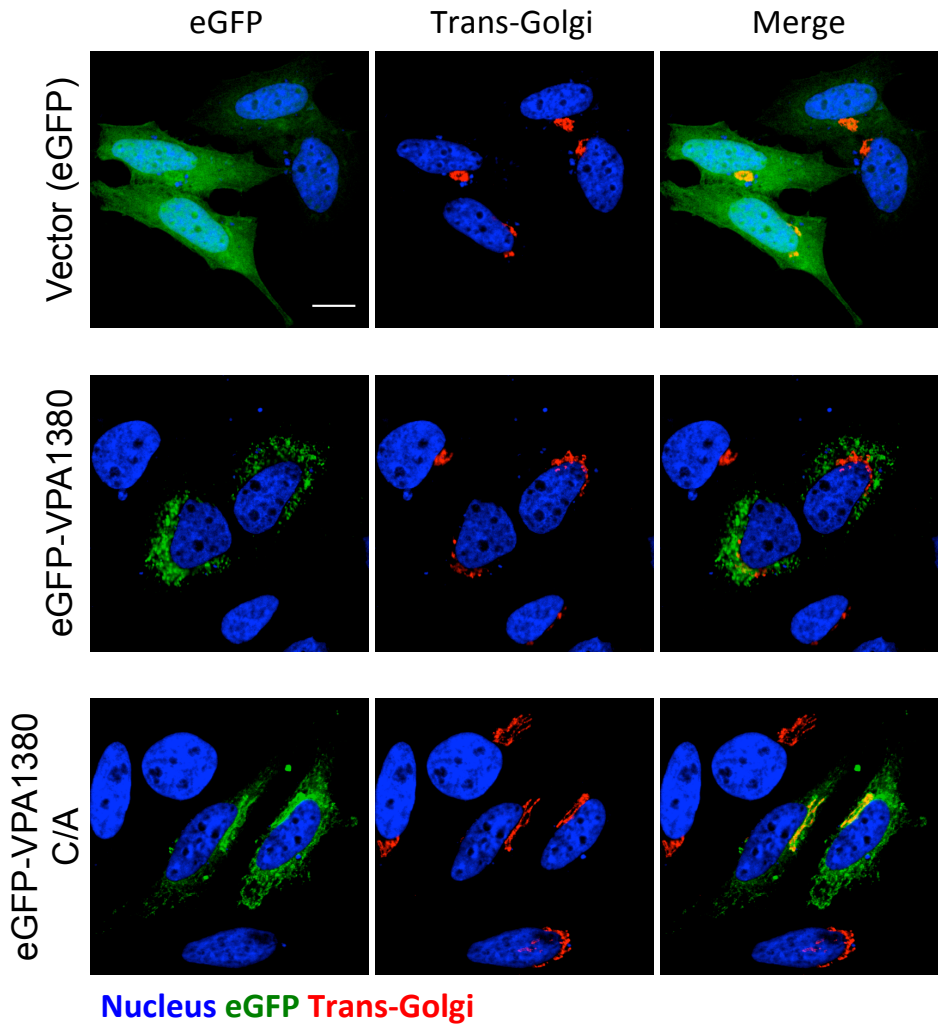

Figure 33. eGFP-VPA1380 (C/A) co-localizes with the trans-Golgi. HeLa cells transfected with pSurf expression vector encoding *egfp*, *egfp-vpa1380,* and *egfp-vpa1380(C/A)*. Nucleus was stained with Hoescht and trans-Golgi was immunostained with mouse anti-TGN97 antibody. Scale bar represents 50 μm.

The punctate phenotype of GFP-VPA1380-V5 suggests the effector may target specific endosomal vesicles. We thus compared the localization of GFP-VPA1380-V5 and GFP-VPA1380-V5 (C/A) to several endosomal markers. Neither protein appeared to co-localize with early endosomes, which appeared in bright spots evenly throughout the cell **(Figure 34)**. We next compared the localization of the effector proteins to recycling endosomes. GFP-VPA1380-V5 and GFP-VPA1380-V5 (C/A) appeared to have a perinuclear localization with their punctate mostly condensed near the nucleus. Recycling endosomes share this perinuclear localization but did not perfectly co-localize with either protein **(Figure 35)**. Similarly, GFP-VPA1380-V5 and GFP-VPA1380-V5 (C/A) did not co-localized with lysosomes, which also have a perinuclear localization **(Figure 36)**. Therefore, future studies are required to determine the vesicle identity of these punctate structures.

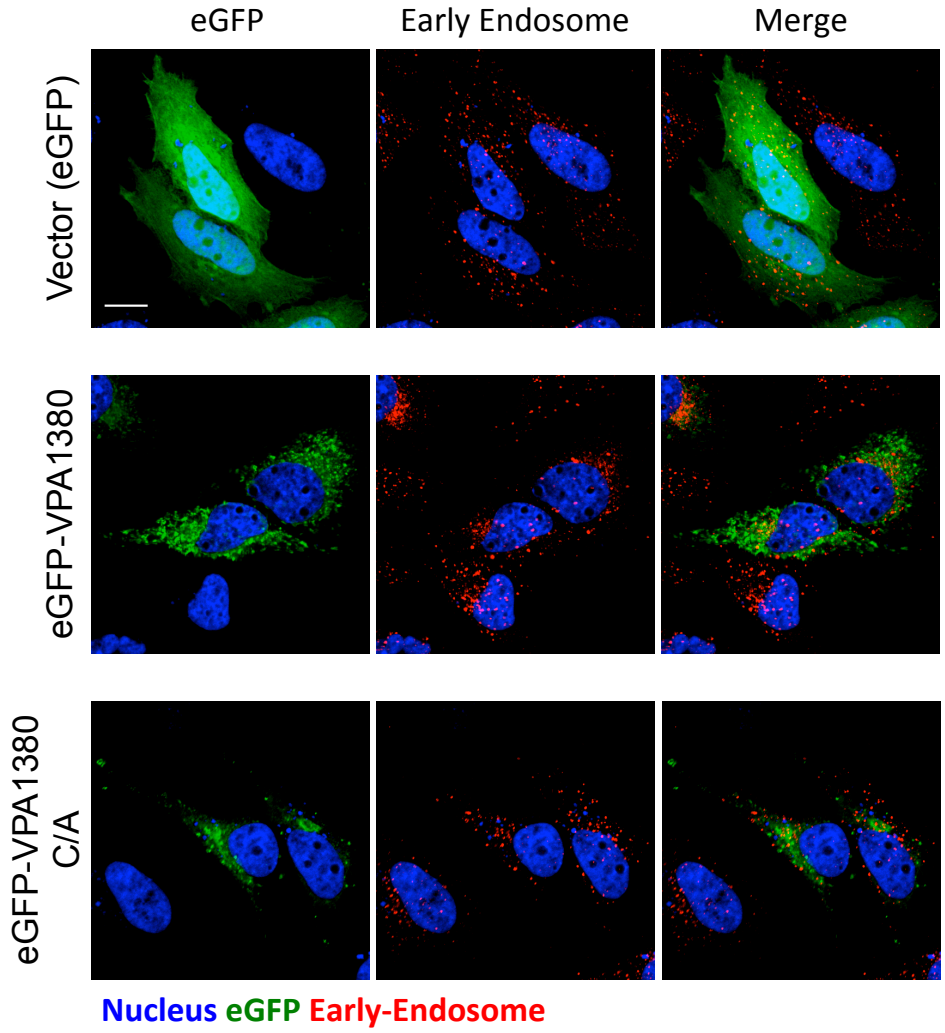

Figure 34. eGFP-VPA1380 does not co-localize with early endosomes. HeLa cells transfected with pSurf expression vector encoding *egfp*, *egfp-vpa1380,* and *egfp-vpa1380(C/A)*. Nucleus was stained with Hoescht and early endosomes were immunostained with mouse anti-EEA1 antibody. Scale bar represents 50 μm.

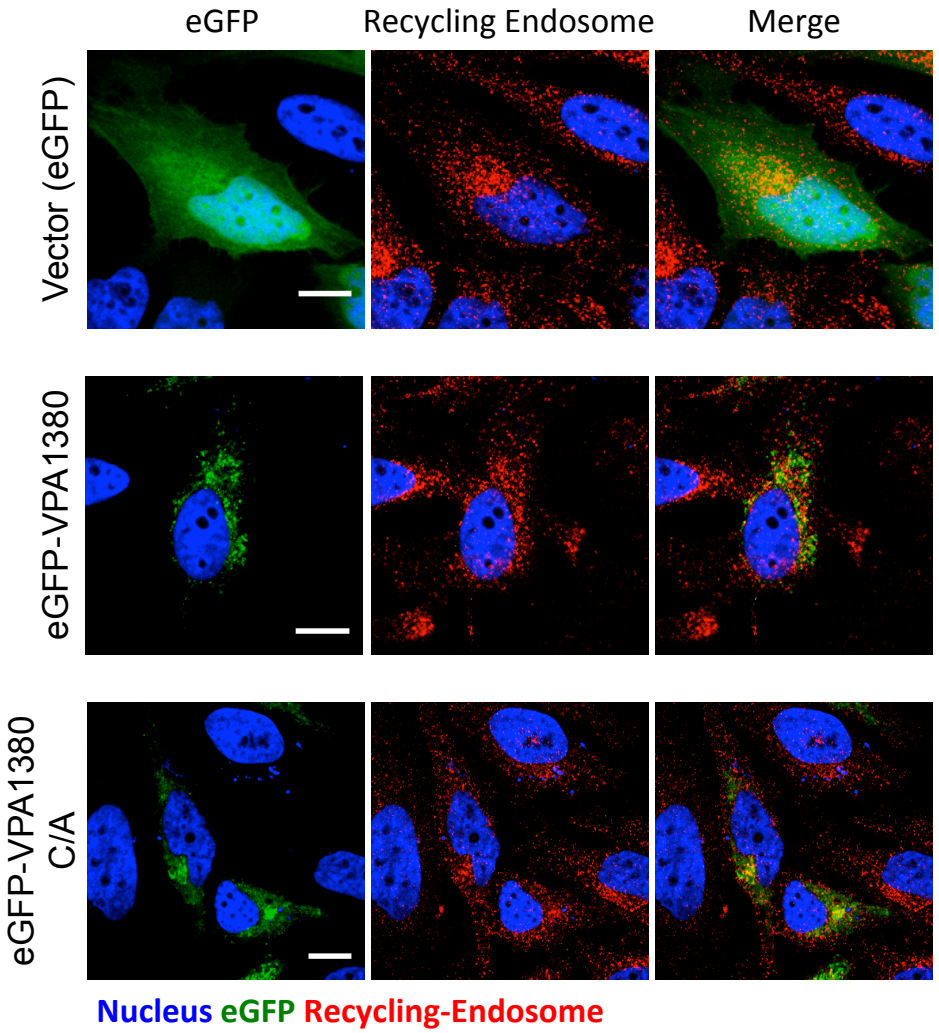

Figure 35. eGFP-VPA1380 does not co-localize with recycling endosomes. HeLa cells transfected with pSurf expression vector encoding *egfp*, *egfp-vpa1380,* and *egfp-vpa1380(C/A)*. Nucleus was stained with Hoescht and recycling endosomes were immunostained with rabbit anti-Rab11 antibody. Scale bar represents 20 µm.

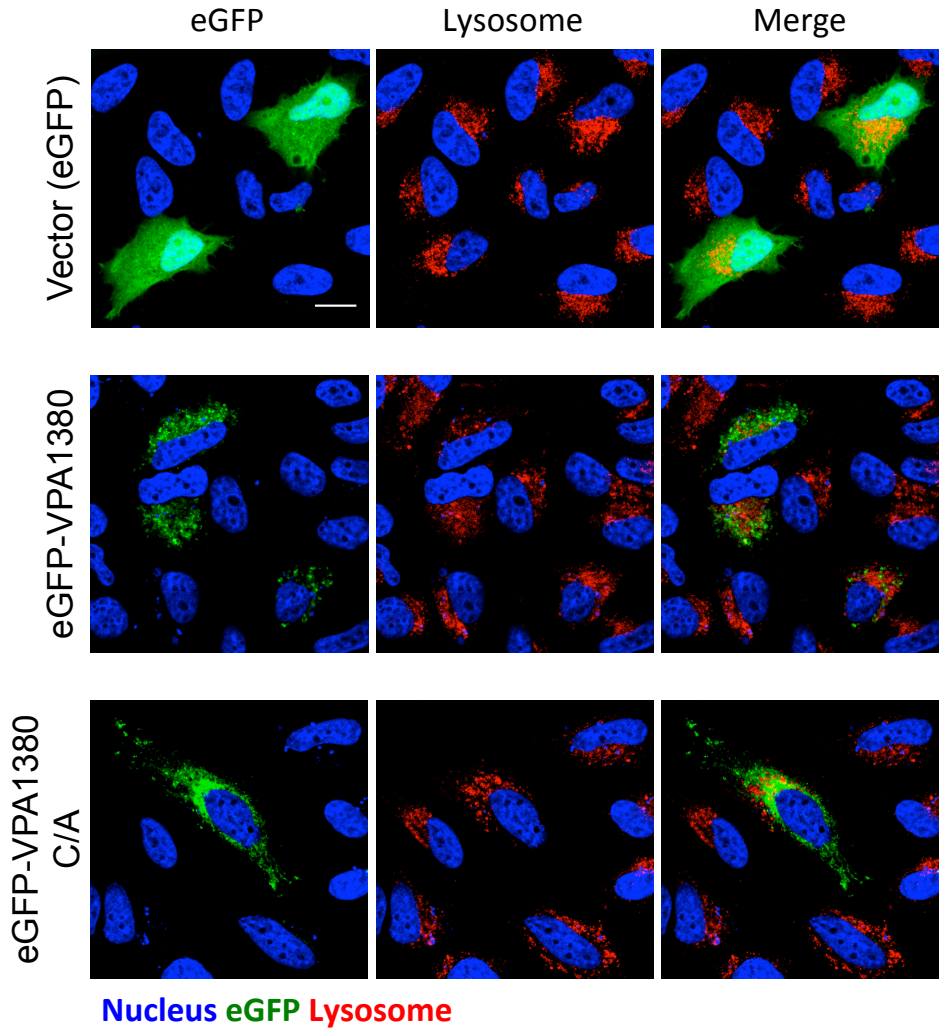

Figure 36. eGFP-VPA1380 does not co-localize with lysosomes. HeLa cells transfected with pSurf expression vector encoding *egfp*, *egfp-vpa1380,* and *egfp-vpa1380(C/A)*. Nucleus was stained with Hoescht and lysosomes were stained with Lysotracker. Scale bar represents 20 μm.

VPA1380 alters retrograde trafficking

Based on the observation that VPA1380 changes localization in the endosomal pathway based on its putative catalytic site and the discovery of two positive yeast 2-hybrid clones, Ndel1 and Vps52, that are involved in vesicle trafficking, we hypothesized that VPA1380 alters vesicle trafficking. Several trafficking markers exist to characterize different trafficking events. In this study, we examine VPA1380's activity-dependent effects on anterograde trafficking, endosome to recycling endosome trafficking, and endosome to lysosome trafficking.

Anterograde trafficking was monitored with the ts045 temperature sensitive mutant protein VSVG (vesicular stomatitis virus G) fused to CFP. This mutant protein is retained in the ER at 40°C due to misfolding. When the incubation temperature is shifted to 32°C, VSVG folds properly and first travels to the Golgi apparatus within 30 minutes and then to recycling endosomes by 60 minutes [134]. The IpaJ effector from *S. flexneri* was used as a positive control because it was recently shown to disrupt Golgi trafficking by permanently cleaving an N-myristoyl molecule from the regulatory protein ARF1 [135]. As expected, cells transfected with GFP-IpaJ caused VSVG-CFP to be retained in the ER at 32°C. In contrast, GFP-VPA1380-V5 and GFP-VPA1380-V5 (C/A) did not appear to block VSVG-CFP transport, because VSVG-CFP was seen in a Golgi-like structure when the HeLa cells were shifted from 40°C to 32°C for 30 minutes. Also, at 60 minutes VSVG-CFP appeared to spread out into vesicles. This localization was similar to the GFP control **(Figure 37)**, which suggests VPA1380 does not disrupt anterograde trafficking from the ER and Golgi apparatus.

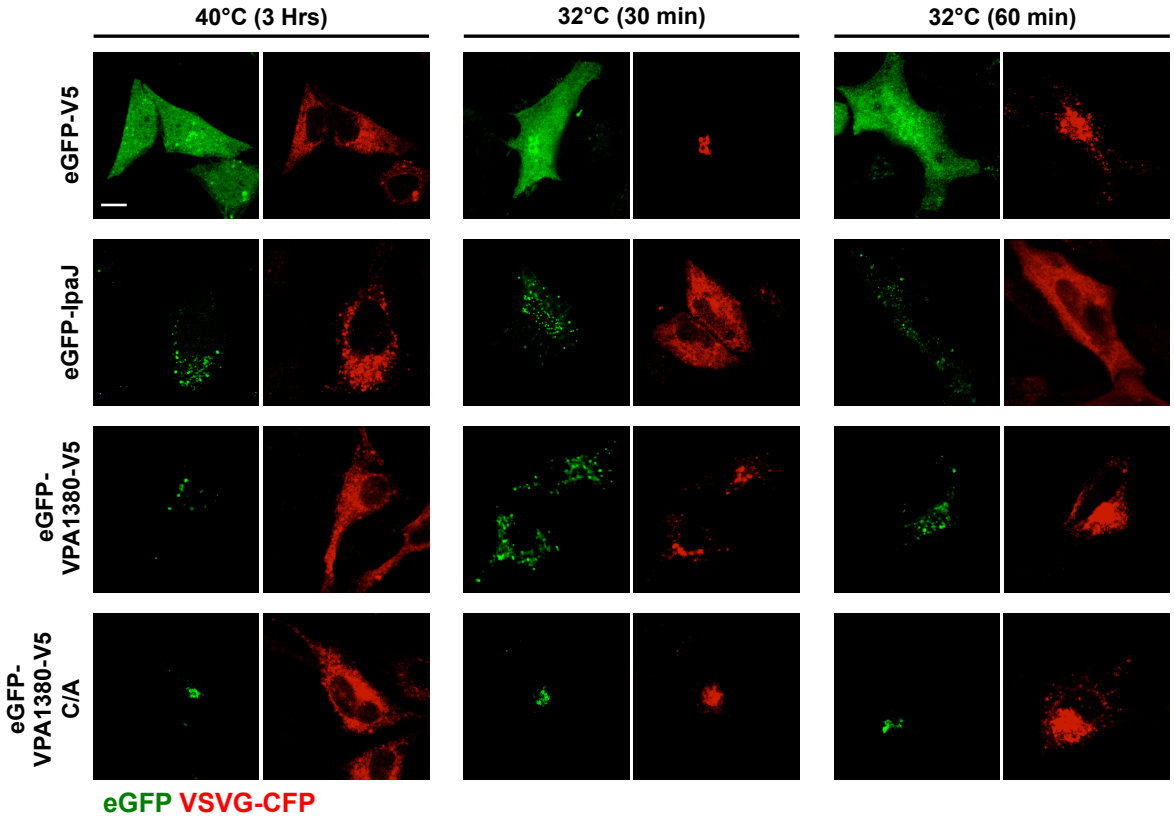

Figure 37. eGFP-VPA1380 does not block vesicle trafficking from ER to recycling endosomes. HeLa cells cotransfected with mammalian expression vectors harboring *egfp* constructs and *cfp-vsvg* and examined by confocal analysis. CFP-VSVG was tracked from the ER (40C 3 Hrs) through the Golgi (32C 30 min) to recycling endosomes (32C 60 min). Scale bar represents 10 μm.

To test if VPA1380 alters endosome-lysosome retrograde trafficking, the fluid phase marker Dextran was utilized. Cells engulf dextran through a process called macropinocytosis, which involves membrane ruffles indiscriminately engulfing extracellular molecules. Upon engulfment, Dextran is internalized in a large vesicle termed the macropinosome. From this point, dextran is either recycled outside the cell or trafficked to late endosomes and lysosomes. Dextran can be used as an endosome-lysosome marker because lysosomes are the final destination of dextran trafficking [136]. With this tool, we found that Texas red dextran localized in the perinuclear region of HeLa cells transfected with peGFP-V5 alone, but was surprisingly absent in cells transfected with peGFP-VPA1380-V5. This effect was dependent on the putative catalytic site of VPA1380 because dextran-Texas red localized in the perinuclear region of HeLa cells transfected with peGFP-VPA1380-V5 (C/A) **(Figure 38A)**. We next tested dextran uptake during an infection with the *Y. pseudotuberculosis* delivery system. In cells infected with *Y. pseudotuberculosis* strains induced for VPA1380-Flag and VPA1380-Flag (C/A) secretion, Texas red dextran appeared to localize normally in the perinuclear region **(Figure 38B)**. Therefore, VPA1380 appears to inhibit endosome-lysosome retrograde trafficking of Texas red dextran when VPA1380 is overexpressed in cells, however we could not confirm VPA1380's inhibition of this pathway during infection with *Y. pseudotuberculosis* secreting VPA1380.

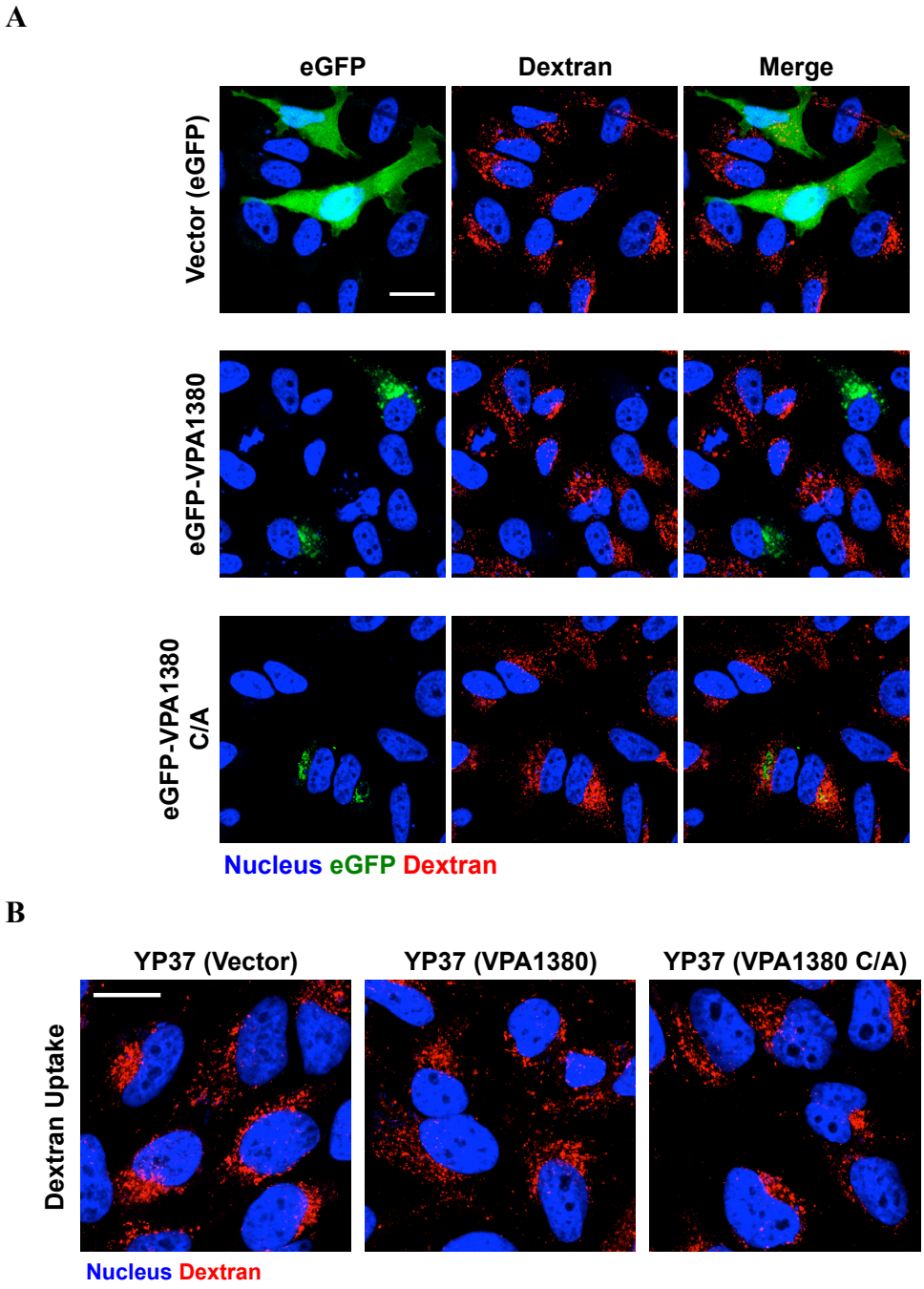

Figure 38. Transfected *egfp-vpa1380-v5* eliminates dextran uptake but VPA1380-Flag secreted from *Y. pseudotuberculosis* exhibits no affect on dextran uptake. (A) HeLa cells transfected with mammalian expression vector encoding *egfp*, *egfp-vpa1380,* and *egfp-vpa1380(C/A)* for 16 hours followed by incubation with Dextran for 3 hours. **(B)** HeLa cells infected with *Y. pseudotuberculosis* strains for 1.5 hours followed by incubation with dextran (Texas Red) for 3 hours. Nucleus was stained with Hoescht and cells were imaged by confocal microscopy. Scale bar represents 50 μm.

The recycling endosome pathway is commonly monitored by tracking transferrin (tfn), an iron-scavenger protein that binds to the Tfn-receptor at the membrane and becomes internalized through a process termed clathrin-mediated endocytosis. Tfn travels from early endosomes to recycling endosomes and then leaves the cell through exocytosis [137]. While this pathway is highly dynamic, we examined cells at a single time point to determine if Tfn-Alexa 680 can be endocytosed. The *Y. pseudotuberculosis* infection model was used as a delivery system to translocate VPA1380-Flag and VPA1380-Flag C/A into cells. Interestingly, VPA1380-Flag did not appear to block Tfn-Alexa 680 uptake but did diminish the perinuclear localization of Tfn-Alexa 680, and this effect was dependent on VPA1380's putative catalytic site **(Figure 39)**. Therefore, VPA1380 may block a step in retrograde trafficking of vesicles derived from clathrin-mediated endocytosis.

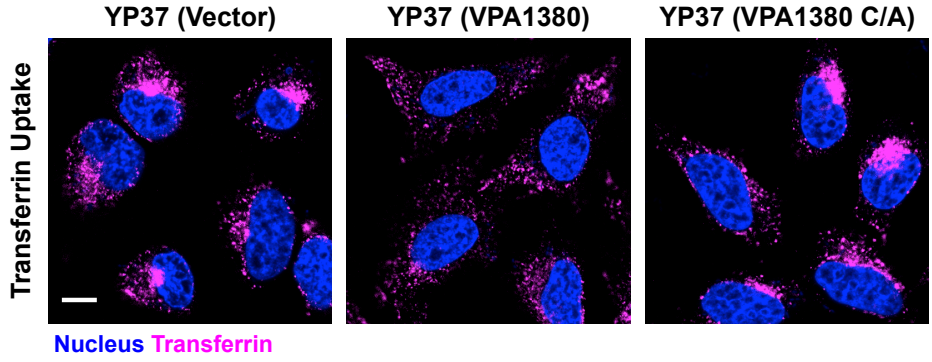

Figure 39. VPA1380-Flag secreted from *Y. pseudotuberculosis* diminishes the retrograde transport of transferrin. HeLa cells infected with *Y. pseudotuberculosis* strains for 1.5 hours followed by incubation with Transferrin (Alexa Fluor 680) for 30 min. Nucleus was stained with Hoescht and cells were imaged by confocal microscopy. Scale bar represents 10 μm.

Discussion

In this work, we identified and characterized a new *V. parahaemolyticus* T3SS2 effector, VPA1380. From bioinformatic analyses, we identified the putative catalytic and IP6-binding residues that are critical for VPA1380's activity in yeast. This supports the comparison of VPA1380 with the CPDs of MARTX and CGT toxins since these toxins also require the conserved catalytic and IP6-binding residues for enzyme activity [110,111,138,139]. Unlike the autoprocessing MARTX and CGT toxins, VPA1380 did not appear to cleave itself since no cleavage fragments were observed **(Figure 23)**. Therefore, VPA1380 is likely a cysteine protease that requires IP6 as an activator and targets a host substrate.

Many T3SS effectors require a eukaryotic factor for their activity. This regulatory control is thought to prevent off target effects prior to translocation that may arise from a promiscuous enzyme [140]. YpkA is an effector from *Yersinia* that requires actin from a host cell for activation of its kinase domain [141]. The OspG effector from *Shigella* binds to the host protein ubiquitin in conjugated, chained or free form to turn on its kinase activity [142]. AvrRpt2 is a T3SS effector from *Pseudomonas syringae* that binds to the protein cyclophilin in *Arabidopsis* plant cells to activate its protease activity [143]. Cyclophilin was found to mediate structural folding of AvrRpt2 through its binding and peptidyl-prolyl isomerase activity [144]. These effectors are representative examples that serve to exemplify how effector-activation by a eukaryotic factor is a strategy widely used by different T3SS effectors from numerous pathogenic bacteria.

VPA1380 is homologous to two partially characterized T3SS effector proteins. A homolog from pathogenic *E. coli* strains, named Ibe, was demonstrated through pull down experiments and localization studies to interact with the scaffolding protein IQGAP1 at the bacterial-induced pedestal [145]. Notably, the putative Cys-His active site in Ibe contains an aspartatic acid residue in place of the histidine **(Figure 20A)**. This substitution suggests the function of Ibe may be independent of its putative protease activity. Another homolog, OspB from *S. flexneri*, was shown to share several traits with the effector OspF that inhibits the MAPK pathway[84], but another study found OspB activates the NFκB pathway in a GEF-H1 dependent manner [85]. While VPA1380 was toxic to yeast in non-stress conditions, OspB was shown to only reduce yeast growth when yeast were grown under stress conditions in the presence of caffeine, a purine analog that elicits pleiotropic effects in yeast. [109]. VPA1380's toxicity was exacerbated by osmotic stress, which is toxic to yeast with disruptions in ion homeostasis or the MAPK equivalent HOG (High Osmolarity Glycerol) pathway [107]. Therefore, VPA1380 may target a different eukaryotic pathway than OspB that is required for growth under normal conditions (in the absence of stress) and osmotic stress.

Additionally, VPA1380 C/A was found to interact with Ndel1 and Vps52 in a yeast 2-hybrid system. Since both Ndel1 and Vps52 are involved in retrograde trafficking, their potential interaction with VPA1380 may play a role in VPA1380's ability to block Dextran uptake and disrupt the retrograde trafficking of Tfn in certain assays. The cytoplasmic dynein motor complex, which includes NdeL1, is required for macropinocytosis of dextran [146] and retrograde transport of Tfn [147]. Vps52 has only been shown to be responsible for

vesicle transport at the TGN [127], but altering Vps52's function may have downstream effects that alter other trafficking networks. Many intracellular and extracellular pathogens produce effector proteins that disrupt host vesicle trafficking in different ways to block innate immunity pathways and prevent phagocytosis [148]. Future studies are required to determine if VPA1380 plays a similar role during *V. parahaemolyticus* infection.

As pathogenic strains of *V. parahaemolyticus* become more prevalent around the world, it is important to understand the bacteria's virulence mechanisms for diagnostic and treatment purposes. The discovery of VPA1380 as a T3SS2 effector adds a new component to the wide repertoire of *V. parahaemolyticus* virulence factors. By understanding VPA1380's similarities to the CPD of MARTX and CGT toxins, we are closer to understanding the function of VPA1380 and identifying its cellular target. Future studies will provide insight on how VPA1380 and its close homologs contribute to the infection process of *V. parahaemolyticus* and other major pathogens, and whether it plays a role in the T3SS2-mediated host cell invasion of *V. parahaemolyticus*.

CHAPTER FIVE
Conclusion and Future Directions

CONCLUSION

V. parahaemolyticus pathogenicity

V. parahaemolyticus is one of the leading causes of seafood-derived gastroenteritis throughout the world [37]. This pathogenic bacterium encodes two T3SS's, T3SS1 and T3SS2, that translocate a separate repertoire of effectors to mediate different cellular effects [92], though only T3SS2 has been linked to the gastroenteritis disease[42,71,78,92]. As *V. parahaemolyticus* has become a major world pathogen, it is important to characterize the factors and regulatory mechanisms involved in pathogenesis to better understand the infection process of this bacterium. To this end, we analyzed different virulence-related systems in relationship to T3SS1 and T3SS2 functionality and regulation, and explored the functional role of the T3SS2 effector VPA1380.

Regulatory versus structural T3SS mutants

From microarray and RNAseq studies, both ExsA and VtrA were shown to control expression of genes outside the T3SS pathogenicity islands [46,70,83]. Therefore, the regulation of T3SS1 and T3SS2 may also be tied to other virulence systems. To address this hypothesis, we investigated the virulence differences between structural and regulatory mutants of *V. parahaemolyticus*. The genes for proteins in the inner membrane ring of the needle apparatus of the T3SS basal structures **(Figure 7A)** were eliminated to create the POR2 and POR3 strains that no longer formed the secretion apparatus for T3SS1 and T3SS2,

respectively **(Table 4)**. Both of these structural mutants provide the same outcome of effector production without effector secretion due to a crippled needle apparatus [37]. The transcriptional regulators of both T3SS1 (*exsA*) and T3SS2 (*vtrA*) were eliminated to create the CAB2 and CAB3 strains, respectively **(Figure 7B and 7C)**. These transcriptional mutants are deficient in both effector and needle production [73] **(Table 4)**. The purpose of this study was to compare the virulence capability of the POR and CAB strains and to speculate about the potential relationships of virulence systems that could be positive or negatively regulated with each T3SS.

Many studies of *V. parahaemolyticus* have shown that swarming and T3SS1 are both induced by quorum sensing at low cell density, surface sensing, and levels of calcium or iron [21,29,99]. Swarming is an important virulence phenotype since many bacteria use lateral flagella to crawl across hard surfaces and migrate to sites of infection [98]. In *V. parahaemolyticus*, the production of lateral flagella genes is controlled by the σ54 dependent master regulator, LafK [19,97], but the relationship between this regulator and T3SS1 gene activation is unknown. Overexpressing *exsA* is also known to down-regulate swarming genes, suggesting that the two systems might operate in a negative feedback loop involving a positive and negative relationship [99]. Despite this complex relationship, which was only observed in environmental strains, we found no variation in swarming between the T3SS mutants in any induction condition. This result demonstrates that swarming genes are independent of T3SS1 and T3SS2 gene regulation, but this regulatory control may also be strain dependent.

Biofilm production is another virulence-related factor in *V. parahaemolyticus* that is important for bacterial survival in harsh environmental conditions [25]. To create these biofilms, *V. parahaemolyticus* produces extra-polysaccharides and two Type IV pili, chitin-regulated pilus (ChiRP) and mannose-sensitive hemagglutinin (MSHA), that are used for surface attachment [24,26]. Studies have shown that biofilm production is inversely regulated with swarming and T3SS1 induction [35,101]. For example, when bacteria were grown in surface-sensing conditions, they down regulated MSHA genes, and increased expression of swarming and T3SS1 genes [21]. While we did not find a difference in biofilm growth from strains under T3SS1 inducing conditions, we found that T3SS2 regulatory mutants could produce larger biofilms than other strains grown in T3SS2 inducing conditions. Furthermore, these other strains that are capable of expressing T3SS2 genes produced less biofilm mass than similar strains in non-induced conditions. This supports the hypothesis that VtrA, the T3SS2 master regulator, directly or indirectly turns off the biofilm state.

This inverse relationship is known to be regulated, in part, by levels of the signaling molecule, cyclic-di-GMP [33]. This second messenger controls many molecular networks in bacteria to induce biofilm growth and repress motility and T3SS expression. Proteins with diguanylate cyclase GGDEF domains are responsible for producing the molecule c-di-GMP, which can then be broken down by phosphodiesterases with an EAL domain [32]. Little data exist to explain T3SS2's involvement in c-di-GMP regulation, but the T3SS2 pathogenicity island contains the gene, *vpa1324*, which encodes a protein with a phosphodiesterase EAL domain. Expression of this gene is induced by bile salts and upon host cell contact [46], which may alter the virulence state and biofilm production ability of the bacterium. The

signaling capabilities of c-di-GMP may explain the inverse relationship seen in this study between T3SS2 gene expression and biofilm growth.

We next tested the POR and CAB strains for differences in effector secretion and found no differences POR and CAB strains. Interestingly, under T3SS1 induction, POR1 and POR3 produced higher levels of effector proteins than POR2 and POR4, which implicates a regulatory factor that requires a functional needle apparatus. ExsE, a T3SS1 negative regulator and secreted substrate [54], is likely responsible for this difference in effector production. In this study, the POR2 and POR4 strains should be unable to secrete ExsE from the bacterium, since they both contain a non-function T3SS1 needle apparatus. Therefore, ExsE is likely trapped in these cells and represses the expression of T3SS1 genes.

From tissue culture infection experiments, we found the POR and CAB equivalent strains caused host cell lysis at a similar rate from either T3SS1 or T3SS2 induction. Therefore, the T3SS structural and regulatory mutants do not differ in the timing of host-cell death. The LDH cell lysis assay only measures the final outcome of infection though, and does not account for the processes occurring between the bacteria and the host cell. To examine other parameters of infection, we monitored actin rearrangement during T3SS1-induced infection and also invasiveness during T3SS2-induced infection. These parameters revealed an interesting finding during T3SS2-induced infection. CAB2, a T3SS1 regulatory mutant, invaded HeLa cells with an efficacy over 10 fold higher than that of POR2, a T3SS1 structural mutant. Since CAB2 and POR2 do not differ in level of effector secretion, the reason for this increase in apparent invasion is unknown. One possibility is that CAB2

transitions into a hyperproliferative state intracellularly that allows it to replicate faster than POR2. This hyperproliferative state has been observed with the bacterium *Salmonella* [103].

Characterization of the T3SS2 effector VPA1380

In this study we confirm that a T3SS2 gene, termed *vpa1380*, encodes an effector protein that is secreted and translocated into host cells in a T3SS2 dependent manner. VPA1380 does not contain any conserved domains, but by analyzing the predicted secondary structure of the protein, we uncovered sequence similarities between VPA1380 and the cysteine protease domain of MARTX and CGT toxins. Importantly, the most similar residues were also necessary for catalytic activity and IP6-activation of these proteases [110,111,138,139].

By studying VPA1380's effects in yeast, we found that the putative catalytic and IP6-binding residues are critical for VPA1380's toxicity in yeast. Since the MARTX and CGT toxins require IP6 to activate the activity of the cysteine protease domain, we expressed VPA1380 in IP6 deficient strains of yeast and confirmed that VPA1380 does in fact require IP6 for toxicity. Notably, the MARTX and CGT toxins are autoprocessing proteases, but we did not observe a cleavage fragment when VPA1380 was expressed in yeast. Therefore, VPA1380 may share functional similarity, as well as amino acid similarity, with the cysteine protease domain of MARTX and CGT toxins, but probably targets a host protein.

VPA1380's role in the host cell is unclear from studies performed on the homologs Ibe from *E. coli* and OspB from *S. flexneri*. The effector Ibe was shown to interact with the scaffolding protein IQGAP1 at the bacterial-induced pedestal site, but the purpose of this

interaction is unknown [145]. Also, Ibe does not contain the conserved histidine within the putative Cys-His active site, suggesting it may have a different mechanism. The role of the effector OspB is currently unclear because it has been shown to inhibit the MAPK pathway [84], but also activate the NFκB pathway in a GEF-H1 dependent manner [85]. Furthermore, no host targets of OspB have been confirmed. Although VPA1380 is homologous to OspB, it may have a different function in the host cell since VPA1380 caused a different level of toxicity in yeast. OspB only reduced yeast growth when the yeast were grown in the presence of caffeine, a stressing agent that causes pleiotrophic effects in yeast [109]. In contrast, VPA1380 was toxic to yeast under non-stressing conditions and caused greater toxicity in the presence of osmotic stress. Therefore, VPA1380 may have a different function in the host cell than its close homologs because of key differences in amino acid composition and host cell toxicity.

To determine the role of VPA1380 in the host cell, we examined VPA1380 C/A in a yeast 2-hybrid system. The positive clones included the Lis1-binding region of Ndel1, which is crucial for dynein motor transport [118,121], and the C-terminus of Vps52, a TGN tethering protein. Both of these hits are involved in moving vesicles in a retrograde direction toward the perinuclear region of the cell [124,127,128]. This is of particular interest because GFP-VPA1380 localized in vesicles in the perinuclear region. Also, GFP-VPA1380 C/A co-localized with the Golgi apparatus, implicating a possible interaction with Vps52. Interestingly, VPA1380 appeared to diminish Ndel1 protein levels when both *gfp-vpa1380-V5* and *ha-Ndel1-flag* were co-transfected in HeLa cells, but this effect was not observed

with the *Y. pseudotuberculosis* infection model. VPA1380 did not appear to alter Vps52 protein levels in co-transfection experiments.

Despite a lack of evidence confirming the interaction of VPA1380 with these crucial components of the retrograde trafficking network, we examined if VPA1380 alters retrograde trafficking. Interestingly, overexpression of VPA1380 in HeLa cells was able to block the uptake of Texas red dextran, which is a fluid-phase marker of macropinocytosis and endosome-lysosome trafficking [136]. This was dependent on the putative catalytic activity of VPA1380 but we could not confirm this effect with the *Y. pseudotuberculosis* infection model. Interestingly VPA1380 did appear to inhibit the perinuclear localization of Tfn, a marker of clathrin-mediated endocytosis and recycling endosome trafficking [137], using the *Y. pseudotuberculosis* infection model. These trafficking results may provide insight on the role of VPA1380 because Ndel1 is required for the macropinocytosis-mediated uptake of dextran [146] and the retrograde transport of Tfn [147]. Vps52 is necessary for vesicle transport at the TGN [127], but disrupting Vps52's function may have downstream effects that alter other trafficking networks. Therefore, VPA1380 may interact with Ndel1 or Vps52 in an unknown manner to disrupt a key component of retrograde trafficking. *V. parahaemolyticus* is an intracellular pathogen, so we may only see these effects in the context of an infection with the bacteria-containing vacuole in the presence of other effectors.

FUTURE DIRECTIONS

Transcriptional differences of POR and CAB strains

To understand the virulence differences between the POR and CAB strains, RNA sequencing technology will be used to determine the transcriptional differences of each POR and CAB strain under T3SS1 and T3SS2 inducing conditions. POR1, POR2, POR3, CAB2, and CAB3 will be induced in DMEM (T3SS1 inducing condition) and LB with 0.05% bile salts (T3SS2 inducing condition) and RNA levels will be examined by RNA-seq. The sequencing data will likely provide information that explains the differences seen in biofilm formation. For example, the strains may differ in levels of transcripts for Type IV pili or proteins containing a GGDEF or EAL domain, which aide or regulate biofilm formation [24-26]. Other significant differences in transcripts may address the mystery of why CAB2 invades better than POR2, and even suggest further virulence differences not examined in this study.

ExsE

As explained above, ExsE is likely the regulatory factor responsible for reducing effector production in POR2 and POR4 strains during T3SS1 inducing conditions. To determine if this effect is transcriptional, and not due to effector degradation, qRT-PCR will be used to examine the relative amount of effector transcripts in the POR1, POR2, POR3, POR4, CAB2, CAB3, and CAB4 strains during T3SS1 inducing conditions. The *exsE* gene can also be knocked out in these strains to confirm that the differences in effector production are due to the regulation by ExsE. These mutant strains should constitutively produce T3SS1 effectors at a similar rate.

Host interaction partners

VPA1380 C/A interacted with Ndel1 and the C-terminus of Vps52 in a yeast 2-hybrid system. To confirm this interaction, pull-downs experiment will be performed *in vitro* with recombinant proteins. Recombinant full-length VPA1380 was insoluble and could not be isolated from bacterial pellets, so VPA1380 will be purified from a eukaryotic system such as yeast or insect cells. This may assist protein folding, since effectors are normally folded in eukaryotic cells. Additionally, the presence of IP6 may help VPA1380 fold, since IP6 is known to alter the protein structure of MARTX and CGT toxins [111,114]. To verify the interaction of VPA1380 with Ndel1 and Vps52 inside cells, *vpa1380-strep* and the yeast 2-hybrid hits will be co-transfected in cells, and VPA1380-strep will be isolated with high affinity Strep-Tactin beads (Qiagen). If binding is confirmed, Ndel1 or Vps52 will be truncated to determine the minimal binding site. While VPA1380 may not cleave Ndel1 or Vps52, it may bind to these proteins for localization purposes. Recombinant VPA1380 and VPA1380-Strep will also be used to identify potential new interaction partners, by performing pull down experiments with eukaryotic cell lysate.

Localization of VPA1380

GFP-VPA1380 and GFP-VPA1380 C/A both formed vesicle-like punctate structures in the cellular perinuclear region, and GFP-VPA1380 C/A also co-localized with the Golgi apparatus. The identity of these vesicles-like punctate structures is unknown because they did not co-localize with early endosomes, recycling endosomes, or lysosomes. Additional endosomal Rab markers will be used to confirm the identity of these vesicles. To determine

VPA1380's localization domain, protein truncations fused to GFP will be examined by cellular localization. Many effectors bind to host phosphoinositides to mediate localization [60,63], so recombinant VPA1380 will be tested for potential interaction with several host phosphoinositides on a filter member. Additionally, bioinformatics analysis will be performed to identify positive charged amino acids that may potentially interact with phosphoinositides.

Retrograde trafficking

VPA1380 appeared to disrupt the uptake of Texas red dextran and the perinuclear localization of Tfn in certain assays. Shiga toxin b-subunit (STxB) is another retrograde trafficking tool that is commonly used to monitor endosome-Golgi trafficking. This subunit is well studied and understood to be receptor-mediated endocytosed into early endosomes and transported through the Golgi in a retrograde direction [129]. This trafficking marker should be used to determine if VPA1380 affects the transport of vesicles to the Golgi. All of the trafficking experiments mentioned above will be confirmed with transfection and infection experiments, including the *Y. pseudotuberculosis* infection model and *V. parahaemolyticus* POR strains. VPA1380 may assist the intracellular lifestyle of *V. parahaemolyticus* because this bacterium is thought to reside within a vacuole during part of its infection process [73]. To fully understand how VPA1380 may assist this process, we will explore if VPA1380 alters dynamics of the bacteria-containing vacuole. First, *V. parahaemolyticus* expressing *gfp* will be monitored during infection with several vesicle markers to determine the identity of the vacuole surrounding the bacteria. Second, the

vacuole will be examined with a *vpa1380* mutant of *V. parahaemolyticus* to determine if VPA1380 alters the maturation of the vacuole. Third, we will determine if VPA1380 is required to prevent the normal lysosomal destruction of endocytosed bacteria. These experiments will help to better understand the infection process of *V. parahaemolyticus*.

BIBLIOGRAPHY

1. Shinoda S (2011) Sixty years from the discovery of Vibrio parahaemolyticus and some recollections. Biocontrol Sci 16: 129-137.
2. Joseph SW, Colwell RR, Kaper JB (1982) Vibrio parahaemolyticus and related halophilic Vibrios. Crit Rev Microbiol 10: 77-124.
3. Yeung PS, Boor KJ (2004) Epidemiology, pathogenesis, and prevention of foodborne Vibrio parahaemolyticus infections. Foodborne Pathog Dis 1: 74-88.
4. Newton A, Kendall M, Vugia DJ, Henao OL, Mahon BE (2012) Increasing rates of vibriosis in the United States, 1996-2010: review of surveillance data from 2 systems. Clin Infect Dis 54 Suppl 5: S391-395.
5. Nair GB, Ramamurthy T, Bhattacharya SK, Dutta B, Takeda Y, et al. (2007) Global dissemination of Vibrio parahaemolyticus serotype O3:K6 and its serovariants. Clin Microbiol Rev 20: 39-48.
6. Iwamoto M, Ayers T, Mahon BE, Swerdlow DL (2010) Epidemiology of seafood-associated infections in the United States. Clin Microbiol Rev 23: 399-411.
7. Su YC, Liu C (2007) Vibrio parahaemolyticus: a concern of seafood safety. Food Microbiol 24: 549-558.
8. Tran L, Nunan L, Redman RM, Mohney LL, Pantoja CR, et al. (2013) Determination of the infectious nature of the agent of acute hepatopancreatic necrosis syndrome affecting penaeid shrimp. Dis Aquat Organ 105: 45-55.
9. De Schryver P, Defoirdt T, Sorgeloos P (2014) Early mortality syndrome outbreaks: a microbial management issue in shrimp farming? PLoS Pathog 10: e1003919.
10. CDC (2013) National Enteric Disease Surveillance: COVIS Annual Summary, 2011.
11. McCarter L (1999) The multiple identities of Vibrio parahaemolyticus. J Mol Microbiol Biotechnol 1: 51-57.
12. Martinez-Urtaza J, Blanco-Abad V, Rodriguez-Castro A, Ansede-Bermejo J, Miranda A, et al. (2012) Ecological determinants of the occurrence and dynamics of Vibrio parahaemolyticus in offshore areas. ISME J 6: 994-1006.
13. Gamble MD, Lovell CR (2011) Infaunal burrows are enrichment zones for Vibrio parahaemolyticus. Appl Environ Microbiol 77: 3703-3714.
14. McLaughlin JB, DePaola A, Bopp CA, Martinek KA, Napolilli NP, et al. (2005) Outbreak of Vibrio parahaemolyticus gastroenteritis associated with Alaskan oysters. N Engl J Med 353: 1463-1470.
15. Garcia K, Bastias R, Higuera G, Torres R, Mellado A, et al. (2013) Rise and fall of pandemic Vibrio parahaemolyticus serotype O3:K6 in southern Chile. Environ Microbiol 15: 527-534.
16. Centers for Disease C, Prevention (2005) Vibrio illnesses after Hurricane Katrina--multiple states, August-September 2005. MMWR Morb Mortal Wkly Rep 54: 928-931.
17. Mudoh MF, Parveen S, Schwarz J, Rippen T, Chaudhuri A (2014) The Effects of Storage Temperature on the Growth of Vibrio parahaemolyticus and Organoleptic Properties in Oysters. Front Public Health 2: 45.

18. Kim YK, McCarter LL (2000) Analysis of the polar flagellar gene system of Vibrio parahaemolyticus. J Bacteriol 182: 3693-3704.
19. Zhu S, Kojima S, Homma M (2013) Structure, gene regulation and environmental response of flagella in Vibrio. Front Microbiol 4: 410.
20. Kim YK, McCarter LL (2004) Cross-regulation in Vibrio parahaemolyticus: compensatory activation of polar flagellar genes by the lateral flagellar regulator LafK. J Bacteriol 186: 4014-4018.
21. Gode-Potratz CJ, Kustusch RJ, Breheny PJ, Weiss DS, McCarter LL (2011) Surface sensing in Vibrio parahaemolyticus triggers a programme of gene expression that promotes colonization and virulence. Mol Microbiol 79: 240-263.
22. Stewart BJ, Enos-Berlage JL, McCarter LL (1997) The lonS gene regulates swarmer cell differentiation of Vibrio parahaemolyticus. J Bacteriol 179: 107-114.
23. Enos-Berlage JL, McCarter LL (2000) Relation of capsular polysaccharide production and colonial cell organization to colony morphology in Vibrio parahaemolyticus. J Bacteriol 182: 5513-5520.
24. Enos-Berlage JL, Guvener ZT, Keenan CE, McCarter LL (2005) Genetic determinants of biofilm development of opaque and translucent Vibrio parahaemolyticus. Mol Microbiol 55: 1160-1182.
25. Yildiz FH, Visick KL (2009) Vibrio biofilms: so much the same yet so different. Trends Microbiol 17: 109-118.
26. Shime-Hattori A, Iida T, Arita M, Park KS, Kodama T, et al. (2006) Two type IV pili of Vibrio parahaemolyticus play different roles in biofilm formation. FEMS Microbiol Lett 264: 89-97.
27. Krachler AM, Ham H, Orth K (2011) Outer membrane adhesion factor multivalent adhesion molecule 7 initiates host cell binding during infection by gram-negative pathogens. Proc Natl Acad Sci U S A 108: 11614-11619.
28. Rutherford ST, Bassler BL (2012) Bacterial quorum sensing: its role in virulence and possibilities for its control. Cold Spring Harb Perspect Med 2.
29. Gode-Potratz CJ, McCarter LL (2011) Quorum sensing and silencing in Vibrio parahaemolyticus. J Bacteriol 193: 4224-4237.
30. McCarter LL (1998) OpaR, a homolog of Vibrio harveyi LuxR, controls opacity of Vibrio parahaemolyticus. J Bacteriol 180: 3166-3173.
31. Wang L, Ling Y, Jiang H, Qiu Y, Qiu J, et al. (2013) AphA is required for biofilm formation, motility, and virulence in pandemic Vibrio parahaemolyticus. Int J Food Microbiol 160: 245-251.
32. Sondermann H, Shikuma NJ, Yildiz FH (2012) You've come a long way: c-di-GMP signaling. Curr Opin Microbiol 15: 140-146.
33. Kim YK, McCarter LL (2007) ScrG, a GGDEF-EAL protein, participates in regulating swarming and sticking in Vibrio parahaemolyticus. J Bacteriol 189: 4094-4107.
34. Trimble MJ, McCarter LL (2011) Bis-(3'-5')-cyclic dimeric GMP-linked quorum sensing controls swarming in Vibrio parahaemolyticus. Proc Natl Acad Sci U S A 108: 18079-18084.

35. Ferreira RB, Antunes LC, Greenberg EP, McCarter LL (2008) Vibrio parahaemolyticus ScrC modulates cyclic dimeric GMP regulation of gene expression relevant to growth on surfaces. J Bacteriol 190: 851-860.
36. Makino K, Oshima K, Kurokawa K, Yokoyama K, Uda T, et al. (2003) Genome sequence of Vibrio parahaemolyticus: a pathogenic mechanism distinct from that of V cholerae. Lancet 361: 743-749.
37. Broberg CA, Calder TJ, Orth K (2011) Vibrio parahaemolyticus cell biology and pathogenicity determinants. Microbes Infect 13: 992-1001.
38. Nishibuchi M, Kaper JB (1995) Thermostable direct hemolysin gene of Vibrio parahaemolyticus: a virulence gene acquired by a marine bacterium. Infect Immun 63: 2093-2099.
39. Meador CE, Parsons MM, Bopp CA, Gerner-Smidt P, Painter JA, et al. (2007) Virulence gene- and pandemic group-specific marker profiling of clinical Vibrio parahaemolyticus isolates. J Clin Microbiol 45: 1133-1139.
40. Park KS, Ono T, Rokuda M, Jang MH, Iida T, et al. (2004) Cytotoxicity and enterotoxicity of the thermostable direct hemolysin-deletion mutants of Vibrio parahaemolyticus. Microbiol Immunol 48: 313-318.
41. Hiyoshi H, Kodama T, Iida T, Honda T (2010) Contribution of Vibrio parahaemolyticus virulence factors to cytotoxicity, enterotoxicity, and lethality in mice. Infect Immun 78: 1772-1780.
42. Ritchie JM, Rui H, Zhou X, Iida T, Kodoma T, et al. (2012) Inflammation and disintegration of intestinal villi in an experimental model for Vibrio parahaemolyticus-induced diarrhea. PLoS Pathog 8: e1002593.
43. Yanagihara I, Nakahira K, Yamane T, Kaieda S, Mayanagi K, et al. (2010) Structure and functional characterization of Vibrio parahaemolyticus thermostable direct hemolysin. J Biol Chem 285: 16267-16274.
44. Matsuda S, Kodama T, Okada N, Okayama K, Honda T, et al. (2010) Association of Vibrio parahaemolyticus thermostable direct hemolysin with lipid rafts is essential for cytotoxicity but not hemolytic activity. Infect Immun 78: 603-610.
45. Ohnishi K, Nakahira K, Unzai S, Mayanagi K, Hashimoto H, et al. (2011) Relationship between heat-induced fibrillogenicity and hemolytic activity of thermostable direct hemolysin and a related hemolysin of Vibrio parahaemolyticus. FEMS Microbiol Lett 318: 10-17.
46. Gotoh K, Kodama T, Hiyoshi H, Izutsu K, Park KS, et al. (2010) Bile acid-induced virulence gene expression of Vibrio parahaemolyticus reveals a novel therapeutic potential for bile acid sequestrants. PLoS One 5: e13365.
47. Radics J, Konigsmaier L, Marlovits TC (2014) Structure of a pathogenic type 3 secretion system in action. Nat Struct Mol Biol 21: 82-87.
48. Galan JE, Wolf-Watz H (2006) Protein delivery into eukaryotic cells by type III secretion machines. Nature 444: 567-573.
49. Marlovits TC, Kubori T, Sukhan A, Thomas DR, Galan JE, et al. (2004) Structural insights into the assembly of the type III secretion needle complex. Science 306: 1040-1042.

50. Chen L, Ai X, Portaliou AG, Minetti CA, Remeta DP, et al. (2013) Substrate-activated conformational switch on chaperones encodes a targeting signal in type III secretion. Cell Rep 3: 709-715.
51. Lara-Tejero M, Kato J, Wagner S, Liu X, Galan JE (2011) A sorting platform determines the order of protein secretion in bacterial type III systems. Science 331: 1188-1191.
52. Yahr TL, Wolfgang MC (2006) Transcriptional regulation of the Pseudomonas aeruginosa type III secretion system. Mol Microbiol 62: 631-640.
53. Zhou X, Shah DH, Konkel ME, Call DR (2008) Type III secretion system 1 genes in Vibrio parahaemolyticus are positively regulated by ExsA and negatively regulated by ExsD. Mol Microbiol 69: 747-764.
54. Kodama T, Yamazaki C, Park KS, Akeda Y, Iida T, et al. (2010) Transcription of Vibrio parahaemolyticus T3SS1 genes is regulated by a dual regulation system consisting of the ExsACDE regulatory cascade and H-NS. FEMS Microbiol Lett 311: 10-17.
55. Rietsch A, Vallet-Gely I, Dove SL, Mekalanos JJ (2005) ExsE, a secreted regulator of type III secretion genes in Pseudomonas aeruginosa. Proc Natl Acad Sci U S A 102: 8006-8011.
56. McCaw ML, Lykken GL, Singh PK, Yahr TL (2002) ExsD is a negative regulator of the Pseudomonas aeruginosa type III secretion regulon. Mol Microbiol 46: 1123-1133.
57. Hovey AK, Frank DW (1995) Analyses of the DNA-binding and transcriptional activation properties of ExsA, the transcriptional activator of the Pseudomonas aeruginosa exoenzyme S regulon. J Bacteriol 177: 4427-4436.
58. Burdette DL, Yarbrough ML, Orvedahl A, Gilpin CJ, Orth K (2008) Vibrio parahaemolyticus orchestrates a multifaceted host cell infection by induction of autophagy, cell rounding, and then cell lysis. Proc Natl Acad Sci U S A 105: 12497-12502.
59. Sreelatha A, Bennett TL, Zheng H, Jiang QX, Orth K, et al. (2013) Vibrio effector protein, VopQ, forms a lysosomal gated channel that disrupts host ion homeostasis and autophagic flux. Proc Natl Acad Sci U S A 110: 11559-11564.
60. Broberg CA, Zhang L, Gonzalez H, Laskowski-Arce MA, Orth K (2010) A Vibrio effector protein is an inositol phosphatase and disrupts host cell membrane integrity. Science 329: 1660-1662.
61. Yarbrough ML, Li Y, Kinch LN, Grishin NV, Ball HL, et al. (2009) AMPylation of Rho GTPases by Vibrio VopS disrupts effector binding and downstream signaling. Science 323: 269-272.
62. Higa N, Toma C, Koizumi Y, Nakasone N, Nohara T, et al. (2013) Vibrio parahaemolyticus effector proteins suppress inflammasome activation by interfering with host autophagy signaling. PLoS Pathog 9: e1003142.
63. Salomon D, Guo Y, Kinch LN, Grishin NV, Gardner KH, et al. (2013) Effectors of animal and plant pathogens use a common domain to bind host phosphoinositides. Nat Commun 4: 2973.

64. Zhang L, Orth K (2013) Virulence determinants for Vibrio parahaemolyticus infection. Curr Opin Microbiol 16: 70-77.
65. Burdette DL, Seemann J, Orth K (2009) Vibrio VopQ induces PI3-kinase-independent autophagy and antagonizes phagocytosis. Mol Microbiol 73: 639-649.
66. Whisstock JC, Wiradjaja F, Waters JE, Gurung R (2002) The structure and function of catalytic domains within inositol polyphosphate 5-phosphatases. IUBMB Life 53: 15-23.
67. Raucher D, Stauffer T, Chen W, Shen K, Guo S, et al. (2000) Phosphatidylinositol 4,5-bisphosphate functions as a second messenger that regulates cytoskeleton-plasma membrane adhesion. Cell 100: 221-228.
68. Casselli T, Lynch T, Southward CM, Jones BW, DeVinney R (2008) Vibrio parahaemolyticus inhibition of Rho family GTPase activation requires a functional chromosome I type III secretion system. Infect Immun 76: 2202-2211.
69. Luong P, Kinch LN, Brautigam CA, Grishin NV, Tomchick DR, et al. (2010) Kinetic and structural insights into the mechanism of AMPylation by VopS Fic domain. J Biol Chem 285: 20155-20163.
70. Kodama T, Gotoh K, Hiyoshi H, Morita M, Izutsu K, et al. (2010) Two regulators of Vibrio parahaemolyticus play important roles in enterotoxicity by controlling the expression of genes in the Vp-PAI region. PLoS One 5: e8678.
71. Pineyro P, Zhou X, Orfe LH, Friel PJ, Lahmers K, et al. (2010) Development of two animal models to study the function of Vibrio parahaemolyticus type III secretion systems. Infect Immun 78: 4551-4559.
72. Qadri F, Alam MS, Nishibuchi M, Rahman T, Alam NH, et al. (2003) Adaptive and inflammatory immune responses in patients infected with strains of Vibrio parahaemolyticus. J Infect Dis 187: 1085-1096.
73. Zhang L, Krachler AM, Broberg CA, Li Y, Mirzaei H, et al. (2012) Type III effector VopC mediates invasion for Vibrio species. Cell Rep 1: 453-460.
74. Aktories K, Barbieri JT (2005) Bacterial cytotoxins: targeting eukaryotic switches. Nat Rev Microbiol 3: 397-410.
75. Okada R, Zhou X, Hiyoshi H, Matsuda S, Chen X, et al. (2014) The Vibrio parahaemolyticus effector VopC mediates Cdc42-dependent invasion of cultured cells but is not required for pathogenicity in an animal model of infection. Cell Microbiol 16: 938-947.
76. Trosky JE, Mukherjee S, Burdette DL, Roberts M, McCarter L, et al. (2004) Inhibition of MAPK signaling pathways by VopA from Vibrio parahaemolyticus. J Biol Chem 279: 51953-51957.
77. Trosky JE, Li Y, Mukherjee S, Keitany G, Ball H, et al. (2007) VopA inhibits ATP binding by acetylating the catalytic loop of MAPK kinases. J Biol Chem 282: 34299-34305.
78. Zhou X, Gewurz BE, Ritchie JM, Takasaki K, Greenfeld H, et al. (2013) A Vibrio parahaemolyticus T3SS effector mediates pathogenesis by independently enabling intestinal colonization and inhibiting TAK1 activation. Cell Rep 3: 1690-1702.

79. Liverman AD, Cheng HC, Trosky JE, Leung DW, Yarbrough ML, et al. (2007) Arp2/3-independent assembly of actin by Vibrio type III effector VopL. Proc Natl Acad Sci U S A 104: 17117-17122.
80. Zahm JA, Padrick SB, Chen Z, Pak CW, Yunus AA, et al. (2013) The bacterial effector VopL organizes actin into filament-like structures. Cell 155: 423-434.
81. Hiyoshi H, Kodama T, Saito K, Gotoh K, Matsuda S, et al. (2011) VopV, an F-actin-binding type III secretion effector, is required for Vibrio parahaemolyticus-induced enterotoxicity. Cell Host Microbe 10: 401-409.
82. Kodama T, Rokuda M, Park KS, Cantarelli VV, Matsuda S, et al. (2007) Identification and characterization of VopT, a novel ADP-ribosyltransferase effector protein secreted via the Vibrio parahaemolyticus type III secretion system 2. Cell Microbiol 9: 2598-2609.
83. Nydam SD, Shah DH, Call DR (2014) Transcriptome analysis of Vibrio parahaemolyticus in type III secretion system 1 inducing conditions. Front Cell Infect Microbiol 4: 1.
84. Zurawski DV, Mumy KL, Faherty CS, McCormick BA, Maurelli AT (2009) Shigella flexneri type III secretion system effectors OspB and OspF target the nucleus to downregulate the host inflammatory response via interactions with retinoblastoma protein. Mol Microbiol 71: 350-368.
85. Fukazawa A, Alonso C, Kurachi K, Gupta S, Lesser CF, et al. (2008) GEF-H1 mediated control of NOD1 dependent NF-kappaB activation by Shigella effectors. PLoS Pathog 4: e1000228.
86. Salomon D, Sessa G (2010) Identification of growth inhibition phenotypes induced by expression of bacterial type III effectors in yeast. J Vis Exp.
87. O'Toole GA (2011) Microtiter dish biofilm formation assay. J Vis Exp.
88. Altschul SF, Madden TL, Schaffer AA, Zhang J, Zhang Z, et al. (1997) Gapped BLAST and PSI-BLAST: a new generation of protein database search programs. Nucleic Acids Res 25: 3389-3402.
89. Soding J, Biegert A, Lupas AN (2005) The HHpred interactive server for protein homology detection and structure prediction. Nucleic Acids Res 33: W244-248.
90. Pei J, Grishin NV (2014) PROMALS3D: multiple protein sequence alignment enhanced with evolutionary and three-dimensional structural information. Methods Mol Biol 1079: 263-271.
91. Cole C, Barber JD, Barton GJ (2008) The Jpred 3 secondary structure prediction server. Nucleic Acids Res 36: W197-201.
92. Park KS, Ono T, Rokuda M, Jang MH, Okada K, et al. (2004) Functional characterization of two type III secretion systems of Vibrio parahaemolyticus. Infect Immun 72: 6659-6665.
93. Salomon D, Klimko JA, Orth K (2014) H-NS regulates the Vibrio parahaemolyticus type VI secretion system 1. Microbiology.
94. Viboud GI, So SS, Ryndak MB, Bliska JB (2003) Proinflammatory signalling stimulated by the type III translocation factor YopB is counteracted by multiple effectors in epithelial cells infected with Yersinia pseudotuberculosis. Mol Microbiol 47: 1305-1315.

95. Hao YH, Wang Y, Burdette D, Mukherjee S, Keitany G, et al. (2008) Structural requirements for Yersinia YopJ inhibition of MAP kinase pathways. PLoS One 3: e1375.
96. Martinez-Urtaza J, Bowers JC, Trinanes J, DePaola A (2010) Climate anomalies and the increasing risk of Vibrio parahaemolyticus and Vibrio vulnificus illnesses. Food Research International 43: 1780-1790.
97. Stewart BJ, McCarter LL (2003) Lateral flagellar gene system of Vibrio parahaemolyticus. J Bacteriol 185: 4508-4518.
98. Kearns DB (2010) A field guide to bacterial swarming motility. Nat Rev Microbiol 8: 634-644.
99. Gode-Potratz CJ, Chodur DM, McCarter LL (2010) Calcium and iron regulate swarming and type III secretion in Vibrio parahaemolyticus. J Bacteriol 192: 6025-6038.
100. Boles BR, McCarter LL (2002) Vibrio parahaemolyticus scrABC, a novel operon affecting swarming and capsular polysaccharide regulation. J Bacteriol 184: 5946-5954.
101. Ferreira RB, Chodur DM, Antunes LC, Trimble MJ, McCarter LL (2012) Output targets and transcriptional regulation by a cyclic dimeric GMP-responsive circuit in the Vibrio parahaemolyticus Scr network. J Bacteriol 194: 914-924.
102. Okada R, Zhou X, Hiyoshi H, Matsuda S, Chen X, et al. (2013) The Vibrio parahaemolyticus effector VopC mediates Cdc42-dependent invasion of cultured cells but is not required for pathogenicity in an animal model of infection. Cell Microbiol.
103. Knodler LA, Vallance BA, Celli J, Winfree S, Hansen B, et al. (2010) Dissemination of invasive Salmonella via bacterial-induced extrusion of mucosal epithelia. Proc Natl Acad Sci U S A 107: 17733-17738.
104. Shimohata T, Takahashi A (2010) Diarrhea induced by infection of Vibrio parahaemolyticus. J Med Invest 57: 179-182.
105. Daniels NA, MacKinnon L, Bishop R, Altekruse S, Ray B, et al. (2000) Vibrio parahaemolyticus infections in the United States, 1973-1998. J Infect Dis 181: 1661-1666.
106. Salomon D, Gonzalez H, Updegraff BL, Orth K (2013) Vibrio parahaemolyticus type VI secretion system 1 is activated in marine conditions to target bacteria, and is differentially regulated from system 2. PLoS One 8: e61086.
107. Salomon D, Bosis E, Dar D, Nachman I, Sessa G (2012) Expression of Pseudomonas syringae type III effectors in yeast under stress conditions reveals that HopX1 attenuates activation of the high osmolarity glycerol MAP kinase pathway. Microbiology 158: 2859-2869.
108. Salomon D, Dar D, Sreeramulu S, Sessa G (2011) Expression of Xanthomonas campestris pv. vesicatoria type III effectors in yeast affects cell growth and viability. Mol Plant Microbe Interact 24: 305-314.
109. Slagowski NL, Kramer RW, Morrison MF, LaBaer J, Lesser CF (2008) A functional genomic yeast screen to identify pathogenic bacterial proteins. PLoS Pathog 4: e9.

110. Lupardus PJ, Shen A, Bogyo M, Garcia KC (2008) Small molecule-induced allosteric activation of the Vibrio cholerae RTX cysteine protease domain. Science 322: 265-268.
111. Pruitt RN, Chagot B, Cover M, Chazin WJ, Spiller B, et al. (2009) Structure-function analysis of inositol hexakisphosphate-induced autoprocessing in Clostridium difficile toxin A. J Biol Chem 284: 21934-21940.
112. Reineke J, Tenzer S, Rupnik M, Koschinski A, Hasselmayer O, et al. (2007) Autocatalytic cleavage of Clostridium difficile toxin B. Nature 446: 415-419.
113. Egerer M, Satchell KJ (2010) Inositol hexakisphosphate-induced autoprocessing of large bacterial protein toxins. PLoS Pathog 6: e1000942.
114. Prochazkova K, Shuvalova LA, Minasov G, Voburka Z, Anderson WF, et al. (2009) Structural and molecular mechanism for autoprocessing of MARTX toxin of Vibrio cholerae at multiple sites. J Biol Chem 284: 26557-26568.
115. York JD, Odom AR, Murphy R, Ives EB, Wente SR (1999) A phospholipase C-dependent inositol polyphosphate kinase pathway required for efficient messenger RNA export. Science 285: 96-100.
116. Chien CT, Bartel PL, Sternglanz R, Fields S (1991) The two-hybrid system: a method to identify and clone genes for proteins that interact with a protein of interest. Proc Natl Acad Sci U S A 88: 9578-9582.
117. To A, Bai Y, Shen A, Gong H, Umamoto S, et al. (2011) Yeast two hybrid analyses reveal novel binary interactions between human cytomegalovirus-encoded virion proteins. PLoS One 6: e17796.
118. Vallee RB, McKenney RJ, Ori-McKenney KM (2012) Multiple modes of cytoplasmic dynein regulation. Nat Cell Biol 14: 224-230.
119. Roberts AJ, Kon T, Knight PJ, Sutoh K, Burgess SA (2013) Functions and mechanics of dynein motor proteins. Nat Rev Mol Cell Biol 14: 713-726.
120. Allan VJ (2011) Cytoplasmic dynein. Biochem Soc Trans 39: 1169-1178.
121. Zylkiewicz E, Kijanska M, Choi WC, Derewenda U, Derewenda ZS, et al. (2011) The N-terminal coiled-coil of Ndel1 is a regulated scaffold that recruits LIS1 to dynein. J Cell Biol 192: 433-445.
122. McKenney RJ, Vershinin M, Kunwar A, Vallee RB, Gross SP (2010) LIS1 and NudE induce a persistent dynein force-producing state. Cell 141: 304-314.
123. Stehman SA, Chen Y, McKenney RJ, Vallee RB (2007) NudE and NudEL are required for mitotic progression and are involved in dynein recruitment to kinetochores. J Cell Biol 178: 583-594.
124. Bradshaw NJ, Hennah W, Soares DC (2013) NDE1 and NDEL1: twin neurodevelopmental proteins with similar 'nature' but different 'nurture'. Biomol Concepts 4: 447-464.
125. Li J, Lee WL, Cooper JA (2005) NudEL targets dynein to microtubule ends through LIS1. Nat Cell Biol 7: 686-690.
126. Derewenda U, Tarricone C, Choi WC, Cooper DR, Lukasik S, et al. (2007) The structure of the coiled-coil domain of Ndel1 and the basis of its interaction with Lis1, the causal protein of Miller-Dieker lissencephaly. Structure 15: 1467-1481.

127. Bonifacino JS, Hierro A (2011) Transport according to GARP: receiving retrograde cargo at the trans-Golgi network. Trends Cell Biol 21: 159-167.
128. Conibear E, Stevens TH (2000) Vps52p, Vps53p, and Vps54p form a novel multisubunit complex required for protein sorting at the yeast late Golgi. Mol Biol Cell 11: 305-323.
129. Johannes L, Popoff V (2008) Tracing the retrograde route in protein trafficking. Cell 135: 1175-1187.
130. Scott CC, Vacca F, Gruenberg J (2014) Endosome maturation, transport and functions. Semin Cell Dev Biol 31C: 2-10.
131. Murshid A, Presley JF (2004) ER-to-Golgi transport and cytoskeletal interactions in animal cells. Cell Mol Life Sci 61: 133-145.
132. Yu IM, Hughson FM (2010) Tethering factors as organizers of intracellular vesicular traffic. Annu Rev Cell Dev Biol 26: 137-156.
133. Hutagalung AH, Novick PJ (2011) Role of Rab GTPases in membrane traffic and cell physiology. Physiol Rev 91: 119-149.
134. Presley JF, Cole NB, Schroer TA, Hirschberg K, Zaal KJ, et al. (1997) ER-to-Golgi transport visualized in living cells. Nature 389: 81-85.
135. Burnaevskiy N, Fox TG, Plymire DA, Ertelt JM, Weigele BA, et al. (2013) Proteolytic elimination of N-myristoyl modifications by the Shigella virulence factor IpaJ. Nature 496: 106-109.
136. Lim JP, Gleeson PA (2011) Macropinocytosis: an endocytic pathway for internalising large gulps. Immunol Cell Biol 89: 836-843.
137. Mayle KM, Le AM, Kamei DT (2012) The intracellular trafficking pathway of transferrin. Biochim Biophys Acta 1820: 264-281.
138. Prochazkova K, Satchell KJ (2008) Structure-function analysis of inositol hexakisphosphate-induced autoprocessing of the Vibrio cholerae multifunctional autoprocessing RTX toxin. J Biol Chem 283: 23656-23664.
139. Egerer M, Giesemann T, Herrmann C, Aktories K (2009) Autocatalytic processing of Clostridium difficile toxin B. Binding of inositol hexakisphosphate. J Biol Chem 284: 3389-3395.
140. Salomon D, Orth K (2013) What pathogens have taught us about posttranslational modifications. Cell Host Microbe 14: 269-279.
141. Juris SJ, Rudolph AE, Huddler D, Orth K, Dixon JE (2000) A distinctive role for the Yersinia protein kinase: actin binding, kinase activation, and cytoskeleton disruption. Proc Natl Acad Sci U S A 97: 9431-9436.
142. Zhou Y, Dong N, Hu L, Shao F (2013) The Shigella type three secretion system effector OspG directly and specifically binds to host ubiquitin for activation. PLoS One 8: e57558.
143. Coaker G, Falick A, Staskawicz B (2005) Activation of a phytopathogenic bacterial effector protein by a eukaryotic cyclophilin. Science 308: 548-550.
144. Coaker G, Zhu G, Ding Z, Van Doren SR, Staskawicz B (2006) Eukaryotic cyclophilin as a molecular switch for effector activation. Mol Microbiol 61: 1485-1496.

145. Buss C, Muller D, Ruter C, Heusipp G, Schmidt MA (2009) Identification and characterization of Ibe, a novel type III effector protein of A/E pathogens targeting human IQGAP1. Cell Microbiol 11: 661-677.
146. Yang Z, Vadlamudi RK, Kumar R (2005) Dynein light chain 1 phosphorylation controls macropinocytosis. J Biol Chem 280: 654-659.
147. Driskell OJ, Mironov A, Allan VJ, Woodman PG (2007) Dynein is required for receptor sorting and the morphogenesis of early endosomes. Nat Cell Biol 9: 113-120.
148. Raymond B, Young JC, Pallett M, Endres RG, Clements A, et al. (2013) Subversion of trafficking, apoptosis, and innate immunity by type III secretion system effectors. Trends Microbiol 21: 430-441.